AD-754 517

INSTRUMENT LANDING SYSTEM SCATTERING

Chin, L. Jordan, et al

Transportation Systems Center

Prepared for:

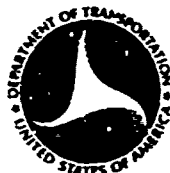Federal Aviation Administration

December 1972

Best
Available
Copy

REPORT NO. FAA-RD-72-137

AD754517

INSTRUMENT LANDING SYSTEM SCATTERING

G. Chin
L. Jordan
D. Kahn
S. Morin
Transportation Systems Center
Kendall Square
Cambridge, Ma. 02142

DECEMBER 1972
FINAL REPORT

NATIONAL TECHNICAL
INFORMATION SERVICE

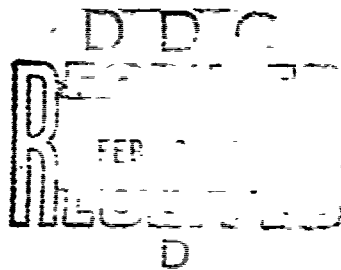| 1. Report No. FAA-RD-72-137	2. Government Accession No.	3. Recipient's Catalog No.
4. Title and Subtitle INSTRUMENT LANDING SYSTEM SCATTERING		5. Report Date December 1972
		6. Performing Organization Code
7. Author(s) G. Chin, L. Jordan, D. Kahn , S. Morin		8. Performing Organization Report No DOT-TSC-FAA-72-28
9. Performing Organization Name and Address Department of Transportation Transportation Systems Center Kendall Square, Cambridge, MA. 02142		10. Work Unit No. R 2103
		11. Contract or Grant No. FA207
		13. Type of Report and Period Covered
12. Sponsoring Agency Name and Address Department of Transportation Federal Aviation Administration Systems Research and Development Service Washington, D.C. 20591		Final Report
		14. Sponsoring Agency Code

15. Supplementary Notes

16. Abstract

The construction of a mathematical model of the Instrument Landing System (ILS) multipath problem has been undertaken. This report presents the theoretical basis for such a model, and newly achieved developments in ILS model construction.

17. Key Words ILS, scattering theory, current deviation indication, derogation, receiver model, Doppler Shift, DDM	18. Distribution Statement Availability is Unlimited. Document may be Released to the National Technical Information Service, Springfield, Virginia 22151, for sale to the Public.

19. Security Classif. (of this report) Unclassified	20. Security Classif. (of this page) Unclassified	21. No. of Pages 140	22. Price

PREFACE

This final report of fiscal year 1972 on ILS scattering contains the new work performed since the publication of the February 1972 report, titled "The ILS Scattering Problem and Signal Detection Model". In order that this report be as self-contained as possible, most of the original work contained in the February 1972 report is reproduced here.

Work performed since the February report is found in Appendix A which contains the development of the Fresnel approximation for use in considering scattering from tall structures; in Section 4 where the closed-form solution for scattering from slanted rectangular walls is derived and where an extension of the electromagnetic scattering problem to non-perfectly conducting slabs is developed; and in Appendix E where the computer program is discussed.

Since publishing the February 1972 report, the model has undergone a validation test and agrees well with the flight data. The model has also been applied to the planned Dallas Fort Worth Regional Airport to predict the expected course deviation indication (CDI) using two different localizers. These results may be found in TSC Report No. DOT-TSC-FAA-72-15, titled "ILS Localizer Performance Study; Dallas Fort Worth Regional Airport and Model Validation - Syracuse Hancock Airport."

TABLE OF CONTENTS

Preceding page blank   v

TABLE OF CONTENTS (CONT.)

LIST OF ILLUSTRATIONS

LIST OF ILLUSTRATIONS (CONT.)

1.0 INTRODUCTION

In the first part of this report, the basic ILS scattering
problem is investigated starting from first principles. Maxwell's
equations are first formally integrated using the vector Green's
theorem. The resulting integral equations express the electric
and magnetic fields at an observation point P inside a volume V in
terms of volume integrals over the charge and current distributions
inside V and surface integrals of the electric and magnetic fields
over the surfaces bounding V. The surface integrals represent con-
tributions to the electromagnetic fields at P from radiation
sources located outside of the volume V and are identically zero
if there are no such external sources.

These integral equations are then applied to the general
problem of electromagnetic scattering. The volume of integration
V is made multiply-connected with an interior and an exterior
boundary. The source of the incident radiation (e.g., an ILS
antenna) is located inside V, while the scatterer is enclosed by
the interior boundary of V. Consequently, the charge and current
distributions which constitute the source of the incident radiation
are the only radiation sources interior to V. Under the assumption
that the perturbations in the current and charge distributions of
the primary source due to the presence of the scatterer can be
neglected (Approx. No. 1), the integral equations for the electric
and magnetic fields at an interior point of V are applied. The
electromagnetic fields are represented as sums of the incident
fields produced by the primary source and the scattered fields
produced by the induced currents and charges in the scatterer. It
is shown that the scattered electric and magnetic fields at the
observation point P can be represented as surface integrals of the
scattered fields over the surface of the scatterer.

To obtain approximate solutions to these surface integral
equations for the scattered fields at P, an iterative approach is
adopted. Specifically, from a knowledge of the boundary conditions
which must be satisfied at the surface of the scatterer, approximate

1

functional relationships among the scattered fields and the known incident fields are developed and then substituted into the surface integral equations. The integrals, which are now expressed in terms of the known incident fields, are then evaluated to produce approximate expressions for the scattered fields at the observation point. The functional relationships among the scattered and incident fields at the surface of the scatterer are extremely complicated in the case of certain structures, for example, for hollow dielectric buildings with various internal structure, but very simple in the case of perfect conductors or buildings with metal walls (or, to a good approximation, metal rod reinforced concrete walls). Because of the difficulties of pursuing the analysis further with non-metal structures and because typical airport scattering objects are well approximated by perfect conductors, we assume, except in Section IV, that the scattering objects are perfect conductors (Approx. No. 2).

Application of the boundary conditions for perfect conductors yields a relationship between the scattered magnetic field at the observation point and the surface integral over the scatterer of the tangential component of the total (incident plus scattered) magnetic field. To approximate the total magnetic field on the surface of the conducting scatterer, we first employ the principles of ray optics. Specifically, we assume as a first approximation that the total magnetic field is zero on the side of the scatterer not directly illuminated by the primary source (Approx. No. 3). This is a good approximation when diffraction effects may be considered as second order effects. Diffraction effects may safely be considered second order when the wavelength of the incident radiation is small compared with the dimensions of the scatterer. This is the case for scattering from hangers; however, it is not the case for scattering from aircraft where the localizer wavelength and fuselage radius are comparable. To treat this case, special care would have to be taken to check that diffraction remains small; for, if it does not, Approximation Number 3 could not be made and an alternate method for relating incident and scattered fields would be needed.

2

Having assumed that the tangential component of the magnetic field is zero on the unilluminated portion of the scatterer, it is next necessary to specify it on the illuminated side. This is done by assuming plane wave reflection (Approx. No. 4). For distances generally encountered in the ILS problem, this approximation is valid (unless the scatterer dimensions are comparable to the wavelength, in which case, Approximations 3 and 4 will have to be modified).

Since we are interested in the values of the scattered fields in the far field of the scatterer (the approaching aircraft being between the outer marker and the far end of the runway), the integral equations for the fields may be expanded asymptotically for large values of the distance between scatterer and observer (Approx. No. 5); a similar far field approximation is made for the antenna-to-scatterer distance. Both the Fraunhofer and Fresnel versions of this approximation are used in this report.

The application of the above approximations in the analysis leads to the final expressions shown in Section 2.4, APPROXIMATE SOLUTIONS TO THE INTEGRAL EQUATIONS OF SCATTERING THEORY, Equations (2.47) and (2.48) for the scattered electromagnetic field. These differ from those used by IBM but are basically the same as the Ohio University expressions. The differences between the theory presented here and IBM's are discussed in Sections 2.5 and 2.6, LOCALIZER SIGNAL SCATTERING and COMPARISON WITH PREVIOUS WORK, where the theory is carefully applied to localizer signal scattering by a rectangular wall. By means of this application of the theory to scattering from a rectangular wall, it is shown our results reduce to Ohio's, if certain additional approximations relating to reflections from the ground plane are made in our equations. The differences between our formulation of the scattering problem and the IBM formulation are of a fundamental nature. The practical consequences of these differences are shown in an accompanying graph in which the example used by IBM for scattering from a vertical rectangular wall is used and the predicted DDM's compared. The differences may often be significant. For very tall

3

structures even larger differences would be found, as is demon-
strated in our Fresnel approximation development, found in
Appendix A.

In addition to the analysis of rectangular wall scattering,
we present (Appendix B) the new scattering formula for vertical
triangles and show how to use these when the triangles are ele-
vated, as in the case of triangular roof structures and tail sec-
tions of aircraft. We also present (Section 4.4.) a closed-form
solution to the slanted rectangular wall (not previously obtained
in the IBM formulation), which should be useful for calculating
reflection from hangars with slanted roofs. New closed-form
solutions for double reflection between two vertical walls are
given in Appendix C.

In Section 3.0, MODELING OF ILS SIGNAL DETECTION, we go from
the scattering problem to the signal detection problem, in which
we try to understand how the DDM must be defined in the presence
of multipath and develop a reasonable model of the ILS signal
detection system. The IBM and Ohio University expressions for DDM
are inadequate for strong multipath environments, since their ex-
pressions are strictly valid only for single carrier signals when
the relative phases of the received carrier and sidebands are the
same. We, therefore, present a unified model of ILS signal recep-
tion which includes the dephasing of carrier and sideband signals,
Doppler effects, different receiving antenna gain patterns and
capture effect systems.

To do this, a general expression for the receiver input cur-
rent is written which includes the polarization and gain vector of
the antenna (the gain vector for a small circular loop receiving
antenna is derived in Appendix D). This is used to help represent
the amplified signal, which appears at the output of the IF stage
of the receiver, in terms of the different transmitted modulation
waveforms and the gains and phase delays associated with the dif-
ferent radiation paths. This IF signal is then passed to a second
detector which generates an audio frequency signal which is passed
through a set of filters to obtain the relative 90 Hz and 150 Hz

4

amplitudes, from which the course deviation indication (CDI) may be determined.

Since the second detector (amplitude modulation detector) is a nonlinear device, its output reflects interactions between the intended ILS signal and the spurious signals received due to multi-pathing or due to transmission of a secondary carrier. In order to estimate the relative passage of this output through the selective 90 Hz and 150 Hz tone filters, Fourier analysis is used to express the detected audio signal in terms of discrete frequency components for which well defined transmissivities by each filter are assumed. The interaction between the course and clearance signals in the general case of a dual carrier frequency system gives rise to the much-utilized "capture effect". Advantage is taken of the large separation between the ILS signal modulation frequencies and the intercarrier beat (8kHz) to find an approximate linear expression for the total detected audio signal in terms of independent course and clearance audio signals.

The isolated course and clearance signals have the character of audio outputs from an AM detector generated by standard single carrier ILS signals, distorted by multipathing. For this single carrier case, a simple relation is found for the principal components of the detected audio signal lying within the passbands of the modulation frequency filters. The analysis in this case is valid in the approximation that the aggregate of interfering signals is somewhat weaker than the direct carrier signal - a reasonable condition for any marginally flyable course.

Doppler modifications of detected signals arise as a consequence of the variation of multipath phase delays which is implicit with the motion of an airborne receiver. In the approximation stated immediately above, each received component of multipath interference may be characterized by the relative Doppler shift of its carrier to the direct path carrier. Sum and difference combinations of modulation and Doppler frequencies can under certain circumstances give net frequencies near the filter center frequencies resulting in possible false signals being passed by the

5

90 Hz or 150 Hz filters. With the aircraft approach speeds used
today, the Doppler may, for example, increase the 90 Hz signal to
the point where it passes through the 150 Hz filter, or it may in-
crease the 150 Hz to the extent that it is excluded from the 150 Hz
filter. These possibilities are investigated by studying the fre-
quency response of a narrowband modulation filter and calculating
all significant contributions in each filter output. Thus, values
are obtained for the two detected modulation amplitudes from which
the apparent DDM and CDI are conventionally determined. As a
practical matter, it appears that the Doppler contributions to sig-
nal derogation cannot be neglected for aircraft speeds in the vicin-
ity of 200 feet/sec. and filter bandwidths around 15 cps.

Thus the new model is capable of calculating the detected audio
frequency signal, including Doppler and capture effects, in the
presence of any moderately strong multipath interference. It may
therefore be applied to determination of the apparent CDI for any
conventional localizer or glide slope system.

In Section 4.0 we present a formulation of the electromagnetic
scattering problem for imperfectly conducting thin flat slabs as a
possible extension of the theory presented in Section 2.0 for use
in situations where the electromagnetic waves are incident upon
non-metallic structures at large angles of incidence.

Finally, in Appendix E, the computer program itself is
discussed.

2.0 THE ILS SCATTERING PROBLEM

2.1 INTRODUCTION

Electromagnetic scattering is one of the most important and most complex topics in classical mathematical physics. Basically, the problem is to determine the field perturbations (scattered fields) which result when various obstacles (the scatterers) are placed in known (incident) electromagnetic fields. To solve a given scattering problem, one attempts to find a solution of Maxwell's equations which has the property that when it is added to the known or incident electromagnetic field the resulting total field satisfies the appropriate boundary conditions at the surfaces of the scattering obstacles. Unfortunately, exact solutions to scattering problems have been obtained in only a limited number of cases. In this report, integral equations for the scattered fields will be developed by directly integrating the electromagnetic field equations. Approximate solutions to these integral equations for the case of perfectly conducting scatterers will then be applied to investigate localizer signal scattering by a flat, vertical wall. Comparisons will be made with previous work.

2.2 INTEGRATION OF MAXWELL's EQUATIONS

The Maxwell's equations in M.K.S. units for a homogeneous, isotropic medium with permittivity ε and permeability μ are given below

$$\vec{\nabla} \times \vec{E} = i\omega\mu\vec{H} \tag{2.1}$$

$$\vec{\nabla} \times \vec{H} = \vec{J} - i\omega\varepsilon\vec{E} \tag{2.2}$$

$$\vec{\nabla} \cdot \vec{H} = 0 \tag{2.3}$$

$$\vec{\nabla} \cdot \vec{E} = \rho/\varepsilon \tag{2.4}$$

In Equations (2.1) through (2.4), it has been assumed that all fields vary harmonically in time as $e^{-i\omega t}$. The quantities $\vec{E}$, $\vec{H}$, $\vec{J}$, and ρ are, respectively, the electric field, the magnetic field, the current distribution, and the charge distribution. Taking the

7

curls of Equations (2.1) and (2.2) we find that $\vec{E}$ and $\vec{H}$ satisfy the following field equations:

$$\vec{\nabla} \times (\vec{\nabla}\times\vec{E}) - k^2\vec{E} = i\omega\mu\vec{J} \qquad , \qquad (2.5)$$

$$\vec{\nabla} \times (\vec{\nabla}\times\vec{H}) - k^2 H = \vec{\nabla}\times\vec{J} \qquad , \qquad (2.6)$$

where $k^2 = \omega^2\epsilon\mu$.

Let V be a closed volume in the medium bounded by a regular surface S. Let $\vec{Q}$ and $\vec{P}$ be vector fields defined at each point in the medium. The vector Green's theorem for $\vec{P}$ and $\vec{Q}$ has the following form:

$$\int_V (\vec{Q}\cdot\vec{\nabla}\times\vec{\nabla}\times\vec{P} - \vec{P}\cdot\vec{\nabla}\times\vec{\nabla}\times\vec{Q})dv$$

$$= \int_S (\vec{P}\times\vec{\nabla}\times\vec{Q} - \vec{Q}\times\vec{\nabla}\times\vec{P})\cdot\hat{n}\ ds \quad , \qquad (2.7)$$

where $\hat{n}$ is the unit normal to the surface S and is directed outward from the volume V.

The integral identity given by Equation (2.7) can be used to directly integrate the field Equations (2.5) and (2.6). To begin with, we define the function $\Psi(\vec{r}',\vec{r})$ as follows:

$$\Psi(\vec{r}',\vec{r}) = \frac{e^{ik|\vec{r}'-\vec{r}|}}{|\vec{r}'-\vec{r}|} \quad . \qquad (2.8)$$

The two point function Ψ is just the Green's function of the Helmholtz equation. That is to say, Ψ satisfies the equation

$$(\nabla^2+k^2)\Psi = -4\pi\delta(\vec{r}'-\vec{r}) \qquad , \qquad (2.9)$$

where $\delta(\vec{r}'-\vec{r})$ is the Dirac Delta Function. The vector $\vec{r}'$ can be thought of as the position vector relative to some origin 0 of an observation point P inside V while $\vec{r}'$ is the position vector relative to the origin of any source point in V or on S. Following Stratton,[1] we first define the vectors $\vec{P}$ and $\vec{Q}$ appearing in Equation (2.7) as follows:

8

$$\vec{P} = \vec{E}(\vec{r})$$

$$\vec{Q} = \hat{a}\ \Psi(\vec{r}',\vec{r}) \tag{2.10}$$

where $\hat{a}$ is a unit vector in some arbitrary, fixed direction.
Referring to Equations (2.5), (2.9), and (2.10), the following
vector relations hold:

$$\vec{\nabla}\times\vec{Q} = \vec{\nabla}\Psi\times\hat{a}$$

$$\vec{\nabla}\times(\vec{\nabla}\times\vec{Q}) = +\hat{a}k^2\Psi + 4\pi\hat{a}\,\delta\,(\vec{r}'-\vec{r}) + \vec{\nabla}(\hat{a}\cdot\vec{\nabla}\Psi) \tag{2.11}$$

$$\vec{\nabla}\times(\vec{\nabla}\times\vec{P}) = k^2\vec{E} + i\omega\mu\vec{J}$$

Substituting these various expressions into the integral
relation (2.7) and integrating with respect to the unprimed source
coordinates, we obtain after a few trivial vector manipulations
the following expression for $\vec{E}(\vec{r}')$

$$\vec{E}(\vec{r}') = \frac{1}{4\pi}\int_V(i\omega\mu\vec{J}\Psi+\frac{1}{\epsilon}\rho\vec{\nabla}\Psi)dv \tag{2.12}$$

$$-\frac{1}{4\pi}\int_S\left[i\omega\mu\,(\hat{n}\times\vec{H})\,\Psi+ (\hat{n}\times\vec{E})\times\vec{\nabla}\Psi+ (\hat{n}\cdot\vec{E})\,\vec{\nabla}\Psi\right]ds$$

The unit vector $\hat{a}$ has been dropped from (2.12) since its orienta-
tion is arbitrary and it would simply scalar multiply both sides
of (2.12). Repeating this analysis with $\vec{P}$ defined as $\vec{H}(\vec{r})$, the
following expression for $\vec{H}(\vec{r}')$ is obtained:

$$\vec{H}(\vec{r}') = \frac{1}{4\pi}\int_V(\vec{J}\times\vec{\nabla}\Psi)dv \tag{2.13}$$

$$+ \frac{1}{4\pi}\int_S\left[i\omega\epsilon\,(\hat{n}\times\vec{E})\,\Psi- (\hat{n}\times\vec{H})\times\vec{\nabla}\Psi- (\hat{n}\cdot\vec{H})\,\vec{\nabla}\Psi\right]ds$$

Equations (2.12) and (2.13) express the electric and
magnetic field intensities at any point P inside the volume V in
terms of volume integrals over the charges and currents inside V
and surface integrals of the fields over the bounding surface S.
The surface integrals represent the contributions to $\vec{E}$ and $\vec{H}$ from
sources located outside V. These two equations will be the basis
for our treatment of electromagnetic scattering.

2.3 INTEGRAL EQUATIONS IN THE THEORY OF ELECTROMAGNETIC SCATTERING

To begin our discussion of electromagnetic scattering, consider the geometry depicted in Figure 2.1. Figure 2.1 depicts a multiply-connected volume V containing a localized source of electromagnetic radiation which occupies a volume V_i in V. This source might, for example, be a glide slope or localizer antenna. The charge and current distributions within V_i will be denoted by ρ_i and $\vec{J}_i$, respectively. Elsewhere in V, $\vec{J}$ and ρ are assumed to be identically zero. Note that the volume V is bounded by an interior boundary surface S_1 and an outer boundary surface S_o. The volume V_1 bounded by S_1 is not included in V. The volume V consists of the region bounded by S_o, excluding the interior of S_1. To apply Equations (2.12)
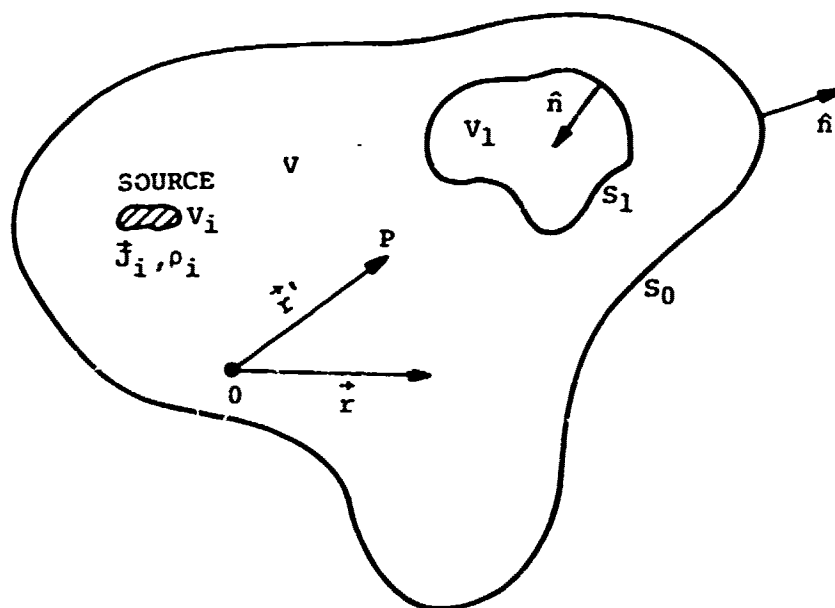
Figure 2.1. Multiply-Connected Region Containing Source

and (2.13) to such a multiply-connected region, the surface integrals must be carried out over both bounding surfaces.

Let us assume that the source occupying the volume V_i in V is the only source of radiation. Let $\vec{E}_i(\vec{r})$ and $\vec{H}_i(\vec{r})$ denote, respectively, the electric and magnetic field intensities produced by this source. The subscript "i" is used to denote incident field. The values of $\vec{E}_i$ and $\vec{H}_i$ at a point P inside V are given by the following equations (Eqs. (2.12) and (2.13)).

$$\vec{E}_i(\vec{r}') = \frac{1}{4\pi}\int_{V_i}(i\omega\mu\vec{J}_i\varphi + \frac{1}{\epsilon}\rho_i\vec{\nabla}\varphi)dv$$

$$-\frac{1}{4\pi}\sum_{j=0}^{1}\int_{S_j}\left[i\omega\mu\,(\hat{n}\times\vec{H}_i)\varphi + (\hat{n}\times\vec{E}_i)\times\vec{\nabla}\varphi + (\hat{n}\cdot\vec{E}_i)\vec{\nabla}\varphi\right]ds \quad (2.14)$$

and

$$\vec{H}_i(\vec{r}') = \frac{1}{4\pi}\int_{V_i}(\vec{J}_i\times\vec{\nabla}\varphi)\,dv$$

$$+\frac{1}{4\pi}\sum_{j=0}^{1}\int_{S_j}\left[i\omega\epsilon\,(\hat{n}\times\vec{E}_i)\varphi - (\hat{n}\times\vec{H}_i)\times\vec{\nabla}\varphi - (\hat{n}\cdot\vec{H}_i)\vec{\nabla}\varphi\right]ds.$$

$$(2.15)$$

Note that in Equations (2.14) and (2.15), the volume integrals are extended only over the volume V_i occupied by the localized source since $\vec{J}$ and ρ are zero elsewhere in V. Note also that each equation contains two surface integrals because of the two surfaces which bound V.

Equations (2.14) and (2.15) represent solutions to the field Equations (2.5) and (2.6) for the electric and magnetic field distributions inside the multiply connected region due to the localized source occupying the volume V_i in V depicted in Figure 2.1. Since this localized source is assumed to be the only source of radiation in the universe, the surface integrals appearing in Equations (2.14) and (2.15) are in fact identically zero. To see that this must be so, consider first the surface integrals, in Equations (2.14) and (2.15) of $\vec{E}_i$ and $\vec{H}_i$ over the interior boundary S_1. Since S_1 encloses no sources ($\vec{J} \equiv 0$ and $\rho \equiv 0$ in V_1), we can

11

contract the surface S_1 down to a new boundary surface $\bar{S}_1$ which is enclosed by S_1 without adding any new charges or currents to the volume of integration. Consequently, the only changes in Equations (2.14) and (2.15) which result from shrinking S_1 down to $\bar{S}_1$ is that the surface integrals of $\vec{E}_i$ and $\vec{H}_i$ over S_1 are now carried out over $\bar{S}_1$. Since the electric and magnetic field intensities at P do not change as a result of this contraction, we must conclude that the surface integrals over $\bar{S}_1$ equal the corresponding surface integrals over S_1. But, the values of the surface integrals in (2.14) and (2.15) of $\vec{E}_i$ and $\vec{H}_i$ over $\bar{S}_1$ can be made arbitrarily small by simply allowing the surface area of $\bar{S}_1$ to go to zero. Consequently, we can conclude that the surface integrals of $\vec{E}_i$ and $\vec{H}_i$ over S_1 appearing in Equations (2.14) and (2.15) are identically zero. That is to say,

$$\int_{S_1} \left[i\omega\mu\,(\hat{n}\mathrm{x}\vec{H}_i)\,\psi + (\hat{n}\mathrm{x}\vec{E}_i)\,\mathrm{x}\vec{\nabla}\psi + (\hat{n}\cdot\vec{E}_i)\,\vec{\nabla}\psi \right] ds \equiv 0 \qquad (2.16)$$

and

$$\int_{S_1} \left[i\omega\epsilon\,(\hat{n}\mathrm{x}\vec{E}_i)\,\psi - (\hat{n}\mathrm{x}\vec{H}_i)\,\mathrm{x}\vec{\nabla}\psi - (\hat{n}\cdot H_i)\,\vec{\nabla}\psi \right] ds \equiv 0 \qquad (2.17)$$

A similar argument can be made regarding the surface integrals of $\vec{E}_i$ and $\vec{H}_i$ over the outer boundary S_o. Since no new sources of radiation are added to the volume of integration by expanding S_o to some new surface $\bar{S}_o$ ($\vec{J} \equiv 0$ and $\rho \equiv 0$ outside S_o); the surface integrals over $\bar{S}_o$ must equal the corresponding integrals over S_o. But if the surface $\bar{S}_o$ is allowed to recede to infinity, the surface integrals over $\bar{S}_o$ go to zero because of the following asymptotic properties of electromagnetic fields produced by localized sources.[1,2]

12

$$\lim_{r \to \infty} r\dot{E} \text{ is finite}$$

$$\left. \lim_{r \to \infty} \; r\left[(\hat{r}\times\vec{H}) + \left(\frac{\varepsilon}{\mu}\right)^{\frac{1}{2}}\vec{E}\right] = 0 \right\} . \tag{2.18}$$

$$\lim_{r \to \infty} r\bar{H} \text{ is finite}$$

$$\left. \lim_{r \to \infty} \; r\left[\left(\frac{\varepsilon}{\mu}\right)^{\frac{1}{2}}(\hat{r}\times\vec{E}) - \vec{H}\right] = 0 \right\} . \tag{2.19}$$

where $\hat{r} = \vec{r}/r$ is a unit vector in the direction of $\vec{r}$. Consequently, we can conclude that the surface integrals of $\vec{E}_i$ and $\vec{H}_i$ over S_o appearing in Equations (2.14) and (2.15) are identically zero. That is to say,

$$\int_{S_o} i\omega\mu(\hat{n}\times\vec{H}_i)\psi + (\hat{n}\times\vec{E}_i)\times\vec{\nabla}\psi + (\hat{n}\cdot\vec{E}_i)\vec{\nabla}\psi \; ds = 0, \tag{2.20}$$

and

$$\int_{S_o}\left[i\omega\varepsilon(\hat{n}\times\vec{E}_i)\psi - (\hat{n}\times\vec{H}_i)\times\vec{\nabla}\psi - (\hat{n}\cdot\vec{E}_i)\vec{\nabla}\psi\right]ds = 0. \tag{2.21}$$

Substituting Equations (2.16), (2.17), (2.20) and (2.21) into Equations (2.14) and (2.15), we obtain the following expressions for $\vec{E}_i(\vec{r}')$ and $\hat{H}_i(\vec{r}')$:

$$\vec{E}_i(\vec{r}') = \frac{1}{4\pi}\int_{V_i}(i\omega\mu\vec{J}_i\psi + \frac{1}{\varepsilon}\rho_i\vec{\nabla}\psi)dv. \tag{2.22}$$

$$\vec{H}_i(\vec{r}') = \frac{1}{4\pi}\int_{V_i}(\vec{J}_i\times\vec{\nabla}\psi)dv . \tag{2.23}$$

Equations (2.22) and (2.23) are the familiar expressions for the electric and magnetic field intensities produced by localized sources of radiation in the absence of boundaries.

13

Suppose now that a scattering object is placed inside the interior boundary S_1. The situation is depicted in Figure 2.2.
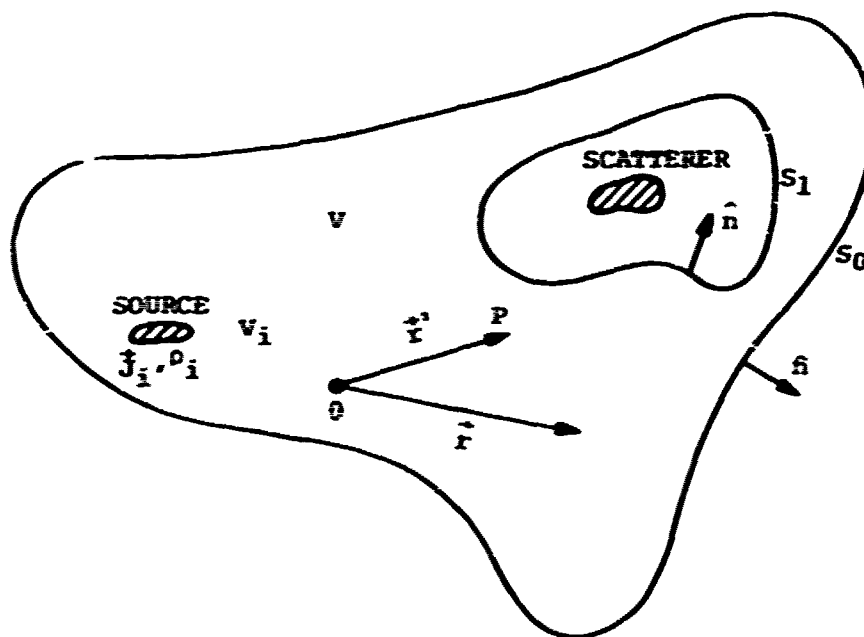
Figure 2.2.   Geometry Illustrating the Arrangement of
Source and Scatterer

The scatterer could be composed of a conducting or dielectric material or a combination of the two. Charges and currents will be induced in the scatterer by the incident fields $\vec{E}_i$ and $\vec{H}_i$ generated by the primary source of radiation occupying the volume V_i in V. These secondary sources will in turn radiate electromagnetic waves. Let $\vec{E}_s(\vec{r})$ and $\vec{H}_s(\vec{r})$ denote, respectively, the electric and magnetic fields generated by the charges and currents induced in the scatterer. The subscript "s" is used to denote scattered field. The total electric and magnetic fields can be represented as follows:

$$\vec{E}(\vec{r}) = \vec{E}_i(\vec{r}) + \vec{E}_s(\vec{r})$$
$$\vec{H}(\vec{r}) = \vec{H}_i(\vec{r}) + \vec{H}_s(\vec{r})$$

(2.24)

The scattered fields $\vec{E}_s$ and $\vec{H}_s$ will of course exert forces on the charges and currents of the primary source. As a result,

14

the charge distribution ρ_i and the current distribution $\vec{J}_i$ will
assume new values which we will denote by ρ_i' and $\vec{J}_i'$, respectively.
However, we will assume that the perturbations of $\vec{J}_i$ and ρ_i due to
the presence of the scatterer are second order effects and that
they can be ignored. That is to say, we will assume that

$$\vec{J}_i' = \vec{J}_i$$
$$\rho_i' = \rho_i \qquad\qquad (2.25)$$

These approximations should be very good for scatterers in the far
field of the primary radiator.[2]

To calculate the total electric and magnetic fields at a
point P inside V, we simply apply Equations (2.12) and (2.13). For
example, the electric field is given by

$$\vec{E}(\vec{r}') = \frac{1}{4\pi} \int_{V_i} (i\omega\mu\vec{J}_i\psi + \frac{1}{\epsilon}\rho_i\vec{\nabla}\psi) \; dv$$

$$- \frac{1}{4\pi} \sum_{j=0}^{1} \int_{S_j} i\omega\mu(\hat{n}\times\vec{H})\psi + (\hat{n}\times\vec{E})\times\vec{\nabla}\psi + (\hat{n}\cdot\vec{E})\vec{\nabla}\psi \; ds \qquad (2.26)$$

where $\vec{E} = \vec{E}_i + \vec{E}_s$ and $\vec{H} = \vec{H}_i + \vec{H}_s$ (Eq. (2.24)). Notice that the
localized source occupying the volume V_i is still the only source
of radiation inside V since the scatterer lies in the volume V_1
bounded by S_1 and this region is excluded from V. Notice also
that we have made use of the approximation (2.25). According to
Equation (2.22), the volume integral appearing in Equation (2.26)
equals $\vec{E}_i(\vec{r}')$. Consequently, since $\vec{E} = \vec{E}_i + \vec{E}_s$, the scattered
electric field at P is given by

$$\vec{E}_s(\vec{r}') = - \frac{1}{4\pi} \sum_{j=0}^{1} \int_{S_j} \left[i\omega\mu(\hat{n}\times\vec{H}_i)\psi + (\hat{n}\times\vec{E}_i)\times\vec{\nabla}\psi + (\hat{n}\cdot\vec{E}_i)\vec{\nabla}\psi \right] ds$$

$$- \frac{1}{4\pi} \sum_{j=0}^{1} \int_{S_j} \left[i\omega\mu(\hat{n}\times\vec{H}_s)\psi + (\hat{n}\times\vec{E}_s)\times\vec{\nabla}\psi + (\hat{n}\cdot\vec{E}_s)\vec{\nabla}\psi \right] ds \qquad (2.27)$$

15

where we have made use of Equation (2.24) and have separated the surface integrals involving the incident and scattered fields. But the integrals of $\vec{E}_i$ and $\vec{H}_i$ over the surfaces S_0 and S_1 have already been shown to be identically zero (Eqs. (2.16) and (2.20)). Furthermore, if the surface S_0 is allowed to recede to infinity, the surface integral over S_0 of the scattered fields will go to zero since $\vec{E}_s$ and $\vec{H}_s$ have the same asymptotic properties as $\vec{E}_i$ and $\vec{H}_i$ (Eqs. (2.18) and (2.19)). Consequently, we finally arrive at the following expression for $\vec{E}_s(\vec{r}')$:

$$\vec{E}_s(\vec{r}') = -\frac{1}{4\pi} \int_{S_1} \left[i\omega\mu\,(\hat{n}\times\vec{H}_s)\psi + (\hat{n}\times\vec{E}_s)\times\vec{\nabla}\psi + (\hat{n}\cdot\vec{E}_s)\vec{\nabla}\psi \right] ds \tag{2.28}$$

Since the surface S_0 has been allowed to recede to infinity, Equation (2.28) is valid for any point P lying outside the surface S_1. The analogous expression for $\vec{H}_s(\vec{r}')$ is

$$\vec{H}_s(\vec{r}') = \frac{1}{4\pi} \int_{S_1} \left[i\omega\epsilon\,(\hat{n}\times\vec{E}_s)\psi - (\hat{n}\times\vec{H}_s)\times\vec{\nabla}\psi - (\hat{n}\cdot\vec{H}_s)\vec{\nabla}\psi \right] ds. \tag{2.29}$$

In fact, the surface S_1 can be collapsed down onto the surface of the scatterer itself so that Equations (2.28) and (2.29) become valid for all points P outside the body of the scatterer. This situation is depicted in Figure 2.3.
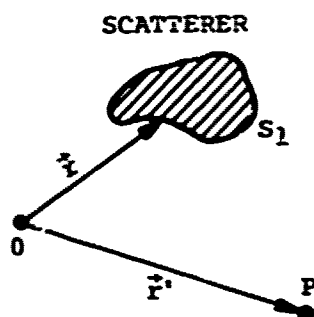
SCATTERER

Figure 2.3. Collapsing Surface S_1 onto Scatterer

Henceforth then, it will be understood that the surface S_1 is the actual surface of the scatterer. The unit normal $\hat{n}$ which appears in Equations (2.28) and (2.29) points into the body of the scatterer.

The integral Equations (2.28) and (2.29) express the scattered electromagnetic fields at an observation point P in terms of integrals of the

16

scattered fields over the surface of the scatterer. These equations represent first order solutions to the scattering problem in that they are based upon the approximation that the charge and current distributions of the primary source are not changed by the fields generated by the scatterer (Equation (2.25)). In the next section, useful approximate solutions to Equations (2.28) and (2.29) will be developed for the case of perfectly conducting scatterers.

2.4 APPROXIMATE SOLUTIONS TO THE INTEGRAL EQUATIONS OF SCATTERING THEORY

Approximate solutions to the integral Equations (2.28) and (2.29) can be obtained by using iterative methods. Specifically, from a knowledge of the boundary conditions which must be satisfied on the surface of the scatterer S_1, approximate functional relationships among $\vec{E}_s$ and $\vec{H}_s$ on S_1 and the known incident fields $\vec{E}_i$ and $\vec{H}_i$ on S_1 are developed and then substituted into the integrals in Equations (2.28) and (2.29). The integrals are then evaluated to produce approximate expressions for $\vec{E}_s$ and $\vec{H}_s$ at an observation point P. This procedure is particularly straightforward for the case of perfectly conducting scatterers because of the relative simplicity of the boundary conditions. In this section we will concentrate exclusively upon perfectly conducting scatterers.

Consider the integral Equation (2.29) for the scattered magnetic field intensity:

$$\vec{H}_s(\vec{r}') = \frac{1}{4\pi} \int_{S_1} \left[i\omega\epsilon\,(\hat{n}x\vec{E}_s)\,\psi - (\hat{n}x\vec{H}_s)\,x\vec{\nabla}\psi - (\hat{n}\cdot\vec{H}_s)\,\vec{\nabla}\psi \right] ds \tag{2.29}$$

For convenience, Equation (2.29) will be modified by making use of the fact that, as shown earlier the surface integral appearing in (2.29) of the incident fields $\vec{E}_i$ and $\vec{H}_i$ is identically zero (Eq. (2.17)). That is to say,

$$0 \equiv \frac{1}{4\pi} \int_{S_1} \left[i\omega\epsilon\,(\hat{n}x\vec{E}_i)\,\psi - (\hat{r}x\vec{H}_i)\,x\vec{\nabla}\psi - (\hat{n}\,\vec{H}_i)\,\vec{\nabla}\psi \right] ds. \tag{2.30}$$

17

Adding Equation (2.30) to (2.29) and recalling that $\vec{E} = \vec{E}_i + \vec{E}_s$ and $\vec{H} = \vec{H}_i + \vec{H}_s$, we obtain the following equation:

$$\vec{H}_s(\vec{r}') = \frac{1}{4\pi} \int_{S_1} \left[i\omega\epsilon (\hat{n}x\vec{E})\Psi - (\hat{n}x\vec{H})x\vec{\nabla}\Psi - (\hat{n}\cdot\vec{H})\vec{\nabla}\Psi \right] ds, \qquad (2.31)$$

where $\vec{E}$ and $\vec{H}$ are the total fields on S_1. At the surface of a perfect conductor, the tangential component of the total electric field and the normal component of the total magnetic field are identically zero. Mathematically, these boundary conditions can be expressed as follows:

$$\hat{n} \times \vec{E} \equiv 0; \quad (\hat{n}x\vec{E}_s = -\hat{n}x\vec{E}_i)$$

$$\hat{n} \cdot \vec{H} \equiv 0; \quad (\hat{n}\cdot\vec{H}_s = -\hat{n}\cdot\vec{H}_i) \qquad (2.32)$$

Consequently, for a perfect conductor, Equation (2.31) takes the following simple form:

$$\vec{H}_s(\vec{r}') = -\frac{1}{4\pi} \int_{S_1} (\hat{n}x\vec{H}) \times \vec{\nabla}\Psi \, ds . \qquad (2.33)$$

To approximate $(\hat{n}x\vec{H})$ on the surface of the scatterer, we first employ the principles of geometrical or ray optics. According to ray optics, there is a deep shadow region (no illumination) on the side of the scatterer not directly exposed to the incident radiation from the primary source. In the shadow region, $\vec{E}$ and $\vec{H}$ are identically zero ($\vec{E}_s = -\vec{E}_i$ and $\vec{H}_s = -\vec{H}_i$). The surface S_1 is thus divided into an illuminated side S_+ and a shadow side S_-, the two sides being separated by a sharp shadow boundary Γ. This situation is depicted in Figure 2.4. If it is assumed that $\vec{E}$ and $\vec{H}$ are identically zero on S_-, then Equation (2.33) becomes

$$\vec{H}_s(\vec{r}') = -\frac{1}{4\pi} \int_{S_+} (\hat{n}x\vec{H}) \times \vec{\nabla}\Psi \, ds , \qquad (2.34)$$

18
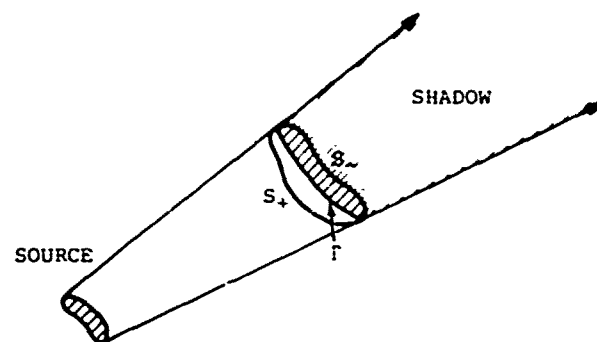
Figure 2.4   Shadow and Illuminated Regions of Scatterer

where the integral is performed only over the illuminated side of
the scatterer. Finally, to specify $(\hat{n} \times \vec{H})$ on S_+, the assumption of
plane wave reflection from the local infinite tangent plane is
made. That is to say, at each point Q on S_+, it is assumed that
$\vec{E}_s(Q)$ and $\vec{H}_s(Q)$ have the values of the reflected fields which
would exist if a plane electromagnetic wave with amplitudes $\vec{E}_i(Q)$
and $\vec{H}_i(Q)$ were incident upon an infinite plane perfectly conducting
boundary tangent to S_+ at Q. The boundary condition satisfied by
the tangential components of the incident and reflected magnetic
fields when a plane wave is incident upon an infinite , plane ,
perfectly conducting boundary is

$$\hat{n} \times \vec{H}_s = \hat{n} \times \vec{H}_i \ , \qquad (2.35)$$

or equivalently,

$$\hat{n} \times \vec{H} = \hat{n} \times (\vec{H}_i + \vec{H}_s) = 2(\hat{n} \times \vec{H}_i) \ . \qquad (2.36)$$

Assuming that Equation (2.36) is valid at each point on S_+,
Equation (2.34) becomes

$$\vec{H}_s(\vec{r}') = -\frac{1}{2\pi} \int_{S_+} (\hat{n} \times \vec{H}_i) \times \vec{\nabla}\psi \ ds \ . \qquad (2.37)$$

The analogous expression for $\vec{E}_s(\vec{r}')$ can be obtained by apply-
ing Equation (2.2) which, in the absence of currents, takes the
form

19

$$\vec{\nabla} \times \vec{H} = - i\omega\epsilon \, \vec{E} \qquad (2.38)$$

Substituting (2.37) into (2.38) the following expression for $\vec{E}_s(\vec{r}')$ is obtained:

$$\vec{E}_s(\vec{r}') = - \frac{i}{2\pi\omega\epsilon} \, \vec{\nabla}' \times \int_{S_+} (\hat{n}\times\vec{H}_i) \times \vec{\nabla}\psi \, ds \quad , \qquad (2.39)$$

where $\vec{\nabla}'$ acts upon the primed or field point coordinates. Equation (2.39) can be rewritten by taking the operator $\vec{\nabla}'\times$ inside the integral and noting that $\nabla\psi$ is the only function under the integral which depends upon $\vec{r}'$:

$$\vec{E}_s(\vec{r}') = - \frac{i}{2\pi\omega\epsilon} \int_{S_+} \left[(\hat{n}\times\vec{H}_i)\vec{\nabla}' \cdot (\vec{\nabla}\psi) - \left\{ (\hat{n}\times\vec{H}_i) \cdot \vec{\nabla}' \right\} \vec{\nabla}\psi \right] ds \qquad (2.40)$$

Since $\vec{\nabla}\psi$ is a function of $|\vec{r}'-\vec{r}|$, the following relationships hold true:

$$\vec{\nabla}' \cdot (\vec{\nabla}\psi) = -\vec{\nabla} \cdot (\vec{\nabla}\psi) = - \nabla^2\psi$$

$$\left[(\hat{n}\times\vec{H}_i) \cdot \vec{\nabla}' \right] \vec{\nabla}\psi = - \left[(\hat{n}\times\vec{H}_i) \cdot \vec{\nabla} \right] \vec{\nabla}\psi \qquad (2.41)$$

Substituting the relations (2.41) into (2.40) and noting that for $\vec{r}'\neq\vec{r}$, $-\nabla^2\psi = k^2\psi$ (Eq. (2.9)), we obtain the following equation for $\vec{E}_s(\vec{r}')$:

$$\vec{E}_s(\vec{r}') = - \frac{ik}{2\pi} \left(\frac{\mu}{\epsilon}\right)^{1/2} \int_{S_+} \left[(\hat{n}\times\vec{H}_i)\psi + \frac{1}{k^2} \left\{ (\hat{n}\times\vec{H}_i) \cdot \vec{\nabla} \right\} \vec{\nabla}\psi \right] ds \qquad (2.42)$$

where we have made use of the fact that $k=\omega\sqrt{\mu\epsilon}$.

We will be primarily concerned with the distributions of $\vec{E}_s$ and $\vec{H}_s$ in the far field or Fraunhofer zone of the scatterer. To obtain expressions for $\vec{E}_s$ and $\vec{H}_s$ in the Fraunhofer zone, Equations (2.37) and (2.42) are expanded asymptotically for large values of $r'=|\vec{r}'|$. For convenience, let the origin of coordinates, 0, lie on the surface of the scatterer. Let D denote some characteristic linear dimension of the scatterer. The Green's function

20

Ψ is given in Equation (2.8):

$$\Psi \approx \frac{e^{ik|\vec{r}'-\vec{r}|}}{|\vec{r}'-\vec{r}|} . \qquad (2.8)$$

Suppose that $r' \gg D$. Then in the denominator of (2.8), $|\vec{r}'-\vec{r}|$ can be approximated very accurately by r'. That is, the variations in the amplitude of Ψ as $\vec{r}$ varies over the surface of the scatterer can be ignored if $r' \gg D$. More care must be exercised in approximating the phase of Ψ because of the oscillatory behavior of the exponential. If $r' \gg D$, then $|\vec{r}'-\vec{r}|$ can be approximated to terms of second order in $r = |\vec{r}|$ as follows:

$$|\vec{r}'-\vec{r}| \approx r' - \hat{r}' \cdot \vec{r} + \frac{r^2}{2r'} - \frac{(\hat{r}' \cdot \vec{r})^2}{2r'} , \qquad (2.43)$$

where $\hat{r}' = \vec{r}'/r'$ is a unit vector in the direction of $\vec{r}'$. In the Fraunhofer zone, $D^2/2r'$ is very small compared to the wavelength $\lambda = 2\pi/k$ of the incident radiation so that the quadratic terms in Equation (2.43) can be ignored in comparison with the other two terms:

$$|\vec{r}'-\vec{r}| \approx r' - \hat{r}' \cdot \vec{r} \qquad \text{(Fraunhofer approximation)} \qquad (2.44)$$

Combining these amplitude and phase approximations, we may write down the following asymptotic expression for Ψ for field points in the radiation zone of the scatterer:

$$\Psi \approx \frac{e^{ikr'}}{r'} e^{-ik(\hat{r}' \cdot \vec{r})} \qquad (2.44A)$$

A similar analysis of $\vec{\nabla}\Psi$ and $(\vec{A} \cdot \vec{\nabla})\vec{\nabla}\Psi$ where $\vec{A}$ is an arbitrary vector leads to the following asymptotic expressions:

$$\vec{\nabla}\Psi \approx - ik \frac{e^{ikr'}}{r'} \cdot e^{-ik(\hat{r}' \cdot \vec{r})} \hat{r}' , \qquad (2.45)$$

$$(\vec{A} \cdot \vec{\nabla})\vec{\nabla}\Psi \approx (\vec{A} \cdot \hat{r}') \hat{r}' k^2 \frac{e^{ikr'}}{r'} e^{-ik(\hat{r}' \cdot \vec{r})} . \qquad (2.46)$$

Substituting the asymptotic forms (2.44), (2.45) and (2.46) into Equations (2.37) and (2.42), we obtain the following asymptotic or far field expressions for $\vec{H}_s$ and $\vec{E}_s$:

$$\vec{H}_s(\vec{r}') = -\frac{ik}{2\pi} \frac{e^{ikr'}}{r'} \cdot \hat{r}' \times \int_{S_+} (\hat{n} \times \vec{H}_i) e^{-ik(\hat{r}' \cdot \vec{r})} ds, \quad (2.47)$$

$$\vec{E}_s(\vec{r}') = \frac{ik}{2\pi} \left(\frac{\mu}{\epsilon}\right)^{1/2} \frac{e^{ikr'}}{r'} \cdot \hat{r}' \times \left[\hat{r}' \times \int_{S_+} (\hat{n} \times \vec{H}_i) e^{-ik(\hat{r}' \cdot \vec{r})}\right] ds, \quad (2.48)$$

where we have made use of the identity $\vec{a} \times (\vec{a} \times \vec{b}) = (\vec{a} \cdot \vec{b})\vec{a} - a^2\vec{b}$ in Equation (2.48). Notice that the asymptotic expressions for $\vec{H}_s$ and $\vec{E}_s$ in Equations (2.47) and (2.48) are related as follows:

$$\hat{r}' \times \vec{H}_s + \left(\frac{\epsilon}{\mu}\right)^{1/2} \vec{E}_s = 0$$

$$\left(\frac{\epsilon}{\mu}\right)^{1/2} \hat{r}' \times \vec{E}_s - \vec{H}_s = 0 \quad (2.49)$$

These results are in agreement with the asymptotic relations given in Equations (2.18) and (2.19).

Equations (2.47) and (2.48) are the basic equations used by the Ohio University[3] researchers and the TSC group for studying localizer signal scattering from metallic airport structures with plane surfaces. However, caution must be exercised in applying these equations since the assumptions upon which they are based are unrealistic for many applications. Generally speaking, Equations (2.47) and (2.48) can be applied with some confidence in situations in which the wavelength $\lambda = 2\pi/k$ of the incident radiation is small compared with the dimensions of the scatterer. When λ is comparable to or greater than the dimensions of the scatterer (length, radius of curvature, etc.) the assumption of a sharp boundary on the surface of the scatterer separating the illuminated side (S_+) from the shadow side (S_-) breaks down because of diffraction. The assumption of local plane wave reflection from the infinite tangent plane also breaks down when λ is comparable to or greater than the radius of curvature of the scatterer. It would for example, be unwise to attempt to use Equations (2.47) and (2.48) to study localizer signal scattering from the fuselages of aircraft

22

since at localizer frequencies, $\lambda \approx 10$ ft which is comparable to or greater than the radii of curvature of all aircraft presently in use. Another fact to be borne in mind is that Equations (2.47) and (2.48) apply to the Fraunhofer zone of the scatterer. That is to say, these equations are based upon the assumption that $D^2/2r'$ is very small compared to a wavelength where D is some characteristic linear dimension of the scatterer. For very large scatterers, and for observation points relatively close to the scatterer, this condition may not be satisfied. One way of circumventing this difficulty is to divide up the illuminated surface S_+ into smaller subsections, apply Equations (2.47) and (2.48) to each subsection, and then add up the contributions from the various subsections to get the total scattered fields. A more direct approach is to simply retain the quadratic terms in the expansion (2.43) and to express the scattered fields in terms of Fresnel integrals. This latter approach has in fact been pursued at TSC. The results of our work to date are presented in Appendix A.

In spite of these various restrictions upon the applicability of Equations (2.47) and (2.48), they can provide a great deal of useful information about scattering phenomena. In the next section, these equations will be used to treat the problem of localizer signal scattering by a flat, vertical wall.

2.5 LOCALIZER SIGNAL SCATTERING

To illustrate the techniques developed in the preceding section, we will treat the important problem of localizer signal scattering by a flat, vertical, rectangular wall. The geometry of the problem is depicted in Figure 2.5. The x-y plane is the ground plane. For simplicity, it is assumed that the ground is perfectly flat and perfectly conducting. The x-axis represents the center line of the runway. The z-axis is perpendicular to the ground and points out of the page. The unit vectors in the x, y, and z directions are denoted by $\hat{e}_x$, $\hat{e}_y$, and $\hat{e}_z$ respectively. The localizer antenna is located a distance H above the ground and has

23

coordinates (0,0,H) relative to the x, y, z coordinate system. H
is typically on the order of 10 feet for the localizer.
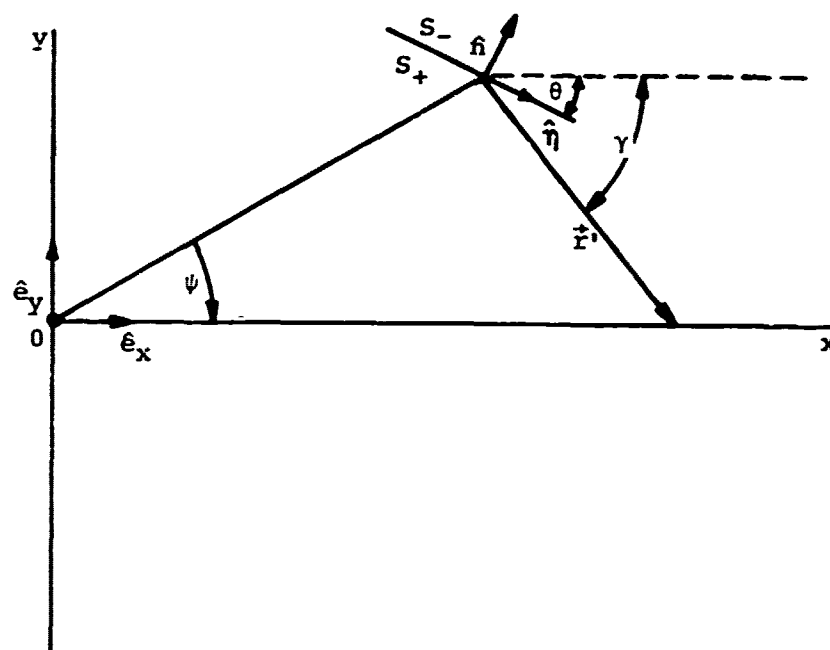
Figure 2.5. Scattering From a Vertical Wall,
Ground Plane Shown

In the far field of the localizer antenna, the electric
field can be written as follows:

$$\vec{E} = \hat{u} \, E_o \, f(\phi) \, \frac{e^{ikR}}{R} \, , \qquad (2.50)$$

where $\hat{u}$ is a unit polarization vector, E_o is an amplitude, R is
the distance from the localizer to the field point, and $f(\phi)$ is
the horizontal field pattern of the antenna. For an arbitrary
field point with coordinates (x,y,z), R and ϕ are defined as
follows:

$$R = \sqrt{x^2 + y^2 + (z-H)^2}$$

$$\phi = \tan^{-1}\left(\frac{y}{x}\right) \qquad (2.51)$$

24

The electric field generated by the localizer is assumed to be polarized parallel to the ground so that $\hat{u}$ is given by

$$\hat{u} = \frac{y \, \hat{e}_x - x \, \hat{e}_y}{D_p} \, , \qquad (2.52)$$

where $D_p = \sqrt{x^2 + y^2}$ is the horizontal distance from the antenna to the field point.

To account for reflections from the perfectly conducting ground plane, an image antenna located at $(0,0,-H)$ is included in the formulation to cancel the E field of the antenna on the ground ($z=0$). The total incident electric field (direct plus ground reflected) is given by

$$\vec{E}_i = \hat{u} \, E_o \, f(\phi) \left[\frac{e^{ikR}}{R} - \frac{e^{ikR_i}}{R_i} \right] \, , \qquad (2.53)$$

where $R_i = \sqrt{x^2 + y^2 + (z+H)^2}$ is the distance from the image antenna to the field point.

Equation (2.53) can be rewritten as follows:

$$\vec{E}_i = \hat{u} \, E_o \, f(\phi) \, \frac{e^{ikR}}{R} \left[1 - \frac{R}{R_i} e^{ik(R_i - R)} \right] . \qquad (2.54)$$

We now make the assumption of small elevation angles. That is to say, we will assume that $D_p = \sqrt{x^2 + y^2}$ is much greater than the magnitudes of $(z-H)$ and $(z+H)$. If $D_p >> |z-H|$ and $|z+H|$, then $D_p \approx R \approx R_i$ and the factor R/R_i in Equation (2.54) can be set approximately equal to 1. However, the path length difference $(R_i - R)$ in the exponential must be approximated more accurately because of the oscillatory behavior of the exponential. To this end, we expand R and R_i in power series retaining only the two leading terms:

$$R \approx D_p + \frac{(z-H)^2}{2D_p} \, , \qquad (2.55)$$

25

$$R_i \approx D_p + \frac{(z+H)^2}{2D_p} \quad . \qquad (2.56)$$

Consequently, the path length difference $(R_i - R)$ is given approximately by

$$R_i - R \approx \frac{2zH}{D_p} \quad . \qquad (2.57)$$

Incorporating these various approximations into Equation (2.54), we obtain the following expression for $\vec{E}_i$ at field points with small elevation angles:

$$\vec{E}_i = \hat{u} \, E_o \, f(\phi) \, \frac{e^{ikR}}{R} \left[1 - e^{2ikzH/D_p} \right] \quad . \qquad (2.58)$$

The corresponding incident magnetic field $\vec{H}_i$ can be derived from Equation (2.58) by recalling that $\vec{E}$ and $\vec{H}$ have the following asymptotic relationship in the far field of a localized source (Eq. (2.19)):

$$\vec{H} = \left(\frac{\varepsilon}{\mu} \right)^{1/2} (\hat{r} \times \vec{E}) \quad . \qquad (2.59)$$

Consequently, $\vec{H}_i$ is given by

$$\vec{H}_i = \left(\frac{\varepsilon}{\mu} \right)^{1/2} E_o \, f(\phi) \, \frac{e^{ikR}}{R} \left[1 - e^{2ikzH/D_p} \right] (\hat{R} \times \hat{u}) \quad , \qquad (2.60)$$

where $\hat{R} = \vec{R}/R$ and $\vec{R} = x\hat{e}_x + y\hat{e}_y + (z-H)\hat{e}_z$. The magnetic polarization vector $(\hat{R} \times \hat{u})$ is given by

$$\hat{R} \times \hat{u} = \frac{\left[x\hat{e}_x + y\hat{e}_y + (z-H)\hat{e}_z \right]}{R} \times \frac{\left[y\hat{e}_x - x\hat{e}_y \right]}{D_p} \quad ,$$

$$\hat{R} \times \hat{u} = -\frac{D_p}{R} \hat{e}_z + (z-H) \frac{(x\hat{e}_x + y\hat{e}_y)}{RD_p} \quad . \qquad (2.61)$$

The magnitude of the second term in Equation (2.61) is $|z-H|/R \approx |z-H|/D_p$ which we are assuming is very small compared to 1. The magnitude of the first term on the other hand is

approximately equal to 1 when $D_p >> |z-H|$. Consequently $\hat{R} \times \hat{u}$ approximately equals $(-\hat{e}_z)$ for small angles of elevation. Making this approximation, Equation (2.60) can be rewritten as follows:

$$\vec{H}_i = - \hat{e}_z \left(\frac{\varepsilon}{\mu}\right)^{1/2} E_o \, f(\phi) \, \frac{e^{ikR}}{R} \left[1 - e^{2ikzH/D_p}\right] . \quad (2.62)$$

It will be assumed that for any point on the vertical wall, $D_p >> |z-H|$ so that Equation (2.62) can be used to accurately describe the variation of $\vec{H}_i$ over the surface of the scatterer.

The length and height of the vertical wall depicted in Figure 2.5 will be denoted by L and h respectively. The coordinates of the midpoint of the base of the wall will be deonoted by (x_1, y_1, o). If

$$D_{p1} = \sqrt{x_1^2 + y_1^2}$$

is much greater than L, then the angle subtended by the wall at the origin of coordinates will be very small. Assuming that this is the case, $f(\phi)$ in Equation (2.62) can be replaced by $f(\psi)$ where $\psi = \tan^{-1}(y_1/x_1)$ to a very good approximation. In other words, we can ignore the variation of the horizontal antenna pattern over the surface of the wall when $D_{p1} >> L$, assuming of course the $f(\phi)$ does not vary too rapidly with ϕ.

Let R_1 denote the distance from the antenna to the mid point of the base of the wall:

$$R_1 = \sqrt{x_1^2 + y_1^2 + H^2} \quad (2.63)$$

When R_1 is much greater than the dimensions of the wall, the distance R from the antenna to any point P on the wall can be represented approximately as follows:

$$R = R_1 + \hat{R}_1 \cdot \vec{r} \quad (2.64)$$

where $\hat{R}_1 = \vec{R}_1/R_1$, $\vec{R}_1 = x_1\hat{e}_x + y_1\hat{e}_y - H\hat{e}_z$, and $\vec{r}$ is a vector in the plane of the wall drawn from the mid point of the base to the point P. Equation (2.64) results from expanding $R = |\vec{R}_1 + \vec{r}|$ to terms of first

27

order in r. Let $\hat{\eta}$ denote a unit vector parallel to the wall and parallel to the x-y plane (Figure 2.5). Using the point $(x_1, y_1, 0)$ as a new origin of coordinates, the vector $\vec{r}$ can be represented as follows:

$$\vec{r} = \eta\, \hat{\eta} + z\, \hat{e}_z \quad , \tag{2.65}$$

where η is variable ranging from $-L/2$ to $+L/2$ and z is just the elevation of the point P on the wall above the ground. The vector $\hat{\eta}$ can be expressed in terms of $\hat{e}_x$ and $\hat{e}_y$ as follows:

$$\hat{\eta} = \cos\theta\, \hat{e}_x - \sin\theta\, \hat{e}_y \tag{2.66}$$

where θ is the angle between $\hat{\eta}$ and the x-axis (Figure 2.5). Substituting (2.66) in (2.65), we obtain the following expression for r:

$$\vec{r} = \eta \cos\theta\, \hat{e}_x - \eta \sin\theta\, \hat{e}_y + z\, \hat{e}_z \quad . \tag{2.67}$$

The path length difference $\hat{R}_1 \cdot \vec{r}$ can now be calculated:

$$\hat{R}_1 \cdot \vec{r} = \eta \left(\frac{x_1}{R_1} \cos\theta - \frac{y_1}{R_1} \sin\theta \right) - \frac{zH}{R_1} \quad . \tag{2.68}$$

Since $R_1 \approx D_{pl}$ ($H \ll D_{pl}$), $x_1/R_1 \approx x_1/D_{pl} = \cos\psi$ and $y_1/R_1 \approx y_1/D_{pl} = \sin\psi$. Making these approximations, Equation (2.68) becomes:

$$\hat{R}_1 \cdot \vec{r} = \eta \cos(\theta + \psi) - \frac{zH}{D_{pl}} \quad . \tag{2.69}$$

Substituting Equation (2.69) into Equation (2.64), we obtain the following approximate expression for the distance R:

$$R = R_1 + \eta \cos(\theta + \psi) - \frac{zH}{D_{pl}} \quad . \tag{2.70}$$

In the denominator of Equation (2.62) R can be simply replaced by R_1 and in the factor $[1 - e^{2ikzH/D_p}]$, D_p can be replaced by D_{pl}. Incorporating all of these approximations into Equation (2.62), we obtain the following expression for $\vec{H}_i$ on the surface of the wall:

28

$$\vec{H}_i = \hat{e}_z \left(\frac{\varepsilon}{\mu}\right)^{1/2} E_o \, f(\psi) \, \frac{e^{ikR_1}}{R_1} \, e^{ikn\cos(\theta+\psi)} \cdot \left[2i \, \sin \, k\left(\frac{zH}{D_{p1}}\right)\right]$$

$$(2.71)$$

The expression for $\vec{H}_i$ given in Equation (2.71) can now be substituted into Equation (2.48) to calculate the scattered electric field $\vec{E}_s$ produced by the wall. The origin of coordinates for this integration will be the mid point of the base of the wall (x_1, y_1, o).

Equation (2.48) is reproduced here for ease of reference

$$\vec{E}_s(\vec{r}') = \frac{ik}{2\pi} \left(\frac{\mu}{\varepsilon}\right)^{1/2} \frac{e^{ikr'}}{r'} \cdot \hat{r}' \times \left[\hat{r}' \times \int_{S_+} (\hat{n} \times \vec{H}_i) \, e^{-ik(\hat{r}' \cdot \vec{r})} \, ds.\right]$$

$$(2.48)$$

The unit normal vector $\hat{n}$ points <u>into</u> S_+ (Figure 2.5). In terms of the unit vectors $\hat{e}_x$, $\hat{e}_y$, and $\hat{e}_z$, $\hat{n}$ is given by

$$\hat{n} = \sin \, \theta \, \hat{e}_x + \cos \, \theta \, \hat{e}_y \qquad (2.72)$$

Clearly, $\hat{n} \times \hat{H}_i$ is parallel to $\hat{n}$ since $\vec{H}_i$ is parallel to $\hat{e}_z$ (Eq. (2.71)).

The vector $\vec{r}'$ is drawn from the point (x_1, y_1, o) to the observation point which is of course the location of the receiving antenna on the aircraft. Let x_2, y_2, z_2 denote the coordinates of the receiver relative to the x, y, and z axes respectively. Then $\vec{r}'$ is given by

$$\vec{r}' = (x_2-x_1) \, \hat{e}_x + (y_2-y_1) \, \hat{e}_y + z_2 \, \hat{e}_z \, . \qquad (2.73)$$

The magnitude r' of the vector $\vec{r}'$ is denoted by R_2:

$$r' \equiv R_2 = \sqrt{(x_2-x_1)^2 + (y_2-y_1)^2 + z_2^2} \qquad (2.74)$$

The horizontal distance of the receiver from the point (x_1, y_1, o) is denoted by D_{p2}:

$$D_{p2} = \sqrt{(x_2-x_1)^2 + (y_2-y_1)^2} \quad . \qquad (2.75)$$

It is assumed that the elevation angle of $\vec{r}'$ is very small. That is to say, it is assumed that $D_{p2} \gg z_2$. The phase term $\hat{r}' \cdot \vec{r}$ appearing in the integral in Equation (2.48) is given by

$$\hat{r}' \cdot \vec{r} = \eta \cos \theta \frac{(x_2 - x_1)}{R_2} - \eta \sin \theta \frac{(y_2 - y_1)}{R_2} + \frac{z\, z_2}{R_2} \quad , \qquad (2.76)$$

where use has been made of Equation (2.67). Since $D_{p2} \gg z_2$, $D_{p2} \approx R_2$. Consequently, the following approximate relationships hold:

$$\frac{(x_2 - x_1)}{R_2} \approx \frac{(x_2 - x_1)}{D_{p2}} = \cos \gamma$$

$$\frac{(y_2 - y_1)}{R_2} \approx \frac{(y_2 - y_1)}{D_{p2}} = -\sin \gamma \quad , \qquad (2.77)$$

where γ is the angle between the projection of the vector $\vec{r}'$ onto the x-y plane and the x-axis (Fig. 2.5). Consequently, Equation (2.76) can be rewritten as follows:

$$\hat{r}' \cdot \vec{r} = \eta \cos (\gamma - \theta) + \frac{z\, z_2}{D_{p2}} \quad . \qquad (2.78)$$

The integral in Equation (2.48) can now be evaluated quite easily. It should be noted that the range of integration of the variable z is $-h \leq z \leq +h$. This range of integration must be used in order to take into account the image of the wall in the ground plane. Carrying out the integrations in η ($-L/2 \leq \eta \leq +L/2$) and z ($-h \leq z \leq +h$), we obtain the following expression for the total scattered field $\vec{E}_s$ (direct plus ground reflected):

$$\vec{E}_s = (\hat{r}' \times (\hat{r}' \times \hat{n}))\, i\, \frac{kLh}{\pi}\, E_o\, f(\phi)\, \frac{e^{ik(R_1 + R_2)}}{R_1 R_2} \cdot \text{sinc}\left[\frac{kL}{2}(\cos(\theta + \phi) - \cos(\gamma - \theta))\right]$$

$$\cdot \left\{ \text{sinc}\left[kh\left[\frac{H}{D_{p1}} - \frac{z_2}{D_{p2}}\right]\right] - \text{sinc}\left[kh\left[\frac{H}{D_{p1}} + \frac{z_2}{D_{p2}}\right]\right] \right\} \quad . \qquad (2.79)$$

30

where $\text{sinc}(x) = \sin x / x$.

For the low angles of elevation which we are assuming, the triple vector product $\hat{r}' \times (\hat{r}' \times \hat{\eta})$ can be simplified greatly. We first expand the triple vector product as follows:

$$\hat{r}' \times (\hat{r}' \times \hat{\eta}) = (\hat{r}' \cdot \hat{\eta}) \hat{r}' - \hat{\eta} \tag{2.80}$$

The unit vector $\hat{r}'$ is given by

$$\hat{r}' = \frac{(x_2 - x_1)}{R_2} \hat{e}_x + \frac{(y_2 - y_1)}{R_2} \hat{e}_y + \frac{z_2}{R_2} \hat{e}_z \quad . \tag{2.81}$$

For small angles of elevation ($R_2 \approx D_{p2} \gg z_2$), we can ignore the z-component of $\hat{r}'$ and use Equation (2.77) to obtain the following expression for $\hat{r}'$.

$$\hat{r}' \approx \cos \gamma \, \hat{e}_x - \sin \gamma \, \hat{e}_y \tag{2.82}$$

Consequently, $\hat{r}' \cdot \hat{\eta} \approx \cos\theta \cos\gamma + \sin\theta \sin\gamma = \cos(\gamma - \theta)$ (Eq. (2.66)). Making these approximations in Equation (2.80), we obtain the following approximate expression for the polarization vector $\hat{r}' \times (\hat{r}' \times \hat{\eta})$:

$$\hat{r}' \times (\hat{r}' \times \hat{\eta}) = -\sin(\gamma - \theta) \left[\sin \gamma \, \hat{e}_x + \cos \gamma \, \hat{e}_y \right] \tag{2.83}$$

which is of course parallel to the ground plane. The magnitude of the vector given in Equation (2.83) is just $\sin(\gamma - \theta)$. Consequently, the magnitude of the scattered field is given by

$$E_s = \frac{ikLh}{\pi}(E_o f(\psi)) \frac{e^{ik(R_1 + R_2)}}{R_1 R_2} \sin(\gamma - \theta) \, \text{sinc} \, \frac{kL}{2} \left[\cos(\theta + \psi) - \cos(\gamma - \theta) \right]$$

$$\cdot \left\{ \text{sinc} \left[kh \left[\frac{H}{D_{p1}} - \frac{z_2}{D_{p2}} \right] \right] - \text{sinc} \left[kh \left[\frac{H}{D_{p1}} + \frac{z_2}{D_{p2}} \right] \right] \right\} \tag{2.84}$$

For an omnidirectional receiving antenna, the expression given in Equation (2.84) is the appropriate one to use for calculating perturbations in the difference in depth of modulation.

31

2.6 COMPARISON WITH PREVIOUS WORK

The result obtained in the preceding section for the scattered electric field produced by a flat vertical wall will now be compared with the solutions to the same problem obtained by the Ohio University and I.B.M researchers.[4]

Our Equation (2.84) for E_s does not differ significantly from the expression obtained by the Ohio University group. This comes as no surprise since our methods of approach are almost identical. Their solution is somewhat simpler in that it does not contain the sinc functions which depend upon the height of the localizer antenna (H), the height of wall (h), and the height of the receiver (z_2) that appear in Equation (2.84). Instead, their expression for E_s is simply proportional to $h^3 H z_2$. The fact that the Ohio University solution has a simpler dependence upon the parameters h, H, and z_2 than does our solution is due to the fact that the Ohio University researchers used a linear approximation to describe ground reflections. Specifically, instead of multiplying the antenna field pattern by the factor $[1 - e^{2ikz/D_p}]$ to account for ground reflections (Eq. (2.58)), as we did, the Ohio University researchers multiplied the antenna field pattern by $(2kzH/D_p)$. That is, they assumed that $(2kzH/D_p) \ll 1$, and essentially expanded $[1 - e^{2ikzH/D_p}]$ in a power series in $(2kzH/D_p)$ retaining only the first two terms. They made a similar approximation to describe the reflections of the scattered fields from the ground plane. Our expression for E_s in fact reduces to the Ohio University expression if the sinc functions involving H, h, and z_2 appearing in Equation (2.84) are approximated by the first two terms in their power series expansions. In essence then, there are no fundamental differences between our treatment of the scattering problem and the Ohio University treatment.

On the other hand, the I.B.M. approach to the problem of localizer signal scattering by a vertical wall differs fundamentally from our approach and that of Ohio University. For convenience, their approach to the problem will be illustrated using our equations and notation.

For ease of reference, Equations (2.28) and (2.29) are reproduced here:

32

$$\vec{E}_s(\vec{r}') = -\frac{1}{4\pi}\int_{S_1}\left[i\omega\mu\,(\hat{n}\times\vec{H}_s)\Psi + (\hat{n}\times\vec{E}_s)\times\vec{\nabla}\Psi + (\hat{n}\cdot\vec{E}_s)\vec{\nabla}\Psi\right]ds,$$

$$\tag{2.28}$$

$$\vec{H}_s(\vec{r}') = \frac{1}{4\pi}\int_{S_1}\left[i\omega\varepsilon\,(\hat{n}\times\vec{E}_s)\Psi - (\hat{n}\times\vec{H}_s)\times\vec{\nabla}\Psi - (\hat{n}\cdot\vec{H}_s)\vec{\nabla}\Psi\right]ds .$$

$$\tag{2.29}$$

Equations (2.28) and (2.29) express the scattered fields outside a scatterer in terms of integrals of the scattered fields over the surface S_1 of the scatterer. For treating perfectly conducting scatterers, we chose to work with Equation (2.29) since the integral simplies greatly for a perfect conductor. The integral in (2.29) was first modified by adding to the right hand side of (2.29) the corresponding integral of the incident fields $\vec{E}_i$ and $\vec{H}_i$. Since the surface integral in (2.28) and (2.29) of $\vec{E}_i$ and $\vec{H}_i$ over S_1 are identically zero, the left hand side of (2.29) was unchanged by this addition and we obtained the following modified expression for $\vec{H}_s(\vec{r}')$:

$$\vec{H}_s(\vec{r}') = \frac{1}{4\pi}\int_{S_1}\left[i\omega\varepsilon\,(\hat{n}\times\vec{E})\Psi - (\hat{n}\times\vec{H})\times\vec{\nabla}\Psi - (\hat{n}\cdot\vec{H})\vec{\nabla}\Psi\right]ds, \quad (2.31)$$

where $\vec{E}$ and $\vec{H}$ are the total fields on S_1 ($\vec{E}=\vec{E}_i+\vec{E}_s$, $\vec{H}=\vec{H}_i+\vec{H}_s$). The analogous expression for the scattered electric field is:

$$\vec{E}_s(\vec{r}') = -\frac{1}{4\pi}\int_{S_1}\left[i\omega\mu\,(\hat{n}\times\vec{H})\Psi + (\hat{n}\times\vec{E})\times\vec{\nabla}\Psi + (\hat{n}\cdot\vec{E})\vec{\nabla}\Psi\right]ds \quad (2.85)$$

For a perfectly conducting scatterer, the surface S_1 is divided into an illuminated side S_+ and a shadow side S_-. On the shadow side, it is assumed as a first approximation that $\vec{E}=\vec{H}=0$ ($\vec{E}_s=-\vec{E}_i$ and $\vec{H}_s=-\vec{H}_i$ on S_-). With this approximation, the integrals in (2.31) and (2.85) are extended only over the illuminated side S_+ of S_1. That is to say, $\vec{E}_s(\vec{r}')$ and $\vec{H}_s(\vec{r}')$ are expressed in terms of surface integrals of the total fields over S_+.

33

Had we chosen to work directly ich Equations (2.28) and (2.29) rather than (2.31) and (2.85) the same result would have been obtained. For example, assuming th.. $\vec{E}_s = -\vec{E}_i$ and $\vec{H}_s = -\vec{H}_i$ on S_-, Equation (2.28) becomes:

$$\vec{E}_s(\vec{r}') = -\frac{1}{4\pi}\int_{S_+}\left[i\omega\mu(\hat{n}x\vec{H}_s)\psi + (\hat{n}x\vec{E}_s)x\vec{\nabla}\psi + (\hat{n}\cdot\vec{E}_s)\vec{\nabla}\psi\right]ds$$

$$+\frac{1}{4\pi}\int_{S_-}\left[i\omega\mu(\hat{n}x\vec{H}_i)\psi + (\hat{n}x\vec{E}_i)x\vec{\nabla}\psi + (\hat{n}\cdot\vec{E}_i)\vec{\nabla}\psi\right]ds \ .$$

$$(2.86)$$

However, we know that the surface integral of $\vec{E}_i$ and $\vec{H}_i$ over the total surface S_1 is identically zero. Consequently, the surface integral in (2.86) of $\vec{E}_i$ and $\vec{H}_i$ over S_- is the negative of the corresponding surface integral of $\vec{E}_i$ and $\vec{H}_i$ over S_+. Therefore, Equation (2.86) can be rewritten as follows:

$$\vec{E}_s(\vec{r}') = -\frac{1}{4\pi}\int_{S_+}\left[i\omega\mu(\hat{n}x\vec{H}_s)\psi + (\hat{n}x\vec{E}_s)x\vec{\nabla}\psi + (\hat{n}\cdot\vec{E}_s)\vec{\nabla}\psi\right]ds$$

$$-\frac{1}{4\pi}\int_{S_+}\left[i\omega_{-}(\hat{n}x\vec{H}_i)\psi + (\hat{n}x\vec{E}_i)x\vec{\nabla}\psi + (\hat{n}\cdot\vec{E}_i)\ \vec{\nabla}\psi\right]ds$$

$$(2.87)$$

Combining these two integrals over S_+ and recalling that $\vec{E}=\vec{E}_i+\vec{E}_s$ $\vec{H}=\vec{H}_i+\vec{H}_s$, we are left with a surface integral over S_+ of the total fields $\vec{E}$ and $\vec{H}$.

The I.B.M. researchers essentially use the same integral Equations (2.28) and (2.29) to treat the problem of localizer signal scattering. To obtain an expression for the scattered electric field produced by a vertical wall, they simply carry out the integral appearing in (2.28) over the illuminated surface of the wall. That is to say, they use the following expression for $\vec{E}_s(r')$:

$$\vec{E}_s(\vec{r}') = -\frac{1}{4\pi}\int_{S_+}\left[i\omega\mu(\hat{n}\times\vec{H}_s)\psi+(\hat{n}\times\vec{E}_s)\times\vec{\nabla}\psi+(\hat{n}\cdot\vec{E}_s)\vec{\nabla}\psi\right]ds \quad .(2.88)$$

That is to say, instead of integrating the total fields over S_+ as we did, they just integrate the scattered fields. In effect, they ignore the integral of $\vec{E}_s$ and $\vec{H}_s$ over S_-, the shadow side of S_1. Instead of setting $\vec{E}_s$ and $\vec{H}_s$ equal to $-\vec{E}_i$ and $-\vec{H}_i$ respectively on the shadow side S_-, they in effect assume that $\vec{E}_s$ and $\vec{H}_s$ are identically zero on S_- which is not true.

Comparing our result for the magnitude E_s of the scattered field produced by a vertical wall with the I.B.M. results, we find that the only real difference between the two expressions is that whereas our Equation (2.84) contains a factor $[2 \sin(\gamma-\theta)]$ to describe the horizontal field pattern of the wall, their Equation (2.43) contains a corresponding factor M_G which is given in our angle notation by:

$$M_G = \left[\sin(\theta+\psi)+\sin(\gamma-\theta)\right]\cos\left[\gamma-\psi-2\theta\right] . \quad (2.89)$$

The effects of this difference on perturbations in the difference in depth of modulation predicted by the two models can be very pronounced as can be seen in some of the accompanying comparative graphs. Figures 2.6 and 2.7 (static and dynamic) show the difference between the new and old (I.B.M.) formulations. Also, as examples of the dependence of the derogation on the building size, location and orientation, we show in Figures 2.8 to 2.18 the micro-amp deviation of a localizer V-ring signal that would be received by an aircraft flying the centerline of the runway in level flight, 50 feet above the ground as predicted by the new math model for scattering off a vertical wall.

These Cal Comp generated figures are presented here as examples of typical output obtained from the computer model and as examples of one way in which this output can be presented. In all figures the x-distance is measured from the Localizer as origin and the y-distance from the centerline of the runway.

In Figure 2.8, the microampere deviation calculated along the runway centerline caused by a 100 foot by 50 foot rectangular wall situated behind the Localizer and 470 feet from the runway center- line is shown to increase markedly as the wall is moved closer to the Localizer. This is expected as more energy is reflected back onto the runway in these cases.

Figure 2.9 shows a similar marked increase in the derogation for buildings located closer to, but in front of the Localizer.

Figures 2.10 and 2.11 show the derogation due to a larger building, 500 feet by 50 feet, which is located further from the runway centerline (1000 feet instead of 470 feet). Well beyond the Localizer in either direction, (-2000 feet or +6250 feet), there is only negligible derogation, while closer in, at -1000 feet and at +500 feet, the derogation is significant.

The explicit variation of the derogation on the building's position relative to the runway centerline is shown in Figures 2.12 and 2.13. There is a dramatic increase in the amount of derogation when the building is placed close to the runway center- line (e.g., when y=4 J feet).

Figures 2.14 and 2.15 show the derogation for different orientations of the building, both in terms of the magnitude and the location of the derogation on the runway centerline. As in- dicated in the accompanying sketches, the different locations of the derogation along the runway centerline occur because of the different specular reflection directions of the various building orientations.

Finally, in Figures 2.16-2.18, the increase in the derogation with the increase of building size is shown.
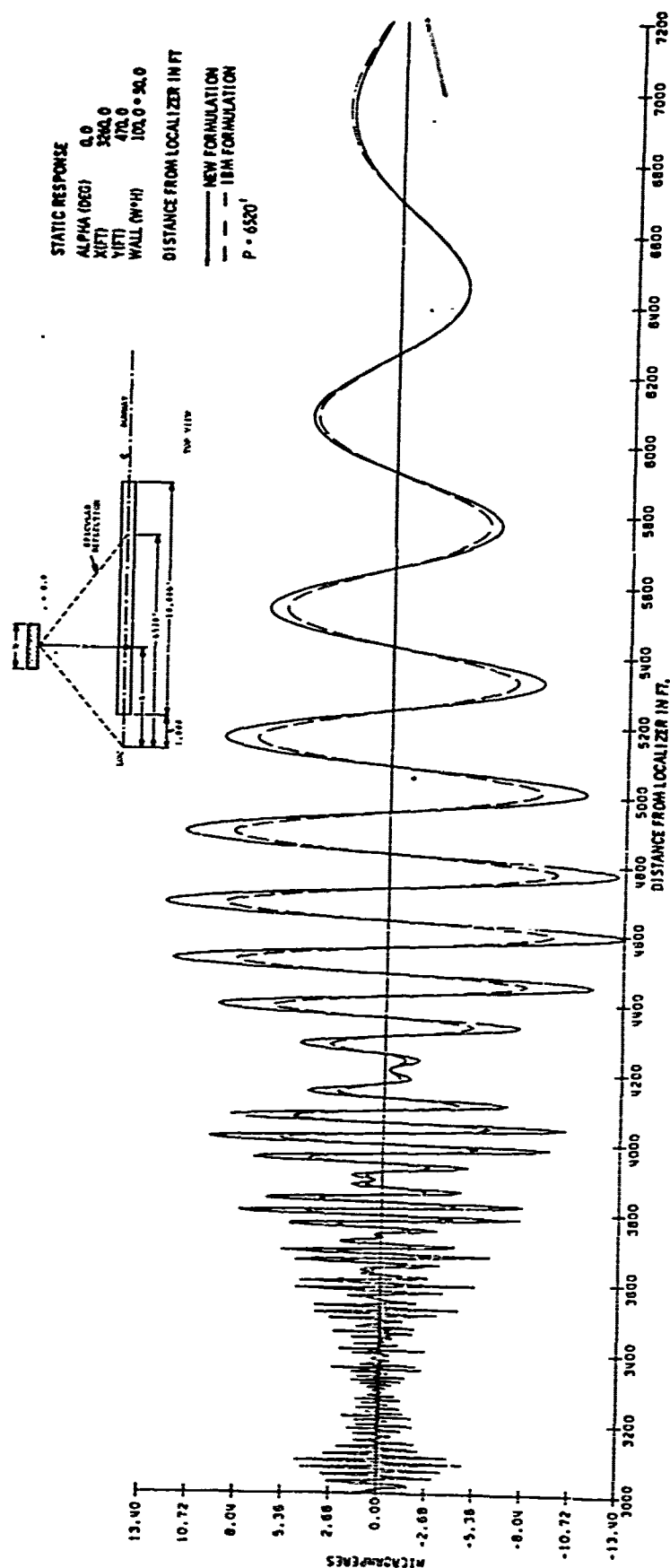
Figure 2.6. Comparison between the I.B.M. and the New Formulation, in the Static Case for a Vertical Flat Wall Parallel to the Runway

Figure 2.7. Same as Figure 2.6
Except the Dynamic Cases are
Compared
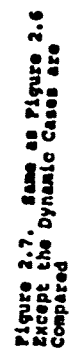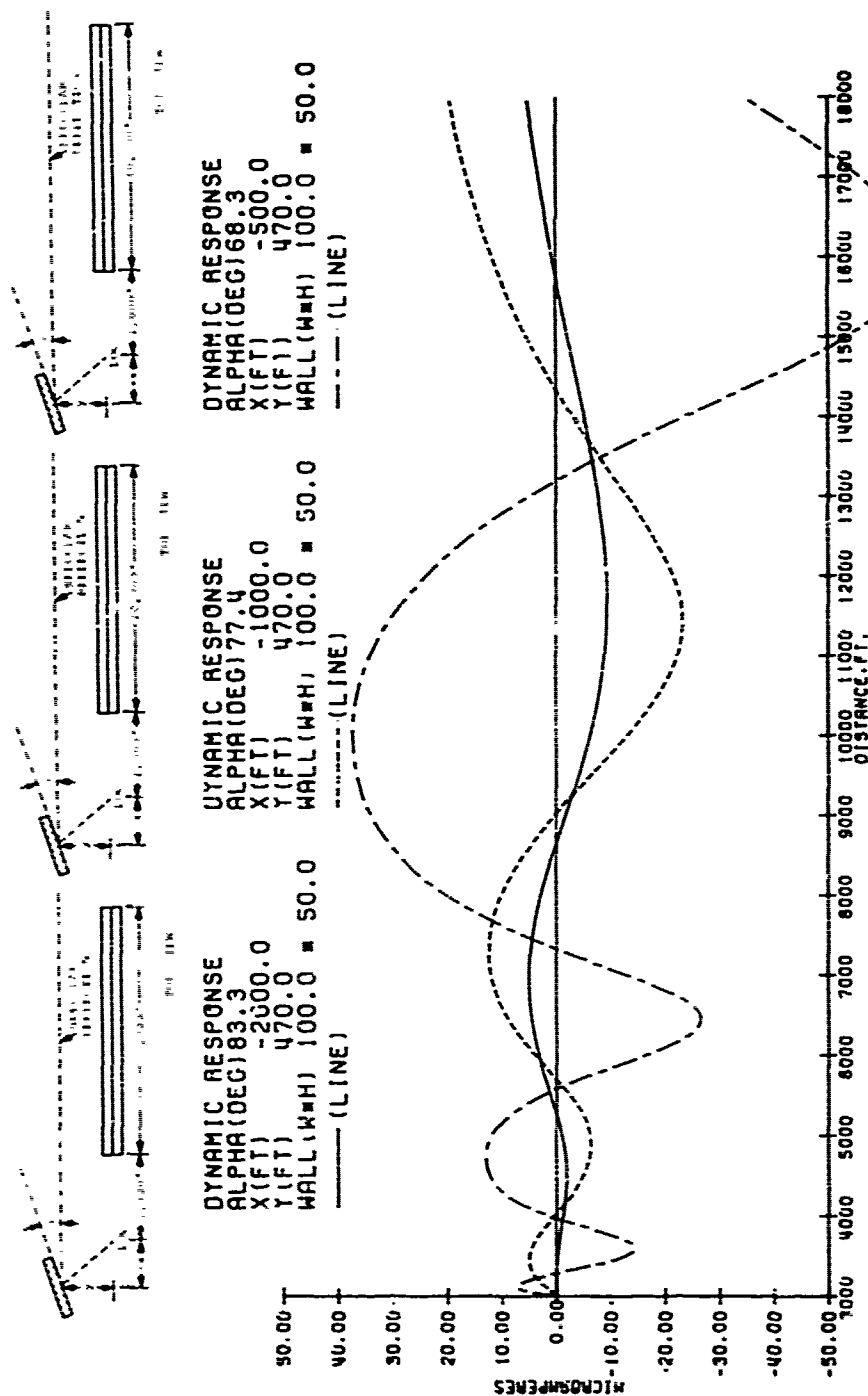
Figure 2.8. The wall's "X" position is changed from -2000ft. to -1000ft. to -500ft. while the "Y" position of 470ft. and the dimensions of the wall are held constant. The angle alpha is varied to give specular reflection parallel to the runway.

41
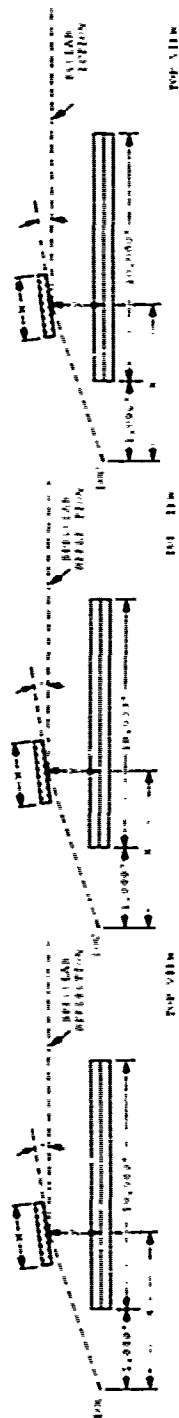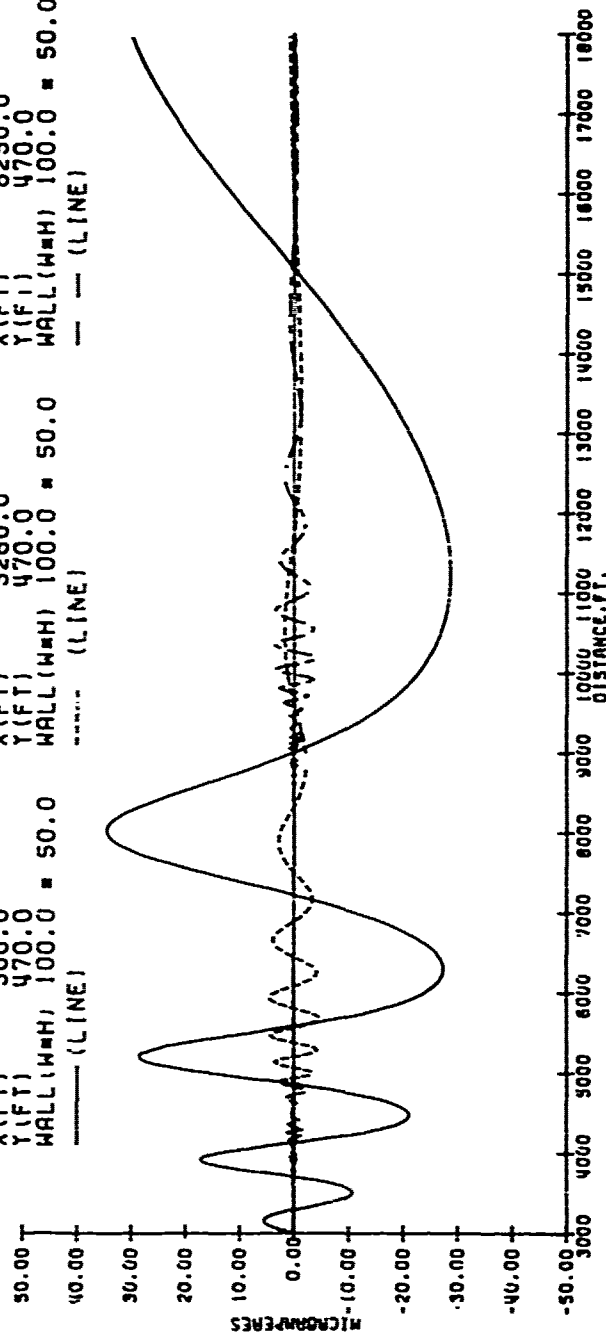
Figure 2.9. The wall's "X" position is changed from 500ft. to 3260ft. and to 8250ft. while the "Y" position of 470ft. and the dimensions of the wall are held constant. The angle alpha is selected so that specular reflection is parallel to the runway.

42
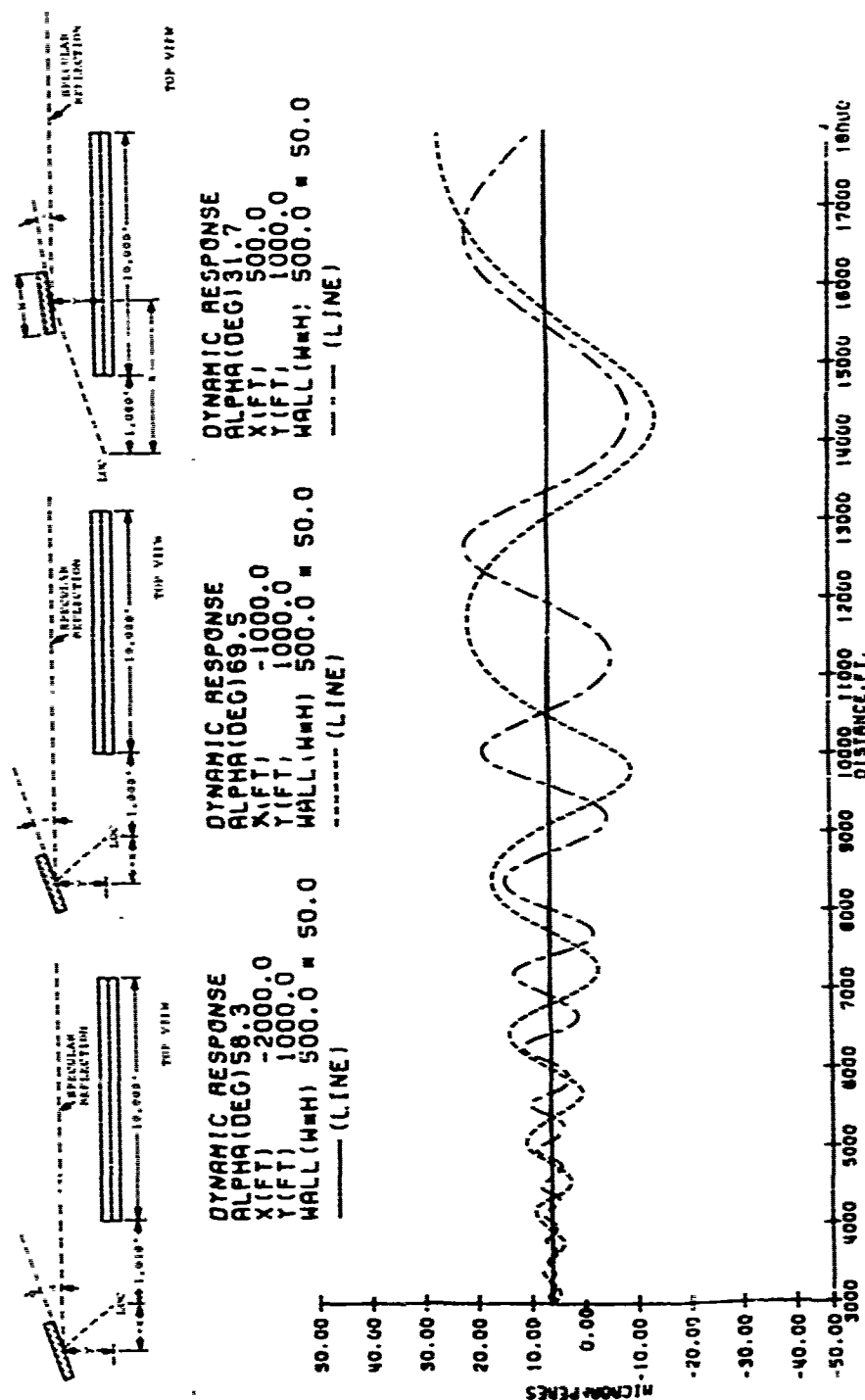
Figure 2.10. The wall's "Y" position is now 1000ft. while the walls "X" position is changed from -2000ft., to -1000 ft. and to 500ft. and the dimensions of the wall are held constant. The angle alpha is varied to give specular reflection parallel to the runway.

43

Figure 2.11. The wall's "X" position is changed from 1000ft. to 2000ft. and to 8250ft. while the "Y" position of 1000 ft. and the dimensions of the wall are held constant. The angle alpha is varied to give specular reflection parallel to the runway.

44
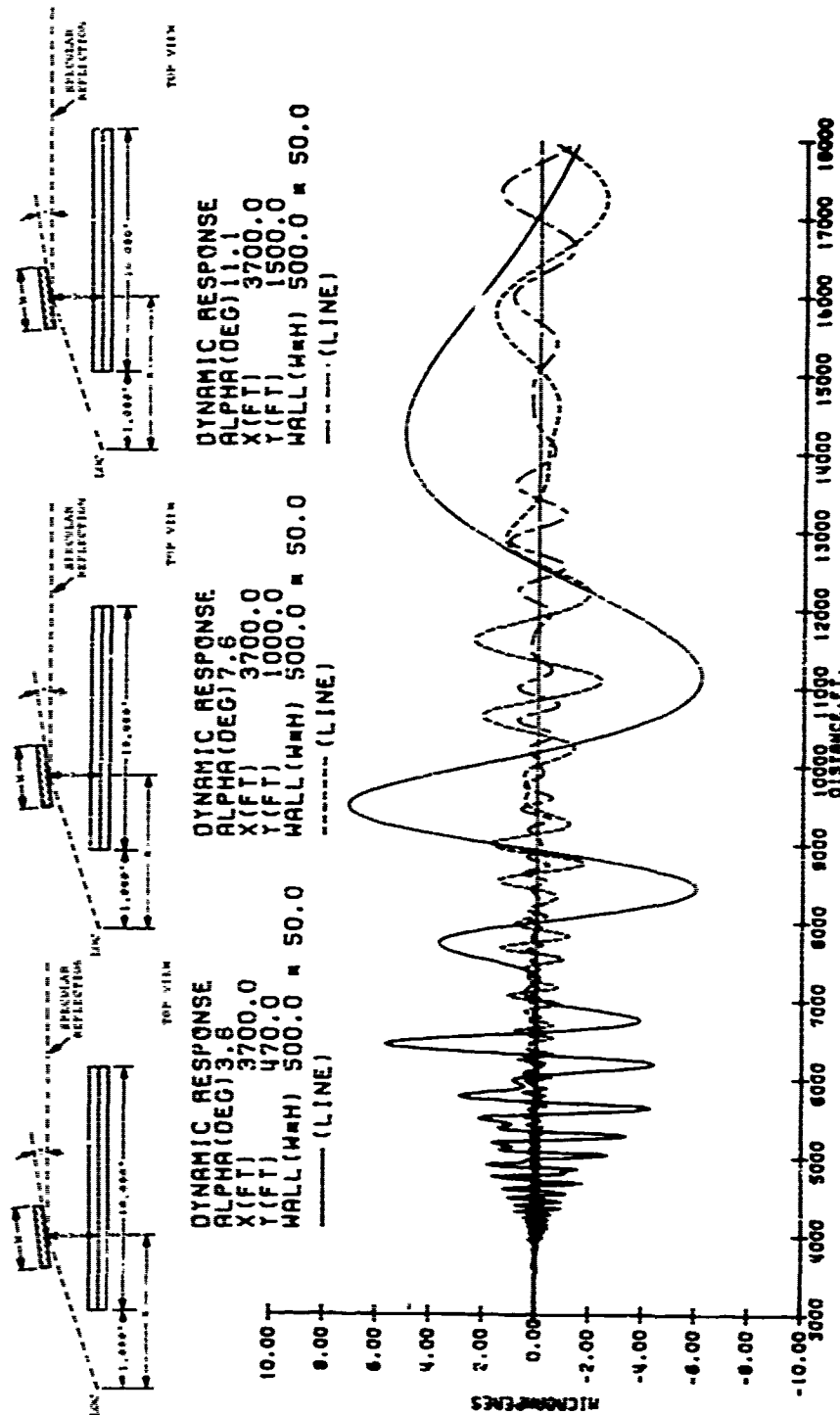
Figure 2.12. The wall's "Y" position is changed from 470ft. to 1000ft. and to 1500ft. while the "X" position and the dimensions of the wall are held constant. The angle alpha is varied to give specular reflection parallel to the runway.

45

DYNAMIC RESPONSE
ALPHA(DEG) 14.2
X(FT)   3700.0
Y(FT)   2000.0
WALL(WxH) 500.0 x 50.0
————(LINE)

DYNAMIC RESPONSE
ALPHA(DEG) 19.5
X(FT)   3700.0
Y(FT)   3000.0
WALL(WxH) 500.0 x 50.0
————(LINE)

DYNAMIC RESPONSE
ALPHA(DEG) 23.6
X(FT)   3700.0
Y(FT)   4000.0
WALL(WxH) 500.0 x 50.0
————(LINE)
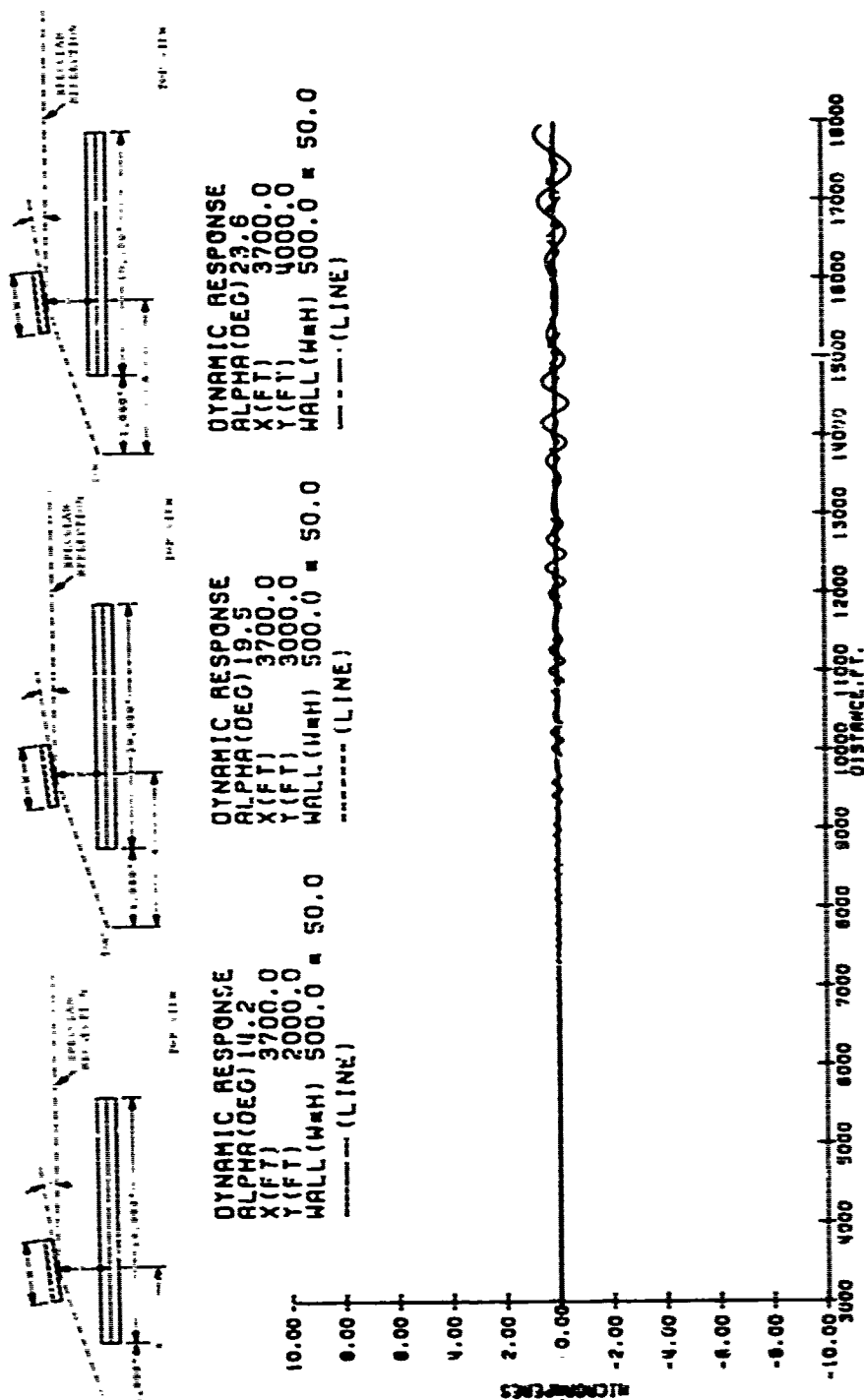
Figure 2.13.   The wall's "Y" position is changed from 2000ft. to
               3000ft. and to 4000ft. while the "X" position and
               the dimension of the wall are held constant. The
               angle alpha is varied to give specular reflection
               parallel to the runway.

46
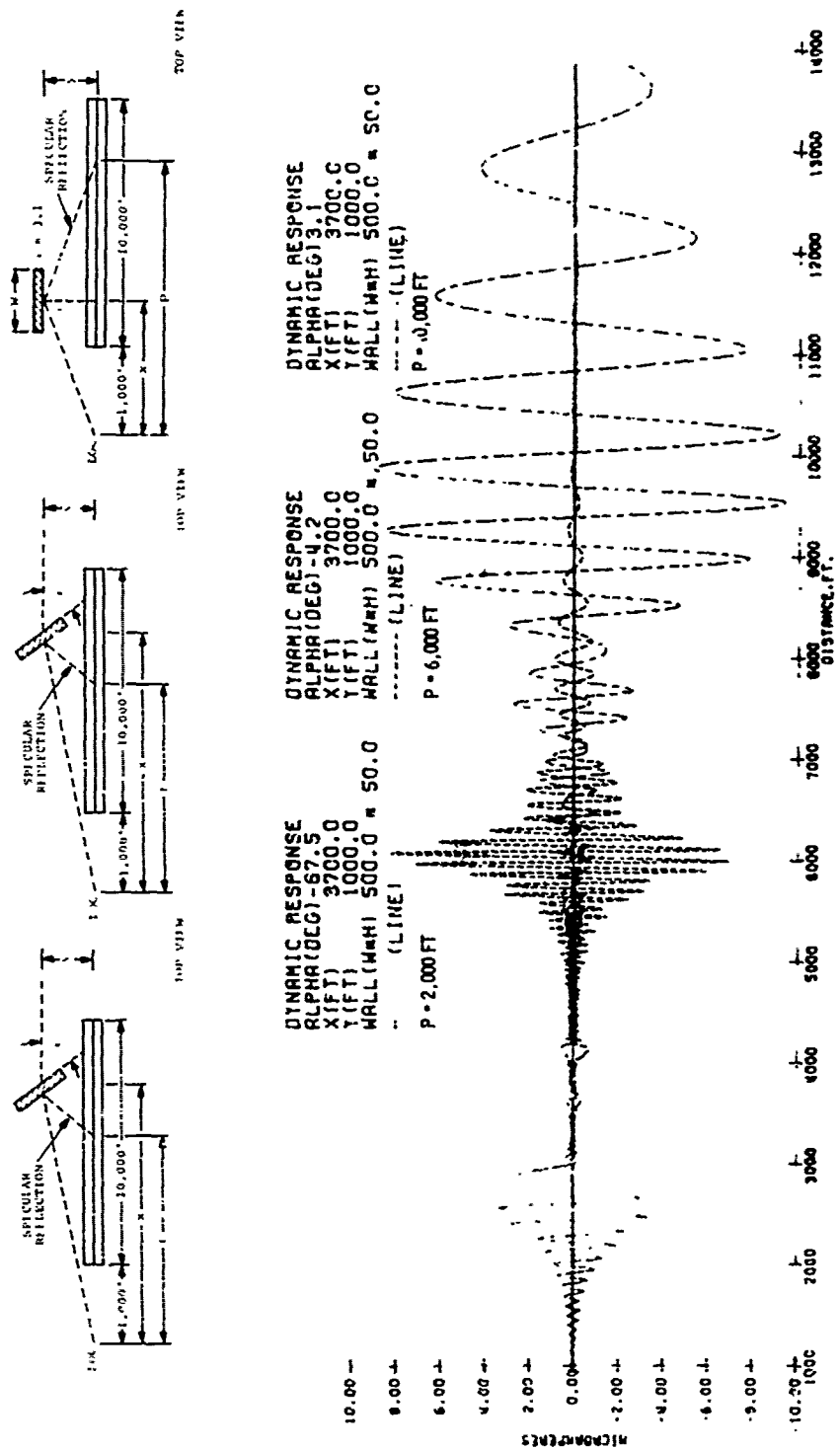
Figure 2.14. Different angles of alpha, -67.5°, -4.2° and 3.1° are used
to place specular reflection at different points along the
runway. The "x" and "y" positions and the dimensions of the
wall are held constant.

47

DYNAMIC RESPONSE
ALPHA(DEG)0.0
X(FT)   3700.0
Y(FT)   1000.0
WALL(WxH) 500.0 x 50.0
—— (LINE)

P = 7400 FT

DYNAMIC RESPONSE
ALPHA(DEG)3.1
X(FT)   3700.0
Y(FT)   1000.0
WALL(WxH) 500.0 x 50.0
—— (LINE)

P = 10,000 FT

DYNAMIC RESPONSE
ALPHA(DEG)14.0
X(FT)   3700.0
Y(FT)   1000.0
WALL(WxH) 500.0 x 50.0
— — (LINE)
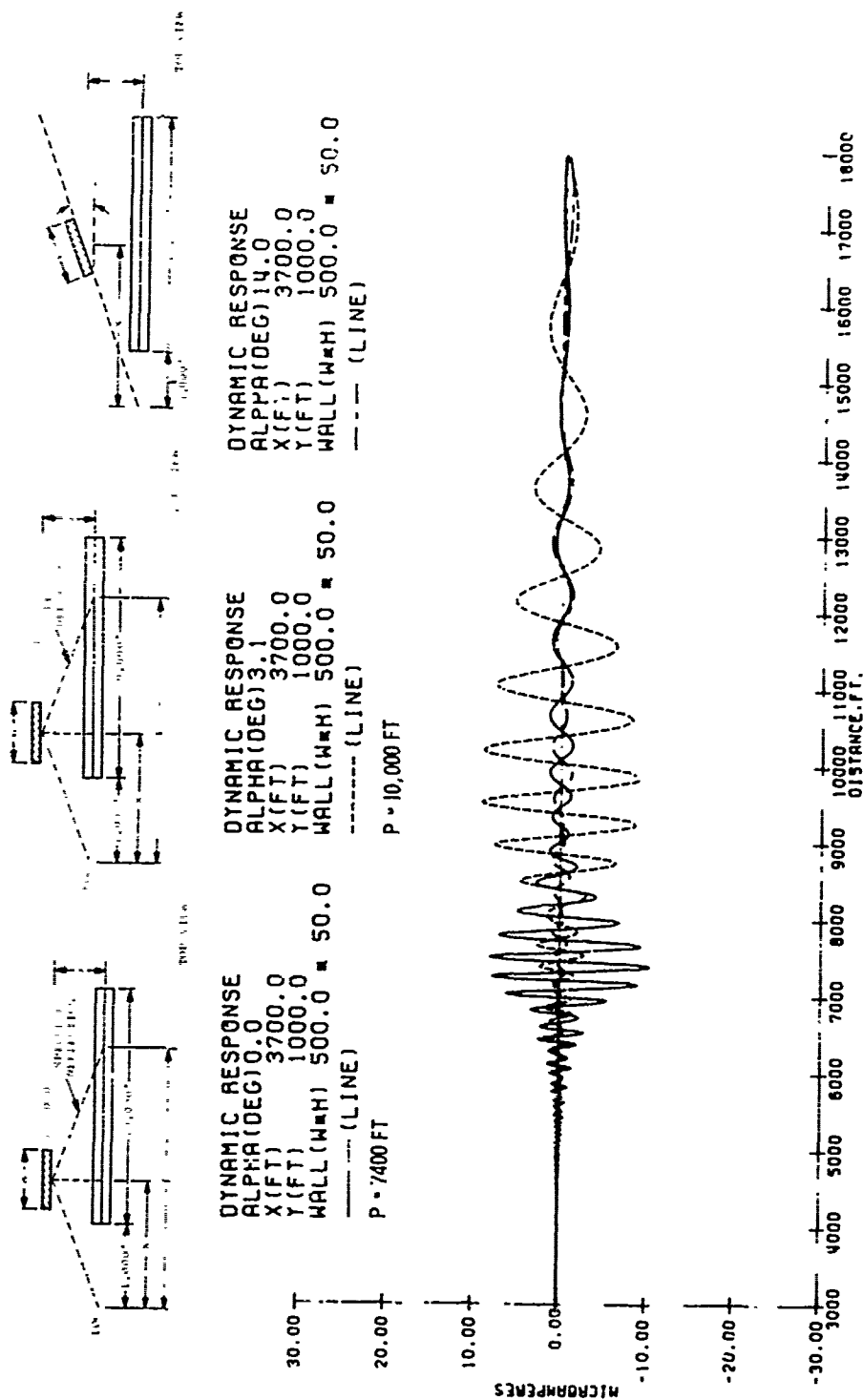
Figure 2.15. Different angles of alpha, 0.0°, 3.1° and 14.0° are used to position the specular reflection at different areas indicated by the sketch. The "x" and "y" positions and the dimensions of the wall are held constant.

48
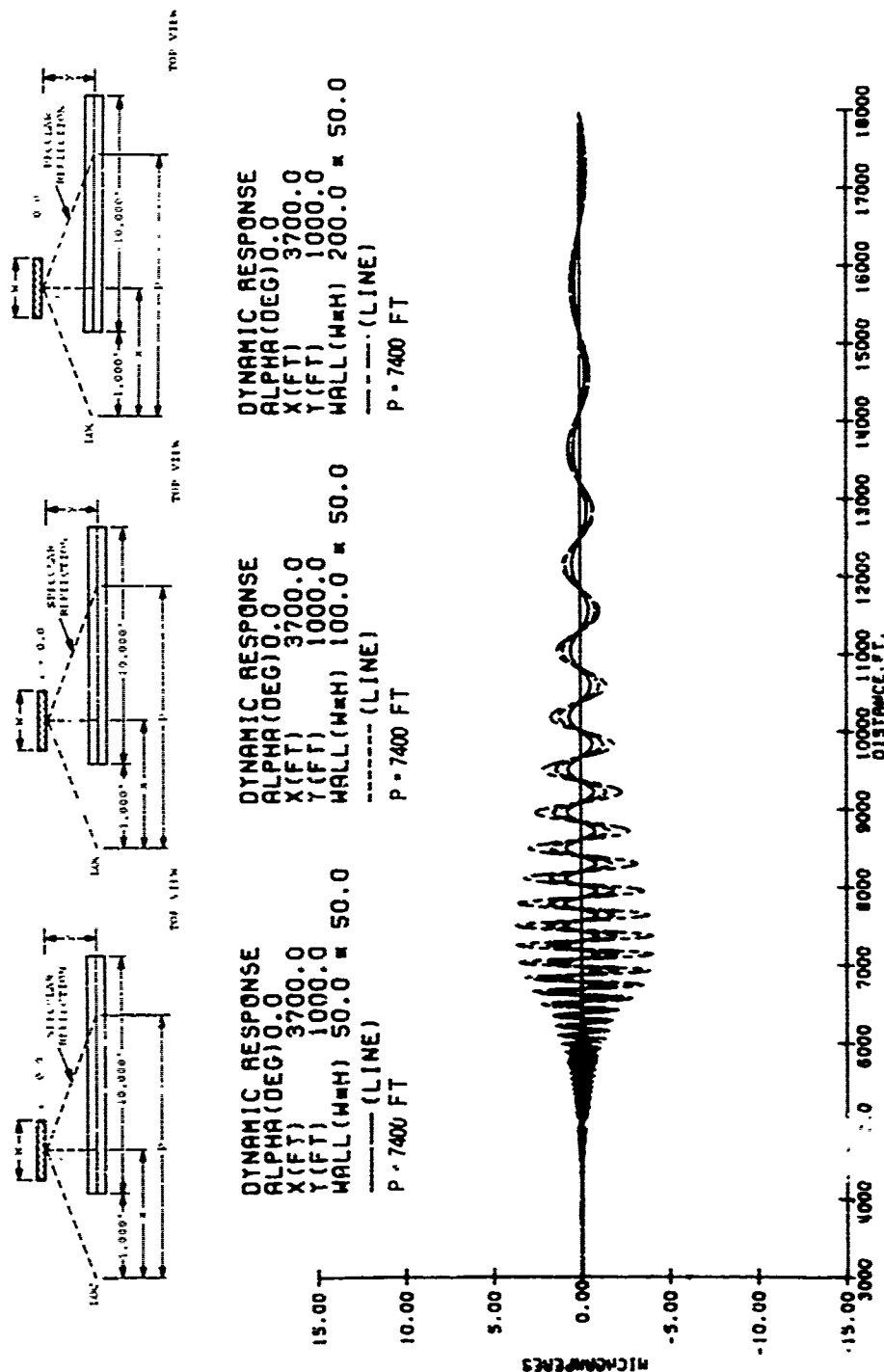
Figure 2.16. Different lengths of the wall, 50ft., 100ft. and 200ft. are used while the "X" and "Y" positions and the height of the wall are held constant.

DYNAMIC RESPONSE
ALPHA(DEG)0.0
X(FT)   3700.0
Y(FT)   1000.0
WALL(HxH) 350.0 x 50.0
——(LINE)
P = 7400 FT

DYNAMIC RESPONSE
ALPHA(DEG)0.0
X(FT)   3700.0
Y(FT)   1000.0
WALL(HxH) 600.0 x 50.0
-----(LINE)
P = 7400 FT

DYNAMIC RESPONSE
ALPHA(DEG)0.0
X(FT)   3700.0
Y(FT)   1000.0
WALL(HxH) 1000.0 x 50.0
—·—(LINE)
P = 7500 FT
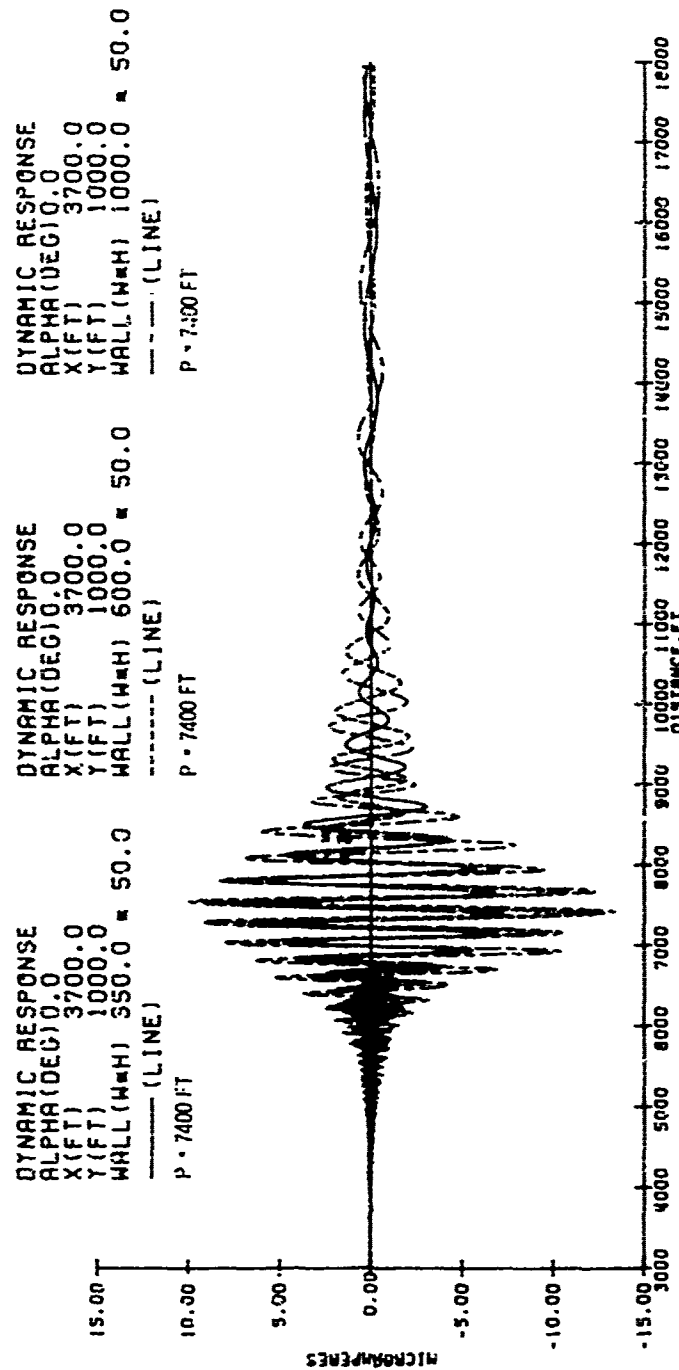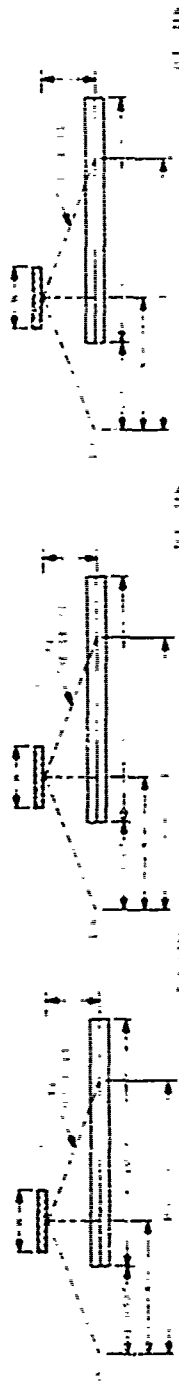
Figure 2.17.   Different lengths of the wall, 350ft., 600ft. and 1000ft. are used while the "X" and "Y" position and the height of the wall are held constant.

50

Figure 2.18. Different heights of the wall, 25ft., 60ft. and 75ft. are used while the "X" and "Y" position and the height of the wall are held constant.

51
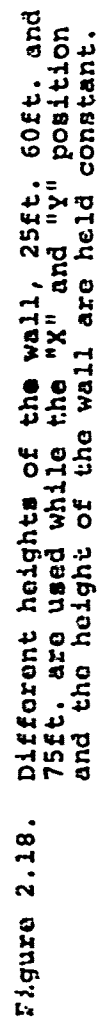
3.0 MODELING OF ILS SIGNAL DETECTION

3.1 INTRODUCTION

In implementing computer prediction of the course deviation indication (CDI) for complex derogating environments and arbitrary selection of the localizer and/or glide slope signal transmitting system, it is desirable to have a unified approach to the modeling of DDM detection by standard aircraft ILS receivers. To effectively treat any existing or future ILS system, a detection model must adequately account for systems utilizing one or two carrier frequencies, for arbitrary relative phasing between different signal components, variation of receiving antenna gain patterns and effects of aircraft speed. The models presently in use fall short of this objective. The I.B.M. code is developed only for the localizer null reference system; the Ohio glide slope programs incorporate null reference, sideband reference and capture effect, but in the latter case the auxilliary carrier signal is ignored.[5] The Ohio codes are further restricted in applicability to moderate derogations near or on the glide course centerline, and none of the foregoing models take any account of relative Doppler effects.

Below we develop a unified model of ILS signal reception that attempts to reach a higher level of completeness and correctness for actual receivers than the previously used models. In the course of the derivation, a number of approximations are inevitably taken. While it is felt that these are all reasonably justified, the overall consequences of the model should be verified by empirical data. The treatment does illuminate the relative significance for the detected ILS signal of carrier and sideband dephasing and of Doppler effects on receiver dynamic response.

3.2 RECEIVER MODEL

Localizer and glide slope signals are assumed to be detected by heterodyne AM receivers similar in basic design to the schematic diagram shown in Figure 3.1. The figure indicates generally how the 90 to 150 Hz modulations are amplified, detected, and

separated and the difference applied to one of the movements of a cross pointer indicator. The sum of the 90 and 150 Hz outputs is held constant by an AGC feedback loop, so that once calibrated, the instrument gives a faithful readout of the apparent CDI (course deviation indication) whenever the incident signal radiation exceeds a minimum level.

The guidance radiation field (localizer or glide slope) is coupled to the receiver input via an antenna which may be assumed to have specified directional and polarization characteristics. Any antenna used in practice may be treated as a linear system. This fact allows us to consider the scalar current transmitted to the receiver input load as the resultant of individual currents generated by various electromagnetic field components incident on the antenna. We shall assume that all incident component fields are transverse and harmonic, and so are adequately described by an electric vector $\vec{E}$ and a unit vector $\hat{k}$ in the direction of propagation. For a number of such component fields incident on a specified antenna, the receiver input current can be expressed in the form:

$$I_{in} = \Sigma \ I_j$$
$$= \Sigma \ \vec{g}(\hat{k}_j) \cdot \vec{E}_j \qquad (3.1)$$

where $\vec{g}(\hat{k})$ conveys both the gain and polarization characteristics of the antenna for plane waves incident in the direction $\hat{k}$.

The ILS radiation fields to be considered may be generated by multiple element antennae and/or waveguide radiators operating on one or two carrier frequencies. In every case, a number of distinct directional modulations are radiated, each in a specific spatial pattern. The separate directional waveforms are comprised of certain combinations of 90 Hz and 150 Hz amplitude modulations with prescribed carrier phases, added to unmodulated carrier in fixed ratios. The measured CDI at a particular aircraft location is based on the relative strengths of 90 Hz and 150 Hz signals detected in the resultant of all direct and scattered ILS radiation reaching the receiving antenna.
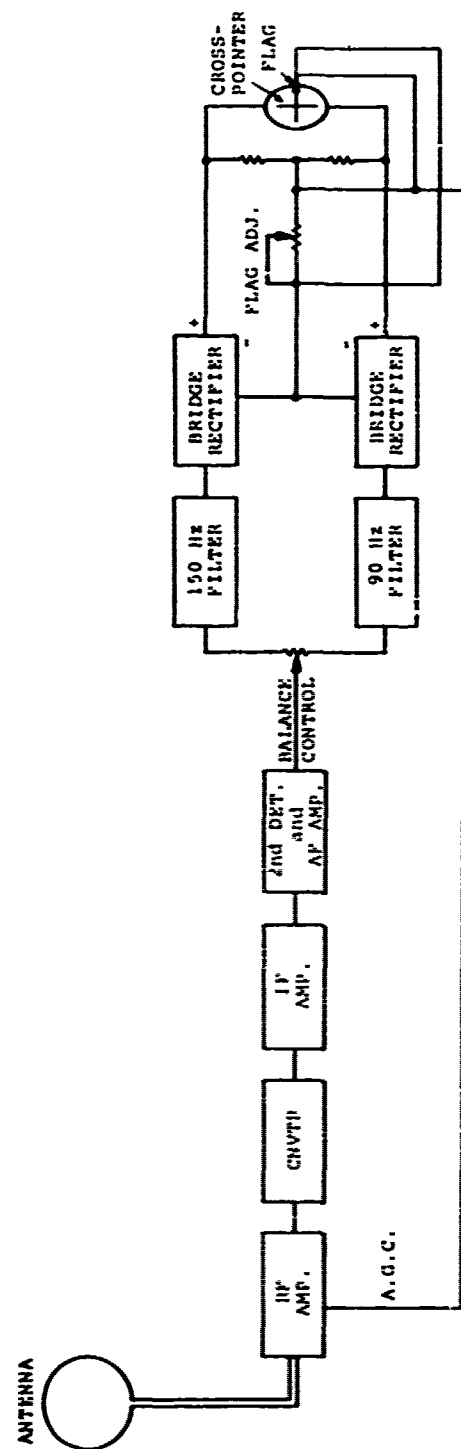
Figure 3.1. Schematic Diagram of Typical ILS Receiver

In treating the total received field numerically, we will
consider the individually computed components to represent radia-
tion travelling approximately by specific point to point paths
between the transmitting antenna and the aircraft. To each such
component field computed at the receiving antenna, there corre-
sponds a component of the amplified signal at the output of the
receiver IF stage, which can be suitably characterized, in the
most general case, by its carrier and sideband amplitudes at the
two carrier frequencies. To state this in convenient complex
rotation, we put:

$$V_{IFp}(t) = e^{-i\omega_c t + i\phi_p} \left(C_p + S_p(t)\right)$$

$$+ e^{-i\omega_c' t + i\phi_p'} \left(C_p' + S_p'(t)\right) \tag{3.2}$$

Here, ω_c and ω_c' are the primary ("course") and secondary ("clear-
ance") carrier frequencies respectively, ϕ_p and ϕ_p' are the cor-
responding phase delays for the specific propagation path denoted
by the subscript p; C_p and C_p' are the respective unmodulated car-
rier amplitudes and $S_p(t)$ and $S_p'(t)$ are the envelopes of the side-
bands-only components. Since the modulation frequencies 90 Hz and
150 Hz have a common subharmonic of 30 Hz and are always rigidly
phase-locked, each sideband envelope can be represented as a two-
term Fourier series:

$$S_p(t) = S_{p3} U_3(t) = S_{p5} U_5(t)$$

$$S_p'(t) = S_{p3}' U_3(t) + S_{p5}' U_5(t). \tag{3.3}$$

where

$$U_m(t) = \cos 60 \pi m t. \tag{3.4}$$

The terms C_p, C_p', S_{pm}, S_{pm}' include as factors the relative
strengths of the initially radiated carrier and sideband amplitudes,
the path attenuation due to field divergence, reflections, etc.,
and the gain factor for the direction of incidence on the receiving
antenna $\vec{g}(\hat{k}_p) \cdot \vec{E}_p$. The total complex IF output signal is the sum
of Equation (3.2) over all multipath modes p.

55

This is passed to the second detector which generates an audio
frequency signal

$$V_{AF}(t) = \left| \sum_p V_{IFp}(t) \right|. \tag{3.5}$$

Determination of the CDI is based on the relative amplitudes of
90 Hz and 150 Hz components found in this audio signal by passing
it through selective filters. Denoting the action of these
filters symbolically by the operators H_{90} and H_{150} (to be defined
presently), we may represent the outputs of an ILS receiver as

$$V_{90}(t) = H_{90} \ [V_{AF}(t)] \tag{3.6a}$$

$$V_{150}(t) = H_{150} \ [V_{AF}(t)]; \tag{3.6b}$$

$$CDI = s_m \frac{\overline{V_{150}} - \overline{V_{90}}}{\overline{V_{150}} + \overline{V_{90}}} \text{ microamperes} \tag{3.7}$$

In Equation (3.7) the factor s_m is the cross-pointer sensitivity
which has the standard values 387.0 for localizer (horizontal)
signals and 576.0 for glide slope (vertical) signals. The magni-
tudes $\overline{V_{150}}$ and $\overline{V_{90}}$ are obtained by rectification of the detected
modulation tone signals $V_{150}(t)$ and $V_{90}(t)$.

3.3 AUDIO SIGNAL DETECTION

3.3.1 Capture Effect

We now seek a reasonably accurate estimate of the detected
90 Hz modulations in the general multipath, capture effect situa-
tion. For this we need an expression for $V_{AF}(t)$ in the form of a
Fourier series, and we need suitable definitions of the filter
operators H_{90} and H_{150}.

It is the possible presence of many signal derogating scatter-
ers in the glidepath environment that makes analytical derivation
of $V_{AF}(t)$ from $V_{IF}(t)$ difficult. Because of the receiving air-
craft's motion, each derogating signal is received with a possibly
significant Doppler shift relative to the direct ILS transmission.

56

The consequence is that a range of frequencies may generally be present in the audio output of the second detector, instead of solely the modulation tone frequencies. The action of the 90 and 150 Hz filters on such complex signals must be considered.

Additional spurious signals occur in reception of radiation from capture effect transmitting systems near all harmonics of the 8 kHz carrier separation frequency. This fact allows a convenient reduction of the audio signal analysis problem, if the capture effect of the detector is treated first. We follow a procedure suggested in part by Manney.[6] The total IF output signal may be written as:

$$V_{IF}(t) = \left[A_1(t) + e^{i\Delta_c t} A_2(t) \right] e^{-i\omega_c t} , \qquad (3.8)$$

where:

$$A_1(t) = \sum_p (C_p + S_p) e^{i\phi_p}$$

$$A_2(t) = \sum_p (C'_p + S'_p) e^{i\phi'_p}$$

$$\Delta_c = \omega_c - \omega'_c \qquad (3.9)$$

The audio signal (Eq. (3.5)) can now be expressed as

$$V_{AF}(t) = \left[|A_1(t)|^2 + |A_2(t)|^2 + 2Re\left(A_1(t)A_2(t)^* e^{-i\Delta_c t} \right) \right]^{1/2} \qquad (3.10)$$

Now the scale of the time variation of the complex frequencies A_1 and A_2 is given by the modulation frequencies 90 Hz and 150 Hz or perhaps by the latter frequency shifted by the upper limit of observed Doppler displacement. In the worst case for glide slope signal reception, the frequency spectral range of A_1 and A_2 is certainly less than 500 Hz, which can be considered small compared to $\Delta_c/2\pi = 8$ kHz. Accordingly, we may expand the instantaneous value of $V_{AF}(t)$ in a power series in $\exp(i\Delta_c t)$, i.e.:

$$V_{AF}(t) = \sum_{-\infty}^{+\infty} V_n(t) e^{ni\Delta_c t} \qquad (3.11)$$

In this expression, because of the spectral narrowness of the factors $V_n(t)$, the term primarily contributing frequencies within the passbands of the modulation filters is $V_o(t)$. This term can be defined by averaging the expression for $V_{AF}(t)$ (Eq. (3.10)) over the phase of $\exp(i\Delta_c t)$, i.e.:

$$V_0(t) = 1/2 \int_0^{2\pi} \left[|A_1(t)|^2 + |A_2(t)|^2 + 2\mathrm{Re}(A_1 A_2^* e^{-i\psi}) \right]^{1/2} d\psi \qquad (3.12)$$

This integral is easily transformed to:

$$V_0(t) = \left[2(|A_1(t)| + |A_2(t)|)/\pi \right] \int_0^{\pi/2} (1 - k^2 \sin^2 \theta)^{1/2} d\theta \qquad (3.13)$$

where:

$$k^2 = 4|A_1(t)A_2(t)| / (|A_1(t)| + |A_2(t)|)^2$$

$$\theta = (\psi + \delta_{12})/2$$

$$e^{i\delta_{12}} = A_1 A_2^* / |A_1 A_2|$$

The integral on the right of Equation (3.13) is a complete elliptic integral of the second kind and is commonly denoted by $E(k)$:

$$E(k) = \frac{\pi}{2} \left(1 - \sum_{n=1}^{\infty} \left[\frac{(2n)!}{(2^n n!)^2} \right]^2 \frac{k^{2n}}{2n-1} \right) \qquad (3.14)$$

Thus for the purpose of determining the detected 90 and 150 Hz modulations, the unfiltered audio signal is to a good approximation

$$V_{AF}(t) \approx \frac{2}{\pi} \left(|A_1(t)| + |A_2(t)| \right) E(k) \qquad (3.15)$$

To put the above expression in usable form, we must carry the approximation somewhat further. Let the magnitude of amplitude $A_1(t)$ be the sum of a constant average value a_{01} and a zero-mean time varying function $a_1(t)$:

$$|A_1(t)| = a_{01} + a_1(t) \qquad (3.16a)$$

58

The quantity $a_1(t)$ represents the total modulation that would be detected if the second carrier were completely absent. Similarly, let

$$|A_2(t)| = a_{02} + a_2(t) \qquad (3.16b)$$

Inserting Equations (3.16) into (3.15) and treating $a_1(t)$ and $a_2(t)$ as small quantities, we obtain an expansion for V_{AF}:

$$V_{AF}(t) = a_0 \sum_{n=0}^{\infty} \sum_{p=0}^{n} \sum_{q=0}^{n} \sum_{r=0}^{\infty} \Gamma_{pqr}^n k_0^{2n} \left(\frac{a_1}{a_{01}}\right)^p \left(\frac{a_2}{a_{02}}\right)^q \left(\frac{a}{a_0}\right)^r \qquad (3.17)$$

Here:

$$a_0 = a_{01} + a_{02}$$

$$a(t) = a_1(t) + a_2(t)$$

$$k_0^2 = 4a_{01}a_{02}/a_0^2$$

$$\Gamma_{pqr}^n = 1 \; ; \; n=0, \; r=0,1$$

$$= 0 \; ; \; n=0, \; r \geq 2$$

$$= (-1)^{r+1} \frac{2n(2n)!(r+2n-2)!}{2^{4n}(n!)^2(n-p)! \; p! \; (n-q)! \; q! \; r!} \; ;$$

$$n \geq 1. \qquad (3.18)$$

After rearrangement we find that the series begins thus:

$$V_{AF}(t) = a_{01} + a_{02} + a_1(t) + a_2(t)$$

$$+ \sum_{n=1}^{\infty} \Gamma_{000}^n k_0^{2n} \left[a_{01} + a_{02} + \left(1-n\frac{a_{01}-a_{02}}{a_{01}}\right) a_1(t) \right.$$

$$+ \left(1-n\frac{a_{02}-a_{01}}{a_{02}}\right) a_2(t)$$

$$+ \left(n(n-1) \; (a_{01}-a_{02})^2/2 - na_{01}a_{02}\right)$$

$$\left. \cdot \left(a_1(t)/a_{01} - a_2(t)/a_{02}\right)^2/a_0 \right]$$

59

$$+ O(k_0^4 a^3) \tag{3.19}$$

$$\approx (a_{01} + a_{02})\ (1 - a_{01} a_{02}/a_0^2 \cdots$$

$$+ a_1(t)\ (1 - a_{02}^2/a_0^2 - \cdots$$

$$+ a_2(t)\ (1 - a_{01}^2/a_0^2 - \cdots$$

$$+ \cdots$$

Summing a finite number of the terms constant and linear in $a_1(t)$ and $a_2(t)$ gives an accurate representation of the audio signal $V_{AF}(t)$ when the parameter $k_0 \ll 1$. The convergence of the series as $k \to 1$ is not easy to discuss because the modulations of ILS transmissions are quite high (40% in the case of localizer signals, 80% for glide slope signals).

3.3.2 Decomposition of Single Carrier Envelopes

It remains to find suitable Fourier expansions for the separate carrier envelopes $A_1(t)$ and $A_2(t)$. In this section we will assume the position of the receiver to be stationary, so that the phases ϕ_p, ϕ_p' are constant. In the next section we treat Doppler effects by varying these phases.

The analysis proceeds below for $A_1(t)$ and is identical for $A_2(t)$. We have

$$A_1(t) = \left| \left(C_p + S_p(t) \right) e^{i\phi_p} \right|$$
$$= \left[\left(C + S(t) \right) \left(C^* + S^*(t) \right) \right]^{1/2}, \tag{3.20}$$

where

$$C = \sum_p C_p e^{i\phi_p} \tag{3.21}$$

$$S(t) = \sum_p S_p(t) e^{i\phi_p} \tag{3.22}$$

60

We may put:

$$C = |C| e^{i\theta_1} \tag{3.23}$$

$$S(t)e^{-i\theta_1} = X + iY , \tag{3.24}$$

and, if $|S| < |C|$, we have:

$$A_1(t) = |C|\left[1+2X/|C| + (X^2+Y^2)/|C|^2\right]^{1/2}$$

$$= |C| + X + Y^2(2|C|)^{-1}(1-X/|C| + \ldots) \tag{3.25}$$

The quantity X represents the sideband component of the received signal which is in phase (or exactly out of phase) with the unmodulated carrier. The quantity Y represents the sideband component which is in quadrature with the carrier. The nonlinear terms of Equation (3.25) may be further expanded in a series of all harmonics of the fundamental frequency 30 Hz. However, we note that the lowest order term $Y^2/(2|C|)$ contributes no correction to the 90 Hz and 150 Hz frequencies. The higher order corrections will be considered unimportant for the present application. Thus in the notation used above, we have

$$a_{01} = |C| \tag{3.26}$$

$$a_1(t) = \sum_p \left(S_{p3}U_3(t) + S_{p5}U_5(t)\right)\cos(\phi_p - \theta_1)$$

$$= \sum_p \sum_m a_{m1p}U_m(t)\cos(\phi_p - \theta_1) \tag{3.27}$$

Similarly,

$$a_{02} = |C'| \tag{3.28}$$

$$a_2(t) = \sum_m \sum_p a_{m2p}U_m(t)\cos(\phi_p' - \theta_2) \tag{3.29}$$

In the above, the carrier phases are determined by

$$\theta_n = \arctan\left(\frac{\sum C_{pn}\sin\phi_{pn}}{\sum_p C_{pn}\cos\phi_{pn}}\right) , \tag{3.30}$$

where

$$(C_{p1}, \phi_{p1}) \text{ correspond to } (C_p, \phi_p)$$

and

$$(C_{p2}, \phi_{p2}) \text{ correspond to } (C_p', \phi_p').$$

3.3.3 Doppler Effects

As a landing aircraft moves there are relative changes in the phases of the various multipath radiation components of the ILS signals received. The amplitudes of the 90 Hz and 150 Hz terms of the detected modulation thus vary with time, and accordingly, each tone acqui s a frequency spread. Since the relative Doppler frequency between direct and s-attered radiation can be as much as 120 Hz in some cases for typical landing approach speeds, the bandwidth of the modulation filters becomes important in determining receiver dynamic response. The effect envisioned here is that certain greatly Doppler shifted signal components may either be severely damped by one filter or unexpectedly passed by the other depending on the circumstances of receiver design, aircraft speed, etc. This is independent of the intentional RC damping that is always introduced into the cross pointer indicator circuits.

To evaluate the possible magnitudes of such phenomena, we consider a particularly simple model for the frequency response of each modulation filter. Though the characteristics of this filter may differ markedly from those of filters in actual receivers, the model is adequate for studying the general effect of filter bandwidth on receiver rejection of ILS interference.

The two detected tones which emerge from the modulation filters were earlier denoted by $V_{90}(t)$ and $V_{150}(t)$ (Eq. (3.6)). We now define these more precisely: Let

$$V_{90 \atop (150)}(t) = \int_0^\infty h_{90 \atop (150)}(\tau) \, V_{AF}(t-\tau)d\tau, \tag{3.31}$$

where $h_f(\tau)$ is the impulse response function of a narrowband filter corresponding to center frequency f. Following Middleton[7], we

62

represent the narrowband filter by the response function

$$h_f(\tau) = h_0(\tau)\cos(2\pi f\tau + \psi) \qquad (3.32)$$

and we select as the particular "window function"

$$h_0(\tau) = 2/T \quad 0 < \tau < T$$

$$= 0 \quad \text{otherwise.} \qquad (3.32a)$$

The output of such a filter when driven by a sinusoidal input
$A\cos(2\pi f_\ell t + \delta_\ell)$ is approximately

$$V_f(t) \simeq (A/2)\operatorname{sinc}(\pi(f-f_\ell)T) \quad .$$

$$\cos[2\pi ft + \delta_\ell + \psi + 2\pi(f_\ell - f)(t = T/2)] \qquad (3.33)$$

whenever $f + f_\ell >> T^{-1}$. The reciprocal of the intergration time T is
the nominal filter bandwidth. The phase ψ is purely additive and
so may be dropped without loss of generality. For brevity we will
put

$$H_0(f) = \operatorname{sinc}(\pi fT).$$

To derive results pertaining to the ILS audio signal (Eq. 3.5)
from Equation 3.33, we assume that the phase shifts of individual
multipath components due to aircraft motion lead to sinusoidal
time variations, and we will neglect the time variation of ampli-
tude coefficients. To this end we may write Equation (3.19) as

$$V_{AF}(t) = B_0(a_{01} + a_{02}) + B_1 a_1(t) + B_2 a_2(t) \qquad (3.34)$$

where the B's can be defined in terms of slowly varying amplitudes
that will be considered constant and the a's (as defined by Equa-
tions (3.26) through (3.30)) will contain typical terms such as:

$$a_{mnp} U_m(t)\cos(\phi_{np} - \theta_n) = 1/2\, a_{mnp}(\cos(60\pi mt + \phi_{np}(t) - \theta_n(t))$$

$$+ \cos(60\pi mt - \phi_n(t) + \theta_n(t))) \qquad (3.35)$$

This form shows that for each multipath component the audio modula-
tion frequencies are modified by sum and difference combinations
with the relative Doppler frequency $d/dt(\phi_{np} - \theta_n)$. Considering all

63

combinations of input modulation frequency and Doppler shift which
may give net frequencies near the filter center frequencies f, we
find the following significant terms in the filter outputs $V_f(t)$
(notation will be detailed below):

1. The average carrier level received by paths with *large*
   Doppler shifts gives rise to a contribution from each
   filter

$$B_0 \sum_m \sum_p a_{onp} H_0 \{f+(\dot{\phi}_{np}-\dot{\theta}_n)/2\pi\} \cos(2\pi fT/2+\theta_n-\phi_{np}) \qquad (3.36)$$

2. The modulation at one frequency modified by a *moderate*
   Doppler shift gives rise to a contribution in the output
   of the opposite frequency filter

$$1/2 \sum_n B_n \sum_p a_{mnp} H_0 (\Delta f) \cos(60\pi mt \mp (2\pi \Delta fT/2+\theta_n-\phi_{np})) \qquad (3.37)$$

   Here the upper or lower sign is taken for filter frequency
   $f = 90$ Hz or 150 Hz respectively and

$$\Delta f = |f-30_m| + (\dot{\phi}_{np}-\dot{\theta}_n)/2\pi.$$

3. In the case of equal modulation and filter frequencies
   the output contribution is

$$\sum_n B_n \sum_p A_{mnp} H_0 ((\dot{\phi}_{np}-\dot{\theta}_n)/2\pi) \cos 2\pi ft \qquad (3.38)$$

The total detected signal at each modulation frequency f is
the sum of the contributions 1, 2, and 3. It may be noted that
only the phase of 3 is well defined in relation to the phase of
the transmitted modulation. This confronts us with the final
problem of this development: we must calculate the rectified
signal derived from each $V_f(t)$ which is passed directly to the
cockpit panel instruments to generate the CDI display. A reason-
able approximation can be reached by assuming the relative phases
of contributions 1, 2, and 3 to be random and defining the final
ILS signals as being the r.m.s. envelope of the $V_f(t)$ obtained
above. We thus arrive at the final formula:

64

$$V_f = \left[B_0^2 \sum \sum a_{mnp}^2 H_0(f + (\dot{\phi}_{np} - \dot{\theta}_n)/2\pi)^2 \Big|_{m=0} \right.$$

$$+ 1/4 \sum_{n=1}^{2} B_n^2 \sum_p a_{mnp}^2 H_0(f - 30_m \pm (\dot{\phi}_{np} - \dot{\theta}_n)/2\pi)^2 \Big|_{f \neq 30m > 0}$$

$$\left. + \left(\sum_{n=1}^{2} B_n \sum_p a_{mnp} \cos(\dot{\phi}_{np} - \dot{\theta}_n) H_0((\dot{\phi}_{np} - \dot{\theta}_n)/2\pi) \right)^2 \Big|_{f = 30m} \right]^{1/2}$$

<div align="right">(3.39)</div>

Again the upper and lower signs refer to filter frequencies of 90
Hz and 150 Hz respectively. As a practical consideration, each of
the terms of Equation (3.39) can be accumulated as the individual
path attenuation factors a_{mp} are calculated, except for the co-
efficients B_0, B_n^2 and B_n, the reference phases θ_n and Doppler fre-
quencies $\dot{\theta}_n$. To facilitate this method of computation we adopt
the approximation

$$\dot{\theta}_n = 2\pi \frac{dR}{dt}/\lambda, \tag{3.40}$$

where R is the instantaneous range of the receiving aircraft to
the transmitting antenna and λ is the carrier wavelength. The
remaining notation of Equation (3.39) is explained in the following
tabulation:

f   = modulation filter frequency 90 Hz or 150 Hz.

m   = transmitted harmonic of 30 Hz; m=3 for 9C Hz, m=5 for
      150 Hz, m=0 for constant or unmodulated carrier terms.

ϕ_{np} = phase delay of a particular transmission path to the
      receiving antenna.

$\dot{\phi}_{np}$ = time derivative of ϕ_{np}.

θ_n = approximate phase of the aggregate of direct and reflected
      carrier amplitudes at the receiver relative to the trans-
      mitted carrier phase (defined by Equation (3.30)). For
      course signal n=1 and for clearance signal n=2.

a_{mnp} = carrier (m=0) or modulation (m=3,5) amplitude component in the received audio signal due to transmission by path p on the course (n=1) or clearance (n=2) carrier.

$$B_0 = \sum_{n=0}^{\infty} r^n_{000} k_0^{2n}$$

$$B_1 = \sum_{n=0}^{\infty} r^n_{000} k_0^{2n} [1-n(a_{01}-a_{02})/a_{01}]$$

$$B_2 = \sum_{n=0}^{\infty} r^n_{000} k_0^{2n} [1-n(a_{02}-a_{01})/a_{02}]$$

r^n_{000}, k_0^2 = special coefficients (defined in Equation (3.18).

The quantities V_{150} and V_{90} determined by Equation (3.39) are inserted in Equation (3.7) to obtain the undamped CDI which would be generated by a moving ILS receiver. The "dynamic" CDI, which incorporates the effect of the RC damping circuit, may be derived from the undamped CDI by the usual numerical techniques of filter simulation.

3.4 MODEL STATUS

The detection model reported here has been incorporated into a computer multipath interference simulation program which is currently under development. To this writing, all results have been consistent with expectation. Additional confirmation will be sought by comparing model predictions directly to measured receiver characteristics.

66

4.0 FORMULATION OF ELECTROMAGNETIC SCATTERING BY IMPERFECTLY CONDUCTING THIN FLAT SLABS

4.1 INTRODUCTION

Predictions of ILS signal derogation based on the assumption of perfectly reflecting scatterers have proven moderately successful in a variety of typical problem situations. Yet the validity of the perfect reflectivity assumption is open to question in situations involving sharp angles of incidence on non-metallic obstructions.

To extend our capability for predicting reflection from such structures, we develop here an approximate model of scattering applicable to flat walls or platforms of arbitrary homogeneous electrical properties. The formalism is general with respect to orientation of scattering surface and is therefore suitable for treating properly the polarization of scattered radiation. However, to avoid difficult questions about field boundary conditions on end faces and at face edges, attention is restricted to thin flat plane parallel slabs. For complex structures which may consist of a number of thin slabs in combination, the problem of multiple reflections remains inadequately treated.

4.2 DEVELOPMENT OF GREEN'S INTEGRAL

We begin with the vector Green's equation for the scattered electric field analogous to Equation (2.31):

$$\vec{E}_s(\vec{r}') = -\frac{1}{4\pi} \int_S ds\left[i\omega\mu(\hat{n}\times\vec{H})\,\psi\right.$$

$$\left. + (\hat{n}\times\vec{E}) \times \nabla\psi + (\hat{n}\cdot\vec{E})\nabla\psi\right] \tag{4.1}$$

where again $\vec{E}$ and $\vec{H}$ are total electric and magnetic fields on a closed surface S enclosing the scatterer, $\hat{n}$ is the inward normal to the surface, and

$$\psi = \exp\,(ik|\vec{r}'-\vec{r}_s|)/|\vec{r}'-\vec{r}_s| \,. \tag{4.2}$$

In the treatment of scattering by perfect conductors, the terms
in Equation (4.1) involving $\hat{n} \times \vec{E}$ and $\hat{n}\cdot\vec{E}$ are discarded on the
grounds that $\hat{n} \times \vec{E}$ vanishes at the surface and $\vec{\tau}_0$ gives only a
longitudinal field. By appeal to the Kirchoff approximation, the
total field $\vec{E}$ and $\vec{H}$ are assumed to be zero on the shadowed portion
of the surface. Consequently, for conducting surfaces, the scat-
tered field is given by an integral of the "current density" $\hat{n} \times \vec{H}$
over the illuminated surface. In the analogous treatment of
scattering by a dielectric or poorly conducting surface, the inte-
grand term $(\hat{n} \times \vec{E}) \times \vec{\tau}_0$ of Equation (4.1) must be retained and the
integration extended to the back side of the object.

Over the illuminated portion of the surface the electric
field appearing in the integrand may be identified as the sum of
the incident field $\vec{E}_i$ and a reflected field $\vec{E}_r$; over the shadowed
portion the combined incident and scattered field may be termed
the transmitted field $\vec{E}_t$. Since, in general, it is virtually
impossible to analytically determine $\vec{E}_r$ and $\vec{E}_t$ over the complete
surface, it might be supposed that this approach would be of
dubious utility in a practical scattering problem. However, we
proceed on the conjecture that perhaps many structural elements
of ILS signal interfering, buildings, hangars, etc., i.e. rein-
forced partitions, may be reasonably modeled as thin plane parallel
slabs with homogeneous electrical properties. This seems to be the
logical extension of our model for conducting surfaces.

The problem considered is that of estimating the scattered
field at a point r' remote from a thin plane parallel slab of
finite dimensions placed with arbitrary orientation in an incident
field, as shown in Figure 4.1. The illuminated face of the slab
is designated S_1, the opposite face S_2. (The peripheral surfaces
of the slab are neglected in the ensuing calculations and presumed
to contribute negligible scattering. This is the most serious
deficiency of the proposed approximation.) Positions and directions
are referred to an origin O, conveniently chosen in the vicinity
of the scatterer. The vector from this origin to a point P on the
front face S_1 is denoted by $\vec{\sigma}$; the vector to the corresponding
point on the back face designated as P' is $\vec{\sigma} + D\hat{n}$, where $\hat{n}$ is the
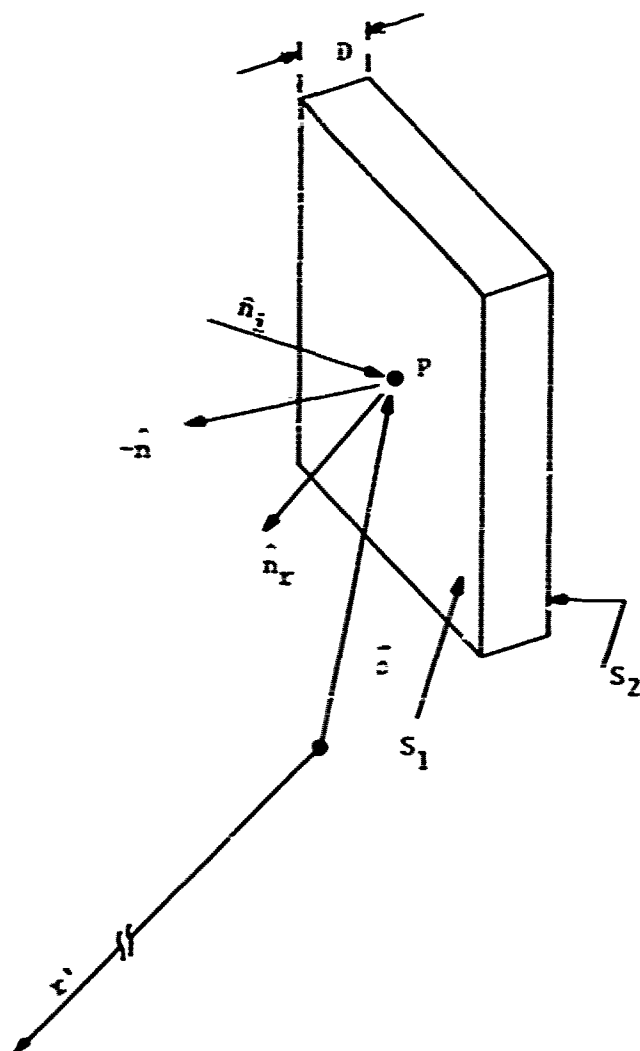
Figure 4.1. Notation for Slab Reflection Model

inward normal to surface S_1 and D is the slab thickness. The
vector $\vec{r}'$ extends from the origin to the remote field point. For
any point on S_1 or S_2 the distance from the reference origin is
always much smaller than distances to the field point. The thick-
ness of the slab D is much smaller than any other dimension.

The evaluation of the integral (4.1) over only the open sur-
faces S_1 and S_2 leads to an estimated scattered field characterized
by unphysical field discontinuities at the edges of S_1 and S_2.
These discontinuities can be compensated for by introducing elec-
tric and magnetic charge distributions on the boundary contours as
has been suggested by Stratton.[1] The resulting corrections to the
calculated field are longitudinal and accordingly may be neglected
in a far field approximation. Thus, to obtain the proper far
field estimate of the scattered field due to the contributions of
surfaces S_1 and S_2 to the integral (4.1), we find the transverse
projection of the field given by·

$$\vec{E}_s(\vec{r}') = \frac{1}{4\pi} \; \vec{r}' \times \left[\vec{r}' \times \left\{ \int_{S_1} - \int_{S_2} \right\} ds \right.$$

$$\left. \left(i\omega \, (\hat{n} \times \vec{H}) + (\hat{n} \times \vec{E}) \times \vec{\nabla}_\partial \right) \right] \tag{4.3}$$

where the difference in sign for the two integrations follows from
the fact that the inward normal to face S_2 is $-\hat{n}$.

The Green's function (4.2) and its gradient may again be
expanded according to a far field approximation:

$$\psi(|\vec{r} - \vec{\rho}|) = \psi(\vec{r}') \; e^{i\Delta(\vec{r}|\vec{\rho})} \tag{4.4}$$

$$\vec{\nabla}_\rho \psi = -ik \, \psi(r) \; e^{i\Delta(\vec{r}|\vec{\rho})} \; \hat{r} \tag{4.5}$$

$$\Delta(\vec{r}|\vec{\rho}) = - k\hat{r} \cdot \vec{\rho} + k \frac{\rho^2 - (\hat{r}\cdot\vec{\rho})^2}{2r} + \ldots \tag{4.6}$$

Here $\vec{\nabla}_p$ indicates a gradient evaluated at point P.

The total $\vec{E}$ and $\vec{H}$ fields   the faces S_1 and S_2 may be con-
sidered as constituted of incident, reflected and transmitted
radiations which very near the slab surface satisfy the boundary

conditions for plane waves:

$$\vec{E} = \vec{E}_i + \vec{E}_r$$

$$\vec{H} = \vec{H}_i + \vec{H}_r \quad \text{on } S_1,$$

$$\vec{E} = \vec{E}_t$$

$$H = \vec{H}_t \quad \text{on } S_2 \tag{4.7}$$

In this "locally plane wave approximation", the incident radiation from a distant localized source is approximated near the point P on S_1 by a plane wave propagating in the direction of a unit vector $\hat{n}_i$; the reflected wave emanating from P propagates in a direction given by n_r and a transmitted wave emanating from face S_2 also propagates in the incident direction $\hat{n}_i$. The relationships between incident, reflected, and transmitted fields will be expressed in terms of certain dyadic forms which hold for the boundary value problem of the plane wave incident on an infinite plane slab. If $\vec{E}_o(\vec{\rho})$ is the incident electric field at point P, the local plane wave approximate fields are

$$\vec{E}_i(\vec{r}) = \vec{E}_o(\vec{\rho}) e^{i(k\hat{n}_i \cdot (\vec{r}-\vec{\rho}) - \omega t)} \tag{4.8}$$

$$\vec{E}_r(\vec{r}) = \overleftrightarrow{R} \cdot \vec{E}_o(\vec{\rho}) e^{i(k\hat{n}_r \cdot (\vec{r}-\vec{\rho}) - \omega t)} \tag{4.9}$$

$$\vec{E}_t(\vec{r}) = \overleftrightarrow{T} \cdot \vec{E}_o(\vec{\rho}) e^{i(k\hat{n}_i \cdot (\vec{r}-\vec{\rho}+D\hat{n}) - \omega t)} \tag{4.10}$$

where $\overleftrightarrow{R}$ and $\overleftrightarrow{T}$ are, as yet, undefined reflection and transmission dyadics. In the following, the periodic time dependence will be suppressed, but is still understood.

Taking advantage of Equations (4.4) through (4.7) and also the relations:

$$i\omega \vec{H}_i = ik\hat{n}_i \times \vec{E}_i$$

$$i\omega \vec{H}_r = ik\hat{n}_r \times \vec{E}_r$$

$$i\omega \vec{H}_t = ik\hat{n}_i \times \vec{E}_t, \tag{4.11}$$

71

we are able to reduce Equation (4.3) to a single surface integral:

$$\vec{E}_s(\vec{r}') = \frac{ik\psi(r')}{4\pi}\, \hat{r}' \times \left| \hat{r}' \times \int_{S_1} ds \right.$$

$$\left(\left[\hat{n} \times (\hat{n}_i \times \vec{E}_i + \hat{n}_r \times \vec{E}_r) - \left(\hat{n} \times (\vec{E}_i + \vec{E}_r) \right) \times \hat{r}' \right] e^{i\Delta(\hat{r}'|\vec{\rho})} \right.$$

$$\left. - \left[\hat{n} \times (\hat{n}_i \times \vec{E}_t) - (\hat{n} \times \vec{E}_t) \times \hat{r}' \right] e^{i\Delta(\hat{r}'|\vec{\rho}+D\hat{n})} \right) \right| \qquad (4.12)$$

where the transmitted field $\vec{E}_t$ associated with the position vector $\vec{\rho}$ is evaluated at the point $\vec{\rho} + D\hat{n}$ of surface S_2. This result can be expressed algebraically as an operator acting on the incident electric field, if we now introduce the dyadic relations (4.8) through (4.10):

$$\vec{E}_s(\vec{r}') = \frac{ik\psi(r')}{4\pi}\, \hat{r}' \times \left| \hat{r}' \times \int_{S_1} ds \right.$$

$$\left(\left[\hat{n}\hat{r}' + \hat{n}_i\hat{n} - \hat{n}\cdot(\hat{r}'+\hat{n}_i)\,\overleftrightarrow{I} \right] e^{i\Delta(\hat{r}'|\vec{\rho})} \right.$$

$$+ \left[\hat{n}\hat{r}' + \hat{n}_r\hat{n} - \hat{n}\cdot(\hat{r}'-\hat{n}_i)\,\overleftrightarrow{I} \right] \overleftrightarrow{R}\, e^{i\Delta(\hat{r}'|\vec{\rho})}$$

$$\left. - \left[\hat{n}\hat{r}' + \hat{n}_i\hat{n} - \hat{n}\cdot(\hat{r}'+\hat{n}_i)\,\overleftrightarrow{I} \right] \overleftrightarrow{T}\, e^{i\Delta(\hat{r}'|\vec{\rho}+D\hat{n})} \right) \cdot \vec{E}_o(\vec{\rho}) \quad (4.13)$$

The dyadic expressions here have the usual linear properties; for example:

$$(\hat{n}\hat{r}' + \hat{n}_i\hat{n}) \cdot \vec{X} = \hat{n}(\hat{r}'\cdot\vec{X}) + \hat{n}_i(\hat{n}\cdot\vec{X}), \qquad (4.14)$$

etc., where $\vec{X}$ is an arbitrary vector; the identity dyadic is denoted by $\overleftrightarrow{I}$:

$$\overleftrightarrow{I} \cdot \vec{X} = \vec{X}$$
$$\overleftrightarrow{I} \cdot \overleftrightarrow{R} = \overleftrightarrow{R} \qquad (4.15)$$

To reduce Equation (4.13) to its most convenient form, we assume that the largest slab dimension is much smaller than the distances to either the radiation source or the point of detection.

This condition must hold if the far field approximations being used are to be valid. This being the case, we will neglect the variation of $\hat{n}_i$, $\hat{n}_r$, and $\hat{r}'$ over the slab face S_1 and set each of these vectors to its respective direction at the fixed reference point O. We shall also expand the phase correction $\Delta(\vec{r}'|\vec{\rho}+D\hat{n})$ and keep only the lowest order term in the dimension D, i.e.:

$$\Delta(\vec{r}'|\vec{\rho}+D\hat{n}) = \Delta(\vec{r}'|\vec{\rho}) - kD(\hat{r}'\cdot\hat{n}) \tag{4.16}$$

This simplification permits us to write (4.13) as:

$$\vec{E}_s(\vec{r}') = \frac{ik\psi(r')}{4\pi} \overleftrightarrow{\mathcal{F}}(\hat{n}_i,\hat{r}',\hat{n}) \cdot \int_{S_1} ds\, \vec{E}_o(\vec{\rho})e^{i\Delta(\vec{r}'|\vec{\rho})} \tag{4.17}$$

Here

$$\overleftrightarrow{\mathcal{F}}(\hat{n}_i,\hat{r}',\hat{n}) = \hat{r}' \times \left[\hat{r}' \times \left(\left(\hat{n}\hat{r}'+\hat{n}_i\hat{n} - \hat{n}\cdot(\hat{r}'+\hat{n}_i)\overleftrightarrow{I}\right)\cdot\left(\overleftrightarrow{I}+\overleftrightarrow{R}-\alpha_D\overleftrightarrow{T}\right) \right. \right.$$
$$\left. \left. + 2(\hat{n}\cdot\hat{n}_i)(\overleftrightarrow{I-\hat{n}\hat{n}})\overleftrightarrow{R} \right) \right] \tag{4.18}$$

with

$$\alpha_D = e^{-ikD(\hat{r}'\cdot\hat{n})} \tag{4.19}$$

and where we have used

$$\hat{n}_r = (\overleftrightarrow{I-2\hat{n}\hat{n}}) \cdot \hat{n}_i \tag{4.20}$$

The application of the foregoing results to scattering by a perfectly conducting slab can be made by putting

$$\overleftrightarrow{R} = 2\hat{n}\hat{n} - \overleftrightarrow{I}$$
$$\overleftrightarrow{T} = 0. \tag{4.21}$$

Equation (4.13) then reduces to

$$\vec{E}_s(\vec{r}') = \frac{ik\psi(r')}{2\pi} \hat{r}' \times\left(\hat{r}'\times \int_{S_1} ds \left[\left(\hat{n}\cdot\vec{E}_o(\vec{\rho})\right)\hat{n}_i - (\hat{n}\cdot\hat{n}_i)\vec{E}_o(\vec{\rho})\right] e^{i\Delta(\vec{r}'|\vec{\rho})}\right) \tag{4.22}$$

which result can be obtained by straightforward manipulations directly from (4.3).

To extend Equation (4.13) to the general case, we must now make a detailed analysis of the slab boundary value problem to determine the dyadics $\overleftrightarrow{R}$ and $\overleftrightarrow{T}$.

4.3 REFLECTION AND TRANSMISSION OF PLANE WAVES BY AN INFINITE PLANE PARALLEL SLAB

In order to apply the local plane wave approximation in our estimates of scattering by thin slabs, we solve the boundary value problem for a plane wave incident on an infinite plane parallel slab of thickness D, with homogeneous electrical properties ϵ, μ and σ which separates two regions of vacuum. Because of the plane symmetry, the problem is two-dimensional, with the incident, reflected, and transmitted wave normals at both slab surfaces all parallel to a common plane of incidence. The incident wave of arbitrary polarization can most easily be treated by decomposition into an "$E_\perp$" component, with the electric vector normal to the plane of incidence, and an "E$\parallel$" component, with the magnetic vector normal to the plane of incidence. We treat the $E_\perp$ case first.

The several secondary waves generated by an electromagnetic wave incident on a slab boundary S_1 are illustrated in Figure 4.2. On the incident side of boundary S_1, we have the reflected wave $\vec{E}_r$ in addition to the incident wave $\vec{E}_i$. In the slab medium, we have a "forward wave" $\vec{E}_f$ and a "backward wave" $\vec{E}_b$. Outside the slab on the transmission side of S_2, we have $\vec{E}_t$. All of these fields are normal to the plane of incidence, and we may drop vector notation for these components. We denote the value of a field at a slab boundary by a subscript 1 or 2; the wave normals are denoted by the vectors $\hat{n}_i$, $\hat{n}_r$, $\hat{n}_f$, $\hat{n}_b$, and $\hat{n}_t$ ($= \hat{n}_i$), as shown in Figure 4.2. A plane wave in the slab has a complex propagation vector K. The real part has the direction of either $\hat{n}_f$ or $\hat{n}_b$ and determines the surfaces of constant phase. The imaginary part is parallel to the boundary normal $\hat{n}$ and determines the surfaces of constant amplitude. Outside the slab, the propagation vectors $k\hat{n}_i$ and $k\hat{n}_r$ are real, with $k = 2\pi/\lambda$.

Following Stratton,[1] the boundary conditions at surfaces S_1 and S_2 for the $E_\perp$ polarization can be written:

74
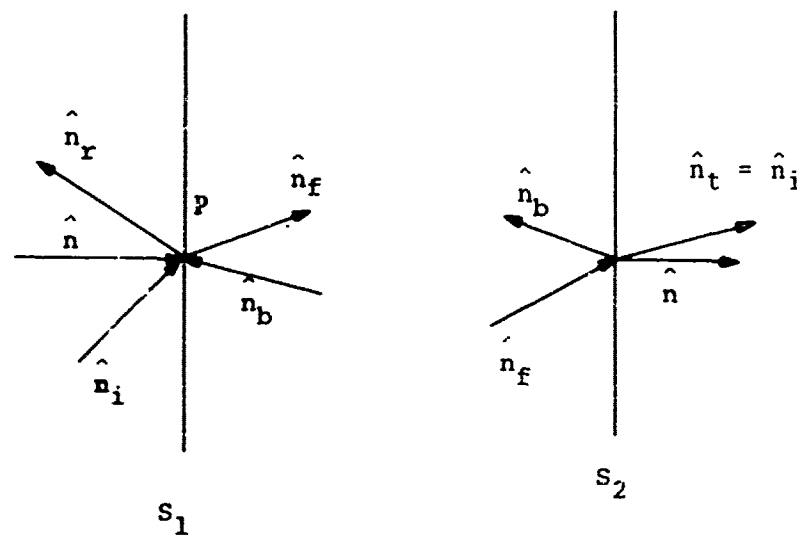
Figure 4.2. Wave Normals of Reflected and Transmitted Electromagnetic Fields Generated by a Wave Propagating in the Direction $\hat{n}_i$ Incident on Boundary S_1. The Reference Normal to the Plane Parallel Slab Bounded by Surfaces S_1 and S_2 is $\hat{n}$.

$$E_i + E_r = E_{f1} + E_{b2} \qquad (4.23)$$

$$\frac{1}{\mu_o}\left((\hat{n}\cdot\vec{k}_i)E_i + (\hat{n}\cdot\vec{k}_r)E_r\right) = \frac{1}{\mu}\left[(\hat{n}\cdot K_f)E_{f1} + (\hat{n}\cdot\vec{K}_b)E_{b1}\right] \qquad (4.24)$$

$$E_{f2} + E_{b2} = E_t \qquad (4.25)$$

$$\frac{1}{\mu}\left[(\hat{n}\cdot K_f)E_{f2} + (\hat{n}\cdot K_b)E_{b2}\right] = \frac{\hat{n}\cdot\vec{k}_i}{\mu_o}E_t \qquad (4.26)$$

Two additional conditions on the six undetermined variables are needed; they may be taken to be:

$$E_{f2} = e^{i(\hat{n}\cdot K_f)D}E_{f1} \qquad (4.27)$$

$$= \beta\, E_{f1}$$

$$E_{b1} = \beta\, E_{b2} \qquad (4.28)$$

where we have used

$$\hat{n}\cdot\vec{K}_f = -\hat{n}\cdot\vec{K}_b \qquad (4.29)$$

which generally holds for plane wave reflection. By making use of the similar relation

$$\hat{n}\cdot\vec{k}_i = k\,\hat{n}\cdot\hat{n}_i$$

$$= -k\,\hat{n}\cdot\hat{n}_r \qquad (4.30)$$

we can reduce Equations (4.23) through (4.28) to the solution for the normal electric vector components:

$$E_r = -\frac{(1-\beta^2)(1-\gamma_E^2)}{\left[(1+\gamma_E)^2 - \beta^2(1-\gamma_E)^2\right]}E_i \qquad (4.31)$$

$$= R_E E_i$$

$$E_t = \frac{4\gamma_E\beta}{\left[(1+\gamma_E)^2 - \beta^2(1-\gamma_E)^2\right]}E_i \qquad (4.32)$$

$$= T_E\, E_i,$$

$$\gamma_E = \frac{\mu(\hat{n}\cdot\vec{k})}{\mu_0(\hat{n}\cdot\vec{k}_f)} \qquad (4.33)$$

We wish to calculate the quantity $\vec{k}_f\cdot\hat{n}$. We have the expansion

$$\vec{k}_f = \hat{n}(\hat{n}\cdot\vec{k}_f) - \hat{n} \times (\hat{n}\times\vec{k}_f). \qquad (4.34)$$

We also have the boundary condition

$$\hat{n} \times \vec{k}_f = \hat{n} \times \vec{k}_i \qquad (4.35)$$

where $\vec{k}_i$ is the incident wave vector.

Then

$$\vec{k}_f^2 = (\hat{n}\cdot\vec{k}_f)^2 + \left[\hat{n}\times(\hat{n}\times\vec{k}_i)\right] \cdot \left[\hat{n} \times (\hat{n}\times\vec{k}_i)\right]$$

$$= (\hat{n}\cdot\vec{k}_f)^2 + (\hat{n}\times\vec{k}_i)\cdot(\hat{n}\times\vec{k}_i)$$

$$= (\hat{n}\cdot\vec{k}_f)^2 + k_i^2 \sin^2 \theta_i \qquad (4.36)$$

But we have also, as shown by Stratton,[1]

$$k_f^2 = \omega^2\mu\epsilon + i\,\omega\mu\sigma. \qquad (4.37)$$

From the above equations, it follows that

$$(\hat{n}\cdot\vec{k}_f) = \sqrt{\omega^2\mu\epsilon - k^2 \sin^2 \theta_i + i\,\omega\mu\sigma} \quad ; \qquad (4.38)$$

hence

$$\gamma_E = \frac{\mu}{\mu_0} \frac{k \cos \theta_i}{\sqrt{\omega^2\mu(\epsilon+i\sigma/\omega) - k^2 \sin^2 \theta_i}} \qquad (4.39)$$

$$\beta = e^{iD\sqrt{\omega^2\mu(\epsilon+i\sigma/\omega) - k^2 \sin^2 \theta_i}} \qquad (4.40)$$

For the $E_\parallel$ polarization case, the magnetic vector is normal to the plane of incidence. Evaluation of the transmitted and re-flected waves follows from the set of boundary conditions similar to (4.23) through (4.28):

$$H_i + H_r = H_{f1} + H_{b1} \qquad (4.41)$$

77

$$\frac{\hat{n}\cdot\vec{k}_i}{\varepsilon_o}\,(H_i - H_r) = \frac{\hat{n}\cdot\vec{K}_f}{\varepsilon + i\sigma/\omega}\,(H_{f1} - H_{b1}) \tag{4.42}$$

$$H_{f2} + H_{b2} = H_t \tag{4.43}$$

$$\frac{\vec{K}_f}{-i\cdots/\omega}\,(H_{f2} - H_{b2}) = \frac{\hat{n}\cdot\vec{k}_i}{\varepsilon_o}\,H_t \tag{4.44}$$

$$H_{f2} = \beta\,H_{f1} \tag{4.45}$$

$$H_{b1} = \beta\,H_{b2} \tag{4.46}$$

We obtain results analogous to Equations (4.31) and (4.32) above with γ_E replaced by γ_H:

$$\begin{aligned}
\gamma_H &= \frac{(\varepsilon + i\sigma/\omega)\,\hat{n}\cdot\vec{k}_i}{\varepsilon_o\,\hat{n}\cdot\vec{K}_f} \\[2mm]
&= \frac{\mu_o\,(\varepsilon + i\sigma/\omega)}{\mu\,\varepsilon_c}\,\gamma_\varepsilon \\[2mm]
&= \frac{(\varepsilon + i\sigma/\omega)k\,\cos\partial_i}{\varepsilon_o\,\sqrt{\omega^2\mu(\varepsilon + i\sigma/\omega) - k^2\sin^2\theta_i}}
\end{aligned} \tag{4.47}$$

$$H_r = R_H\,H_i \tag{4.48}$$

$$H_t = T_H\,H_i \tag{4.49}$$

$$R_H = -\,\frac{(1-\gamma_H^2)(1-\beta^2)}{(1-\beta^2)(1+\gamma_H^2) + 2(1+\beta^2)\gamma_H} \tag{4 50}$$

$$T_H = \frac{4\gamma_H\beta}{(1-\beta^2)(1+\gamma_H^2) + 2(1+\beta^2)\gamma_H} \tag{4.51}$$

To use (4.31), (4.32), (4.48), and (4.49) in the general case, we must decompose the incident, reflected and transmitted electric vectors into polarization components normal and parallel to the plane of incidence. For example, the component of an incident wave perpendicular to both the boundary normal $\hat{n}$ and the wave normal $\hat{n}_i$ may be expressed by the equation:

$$\vec{E}_{i\perp} = \frac{1}{\sin^2\theta_i} \; (\hat{n}_x\hat{n}_i)(\hat{n}_x\hat{n}_i\cdot\vec{E}_i) \qquad (4.52)$$

In anticipation of dyadic relations to be developed shortly, it is appropriate to introduce a special dual set of basis vectors to express such polarization relations. Consider the linearly independent basis:

$$\vec{e}_1 = \frac{\hat{n}}{\sin\theta_i}$$

$$\vec{e}_2 = \frac{\hat{n}_i}{\sin\theta_i}$$

$$\vec{e}_3 = \frac{\hat{n} \times \hat{n}_i}{\sin\theta_i} \qquad (4.53)$$

(see Figures 4.3A and 4.3B).

These vectors are dual to the set

$$\vec{e}^1 = \frac{1}{\sin\theta_i} \left(\hat{n} - (\hat{n}\cdot\hat{n}_i)\hat{n}_i \right)$$

$$\vec{e}^2 = \frac{1}{\sin\theta_i} \left(\hat{n}_i - (\hat{n}\cdot\hat{n}_i)\hat{n} \right)$$

$$\vec{e}^3 = \frac{1}{\sin\theta_i} \; (\hat{n}_x\hat{n}_i) \qquad (4.54)$$

in the sense that:

$$\vec{e}_i\cdot\vec{e}^j = \delta_{ij} \qquad (4.55)$$

The set $\{\vec{e}^j\}$ is the appropriate basis for representing the incident electric field on a medium interface normal to $\hat{n}$. If we make

$$\vec{E}_i = (E_i)_j \; \vec{e}^j \qquad (4.56)$$

where the repeated Roman index here and in the following will imply a summation

$$\sum_{j=1}^{3} , \qquad \text{then:}$$

79
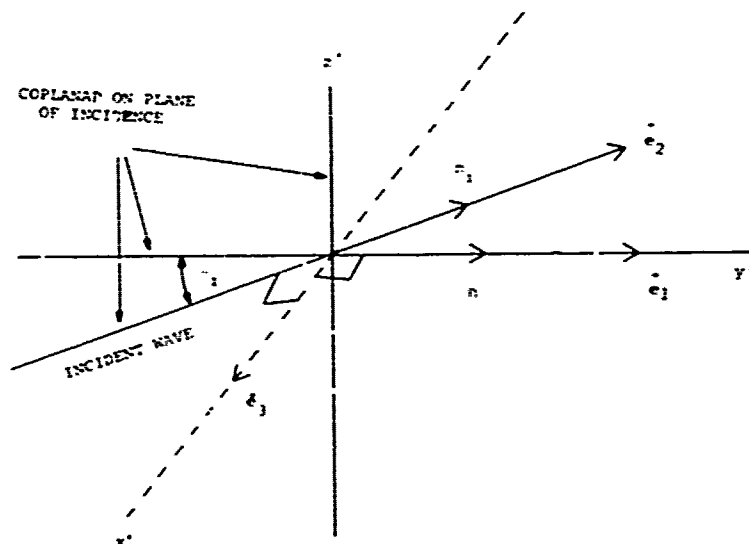
Figure 4.3A. Geometry for the Vectors $\vec{e}_1$, $\vec{e}_2$ and $\vec{e}_3$. x',y',z'
Form a Right-Handed Triad, z' and y' Lie on the
Surface of the Slab. z', $\hat{n}_i$ and $\hat{n}$ Lie on the
Plane of Incidence. Then $\vec{e}_3$ is in the Direction
of x' and is $\perp$ to the Plane of Incidence. (z' is
Not Necessarily in the Vertical Direction.)
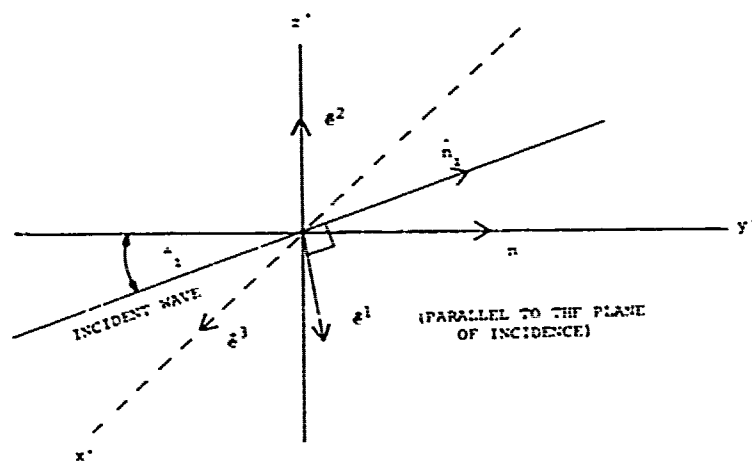
Figure 4.3B. Geometry for the Vectors $\vec{e}^1$, $\vec{e}^2$ and $\vec{e}^3$. z', $\hat{n}_i$
and $\hat{n}$ Lie on the Plane of Incidence, $\vec{e}^3$ is $\perp$ to
this Plane, While $\vec{e}^1$ is Parallel to it and is $\perp$
to $\hat{n}_i$.

$$(E_i)_j = \vec{e}_j \cdot \vec{E}_i \tag{4.57}$$

Upon comparison with Equation (4.52), we see that $\vec{e}^3(\vec{e}_3 \cdot \vec{E}_i)$ is the perpendicular component E_i, that $(\vec{e}_2 \cdot \vec{E}_i)$ is always zero for a transverse wave, and the $\vec{e}^1(\vec{e}_1 \cdot \vec{E}_i)$ is the parallel polarization component of the incident wave.

The reflected and transmitted electric vectors for each polarization are now easily calculated. First, in the perpendicular polarization case we have:

$$\vec{E}_{r\perp} = R_E \, \vec{e}^3(\vec{e}_3 \cdot \vec{E}_i) \tag{4.58}$$

$$\vec{E}_{t\perp} = T_E \, \vec{e}^3\left(\vec{e}_3 \cdot \vec{E}_i\right) \tag{4.59}$$

In the parallel polarization case, we have:

$$\vec{E}_{r||} = -\frac{k}{\omega\epsilon_o} \hat{n}_r \times \vec{H}_{r\perp}$$

$$= -R_H \frac{k}{\omega\epsilon_o} \hat{n}_r \times \vec{H}_{i\perp}$$

$$= -R_H \, \hat{n}_r \times (\hat{n}_i \times \vec{e}^1)(\vec{e}_1 \cdot \vec{E}_i). \tag{4.60}$$

By a similar analysis, we find:

$$\vec{E}_{t||} = -T_H \, \hat{n}_i \times (\hat{n}_i \times \vec{e}^1)(\vec{e}_1 \cdot \vec{E}_i) \tag{4.61}$$

Since the sum of the two polarization cases gives the total reflected and transmitted fields, we are now able to write down the dyadics $\overleftrightarrow{R}$ and $\overleftrightarrow{T}$:

$$\overleftrightarrow{R} = -R_H \, \hat{n}_r \times (\hat{n}_i \times \vec{e}^1)\vec{e}_1 + R_E \, \vec{e}^3\vec{e}_3 \tag{4.62}$$

$$\overleftrightarrow{T} = -T_H \, \hat{n}_i \times (\hat{n}_i \times \vec{e}^1)\vec{e}_1 + T_E \, \vec{e}^3\vec{e}_3 \tag{4.63}$$

Here, $\hat{n}_r$ is the wave normal of the reflected wave generated by the given incident wave in the local plane wave approximation, i.e.:

$$\hat{n}_r = \hat{n}_i - 2(\hat{n} \cdot \hat{n}_i)\hat{n} \tag{4.64}$$

81

We may insert the expressions (4.62) and (4.63) into Equation (4.18) for the scattering dyadic:

$$\vec{\mathcal{J}}(\hat{n}_i,\hat{r},\hat{n}) = \hat{r} \times \Big\{ \hat{r} \times$$

$$\Big[(1-\alpha_D T_H)\Big(\hat{r} \times (\hat{n}\times\vec{e}^1) + \hat{n} \times (\hat{n}_i\times\vec{e}^1)\Big)\vec{e}_1$$

$$+ (1-\alpha_D T_E)\Big(\hat{r} \times (n\times\vec{e}^3) + n \times (\hat{n}_i\times\vec{e}^3)\Big)\vec{e}_3$$

$$- R_H \Big(\hat{r} \times (\hat{n}\times(\hat{n}_r\times(\hat{n}_i\times\vec{e}^1))) + \hat{n} \times \Big(\hat{n}_r \times (\hat{n}_r\times(\hat{n}_i\times\vec{e}^1))\Big)\Big)\vec{e}^1$$

$$+ R_E \Big(\hat{r} \times (\hat{n}\times\vec{e}^3) + \hat{n} \times (\hat{n}_r\times\vec{e}^3)\Big)\vec{e}_3\Big]\Big\} \qquad (4.65)$$

The equation can be reduced by noting such relations as:

$$\hat{n} \times \vec{e}^1 = - (\hat{n}\cdot\hat{n}_i)\vec{e}^3 \qquad (4.66)$$

$$\hat{n} \times \vec{e}^3 = - \vec{e}^2 \qquad (4.67)$$

$$\hat{n}_i \times \vec{e}^1 = - \vec{e}^3 \qquad (4.68)$$

$$\hat{n}_i \times \vec{e}^3 = \vec{e}^1 \qquad (4.69)$$

$$\hat{n} \times (\hat{n}_r\times\vec{e}^3) = (\hat{n}\cdot\hat{n}_i)\vec{e}^3 \qquad (4.70)$$

The form thus obtained is

$$\vec{\mathcal{J}}(\hat{n}_i,\hat{r},\hat{n}) = \hat{r} \times \Big\{ \hat{r} \times$$

$$-\Big[(1-\alpha_D T_H) \Big(\hat{n} + (\hat{n}\cdot\hat{n}_i)\hat{r}\Big) \times \vec{e}^3\vec{e}_1$$

$$- R_H \Big(\hat{n} - (\hat{n}\cdot\hat{n}_i)\hat{r}\Big) \times \vec{e}^3\vec{e}_1$$

$$+ (1-\alpha_D T_E) \Big(-\hat{r}\times\vec{e}^2 - (\hat{n}\cdot\hat{n}_i)\vec{e}^3\Big)\vec{e}_3$$

$$+ R_E \Big(-\hat{r} \times \vec{e}^2 + (\hat{n}\cdot\hat{n}_i)\vec{e}^3\Big) \vec{e}_3\Big]\Big\} \qquad (4.71)$$

It can be checked again that, in the case of a perfect conductor,

$$R_E \rightarrow - 1$$

$$R_H \rightarrow + 1$$

$$\vec{\overline{\mathcal{J}}} \rightarrow - \hat{r} \times \left(\hat{r} \times \left[-\vec{e}^2 \vec{e}_1 + (\hat{n} \cdot \hat{n}_i) \vec{e}^3 \vec{e}_3 \right] \right) \qquad (4.72)$$

as they should.

4.4 SCATTERING FROM A SLANTED RECTANGULAR CONDUCTIVE SLAB

In this section we will calculate the far field scattering from a slanted rectangular conductive slab, the top and bottom edges being parallel to an infinitely conductive flat ground plane. The general method given in Sections 4.1 and 4.2 will be applied to this problem. Figures 4.4A,B and C show the geometry for this problem. $\hat{n}_i$, the incident wave direction, is approximated by $\hat{R}'$, the unit vector from the antenna to the reference point 0 on the midpoint of the slab's lower edge.

$$\hat{n}_i \cong \hat{R}' = \hat{i} \cos\theta_1 \cos\psi + \hat{j} \cos\theta_1 \sin\psi + \hat{k} \sin\theta_1 \qquad (4.73)$$

where

$$\sin\theta_1 = (M-H_A)/R'$$

$$\cos\theta_1 = D_{p1}/R'$$

$$R' = \left[D_{p1}^2 + (M-H_A)^2 \right]^{1/2}$$

The incident electric field vectors (with the inclusion of ground reflection) for small elevation angles is

$$\dot{E}_0(\rho) = \hat{U} \, E_0 \, f(\psi) \, \frac{e^{ikR}}{R} \left[1 - e^{ik\left(2z'H_A/D_p\right)} \right] \qquad (4.74)$$

(Compare Eq. (2.58).) Here, the angle

$$\psi = \tan^{-1} (y_1/x_1),$$

x_1 and y_1 being the horizontal coordinates of the reference point 0 on the slab with the horizontal edge of length L. We make the approximation $D_p \cong D_{p1}$ and again from the expansion

Figure 4.4A. General View

Figures 4.4A, B, and C. Geometric Configuration for Scattering from a slanted rectangular slab with top and bottom edges parallel to the ground plane.
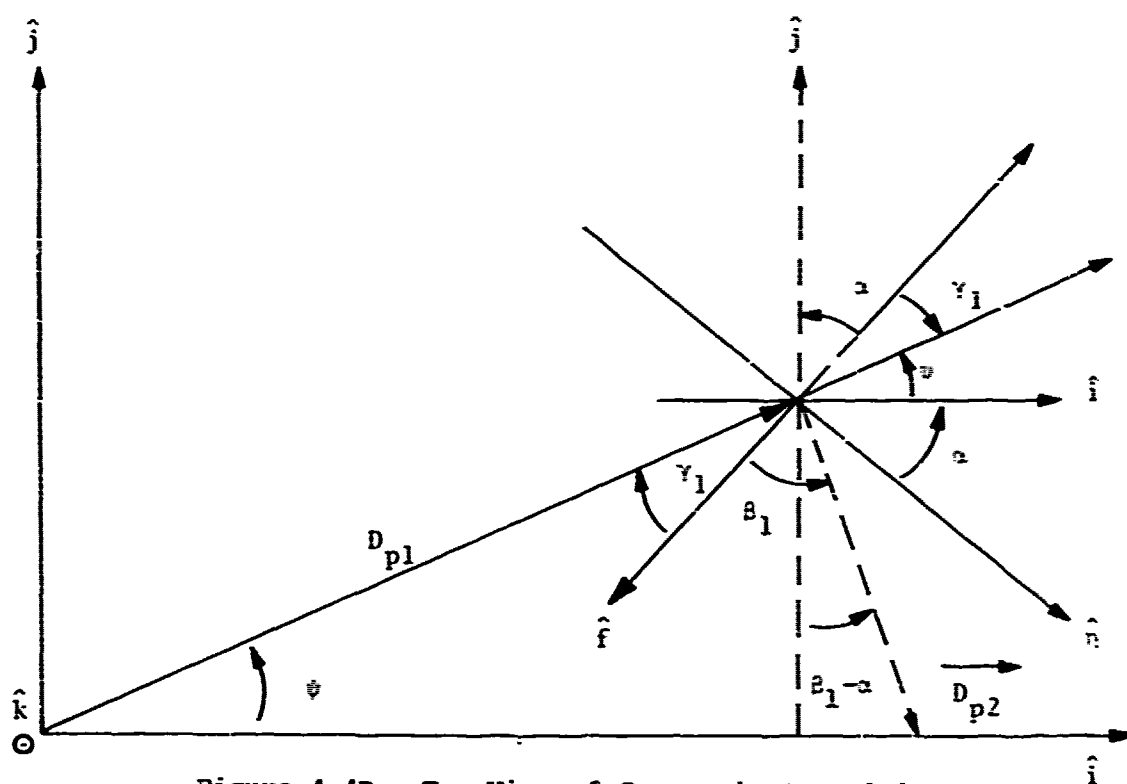
Figure 4.4B. Top View of Geometric Quantities

$\alpha + \psi + \gamma_1 = \pi/2$. $\hat{n}$ is $\perp$ to $\hat{f}$
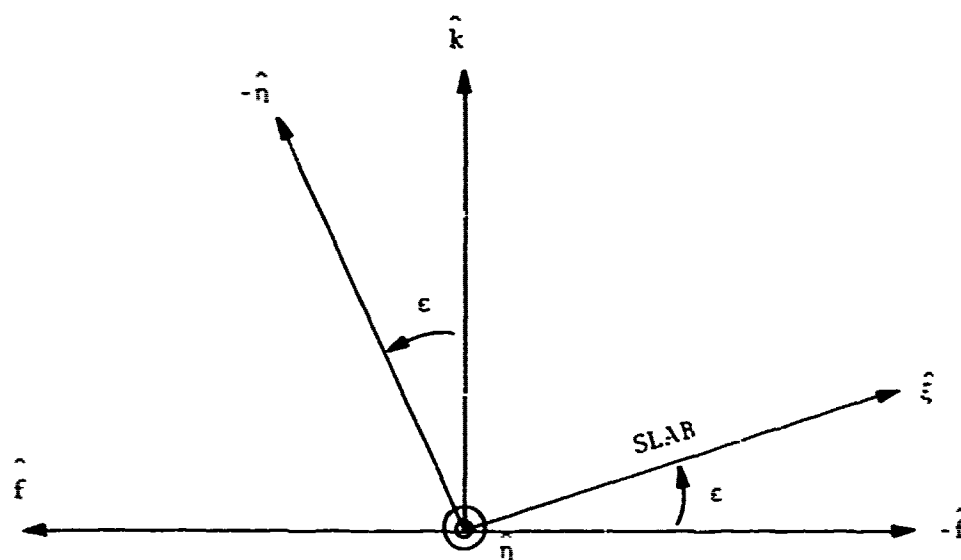
Figure 4.4C. Side View of Slanted Slab

$$R = R' + \hat{R}' \cdot \vec{\rho} + \left[\rho^2 - (\hat{R}' \cdot \vec{\rho})^2\right]/2R' + \ldots \quad (4.75)$$

we obtain (supposing that $k\rho^2/2R' \ll 1$) the Fraunhoffer approximation for the incident field

$$\frac{e^{ikR}}{R} \cong \frac{e^{ikR'}}{R'} e^{ik(\hat{R}' \cdot \vec{\rho})} \quad (4.76)$$

From Equation (4.22) we have the scattered field from a conductive flat surface

$$\vec{E}_s = \frac{ik}{2\pi} \frac{e^{ikr'}}{r'} \hat{r}'$$

$$\times \left\{ \hat{r}' \times \left[\left((\hat{n}_i \hat{n} \cdot) - (\hat{n} \cdot \hat{n}_i)\right) \int_{S_1} ds \vec{E}_o(\vec{\rho}) \times e^{i\Delta(\vec{r}'/\vec{\rho})} \right] \right\} \quad (4.77)$$

where S_1 is the illuminated front surface, and where

$$\Delta(\vec{r}'/\vec{\rho}) = -k\hat{r} \cdot \vec{\rho} + k\left[\rho^2 - (\hat{R} \cdot \vec{\rho})^2\right]/2r' + \ldots \quad (4.78)$$

In the calculation in this section we assume the Fraunhofer field condition to hold for the scattered field,

$$\frac{k\rho^2}{2r'} = \frac{\pi\rho^2}{\lambda r'} \ll 1 \quad (4.79)$$

so that

$$\Delta(\vec{r}'/\vec{\rho}) \cong -k \hat{r}' \cdot \vec{\rho} \quad (4.80)$$

Then,

$$\vec{E}_s = \hat{r}' \times \left\{ \hat{r}' \times \left[\hat{n}_i(\hat{n} \cdot \hat{U}) - \hat{U}(\hat{n} \cdot \hat{n}_i)\right] \right\} I_b \quad (4.81)$$

where

$$I_b = \frac{ik E_c f(\psi)}{2\pi} \exp\left[ik(r'+R')\right] I_c/r'R' \quad (4.82)$$

and

$$I_c = \int d\eta \, d\xi \left\{ \exp\left[ik(\hat{R}' \cdot \vec{\rho})\right] \left[1 - \exp(ik2z'H_N/D_{p1}\right] \cdot \exp(-ik\hat{r}' \cdot \vec{\rho})\right\} \quad (4.83)$$

With

$$\hat{R}' \cdot \vec{D} = \eta \cos\theta_1 \cos(\psi+\alpha) + \xi\left[\cos\theta_1 \cos\epsilon \sin(\psi+\alpha) + \sin\theta_1 \sin\epsilon\right]$$

$$= A\eta + B\xi, \tag{4.84}$$

$$\hat{r}' \cdot \vec{D} = (\eta_2/r')\eta + (\xi_2/r')\xi, \tag{4.85}$$

we have

$$I_C = \int_{-L/2}^{L/2} d\eta \, \exp\left\{ik\left[A-(\eta_2/r')\right]\eta\right\} \times \int_0^h d\xi \, \exp\left[ik\left(B-(\xi_2/r')\right)\xi\right]$$

$$- \exp\left[ik 2H_A M/D_p\right] \int_0^h d\xi \, \exp\left[ik\left(B-(\xi_2/r') + \frac{2H_A \sin\epsilon}{D_p}\right)\xi\right] \Bigg\} \quad (4.86)$$

Integrating gives

$$I_C = L\left[\operatorname{sinc}(kA'L/2)\right] \left\{ \frac{-i}{kB'} \left(e^{ikB'h}-1\right) \right.$$

$$\left. - e^{ik 2H_A M/D_p}\left[\frac{-i}{kB''} \left(e^{ikB''h}-1\right)\right]\right\} \quad, \tag{4.87}$$

where

$$A' = A - \eta_2/r'$$

$$B' = B - \xi_2/r'$$

$$B'' = B' + \frac{2H_A \sin\epsilon}{D_p} \tag{4.88}$$

with $\alpha + \psi + \gamma_1 = \pi/2$,

$$A = \cos\theta_1 \cos(\psi+\alpha) = \cos\theta_1 \sin\gamma_1$$

$$B = \cos\theta_1 \cos\epsilon \sin(\psi+\alpha) + \sin\theta_1 \sin\epsilon$$

$$= \cos\theta_1 \cos\epsilon \cos\gamma_1 + \sin\theta_1 \sin\epsilon \tag{4.89}$$

and

$$\xi_2/r' = -\cos\epsilon_2 \cos\beta_1 \cos\epsilon + \sin\epsilon_2 \sin\epsilon$$

$$\eta_2/r' = \cos\epsilon_2 \sin\beta_1 \tag{4.90}$$

87

with

$$\sin\epsilon_2 = (z_2-M)/r' \qquad (4.91)$$

Also in Equation (4.81) we have

$$\hat{n}_i(\hat{n}\cdot\hat{U}) - (\hat{n}\cdot\hat{n}_i)\hat{U} = \hat{n} \times (\hat{n}_i\times\hat{U}) \qquad (4.92)$$

The induced voltage at the aircraft antenna is

$$V = c_o(\hat{k}\times\hat{r}') \cdot \vec{E}_s \qquad (4.93)$$

$$V = c_o \left\{ (\hat{k}\times\hat{r}') \cdot \hat{r}' \times \left[\hat{r}' \times \left(\hat{n} \times (\hat{n}_i\times\hat{U}) \right) \right] \right\} I_b \qquad (4.94)$$

where I_b is given by Equations (4.82) and (4.87). We have, finally,

$$V/c_o I_b = \left\{ \left[(\hat{k}\times\hat{r}') \times \hat{r}' \right] \times \hat{r}' \right\} \cdot \left[\hat{n} \times (\hat{n}_i\times\hat{U}) \right]$$

$$= - \hat{r}' \times \hat{k} \cdot \left[(\hat{n}_i\times\hat{U}) \times \hat{n} \right]$$

$$= - \hat{r}' \cdot \left\{ \hat{n} \cos\theta_1 + \sin\theta_1 (\hat{k}\times\hat{U})\hat{k}\cdot\hat{n} \right.$$

$$\left. - \cos\theta_1 \hat{k}(\hat{k}\cdot\hat{n}) \right\} \qquad (4.95)$$

Assuming the unit vector $\hat{U}$ to be horizontally polarized

$$\hat{U} = - (\hat{k}\times\hat{n}_i)/\cos\theta_1 \qquad (4.96)$$

we obtain for the voltage function

$$V/c_o I_b = \cos\epsilon_2\left[\cos\theta_1 \sin\epsilon \cos\theta_1 + \sin\theta_1 \cos\epsilon \cos(\beta_1+\gamma_1)\right] \qquad (4.97)$$

In order to obtain the voltage due to the direct scattering from the wall, we set (see Figure 4.5):

$$\sin\epsilon_2 = (z_2-M)/r' \qquad (4.98)$$

$$r' = \left[D_{p2}^2 + (z_2-M)^2 \right]^{1/2} \qquad (4.99)$$

$$\cos\epsilon_2 = D_{p2}/r' \qquad (4.100)$$

88

REFERENCE PT. ON SLAB
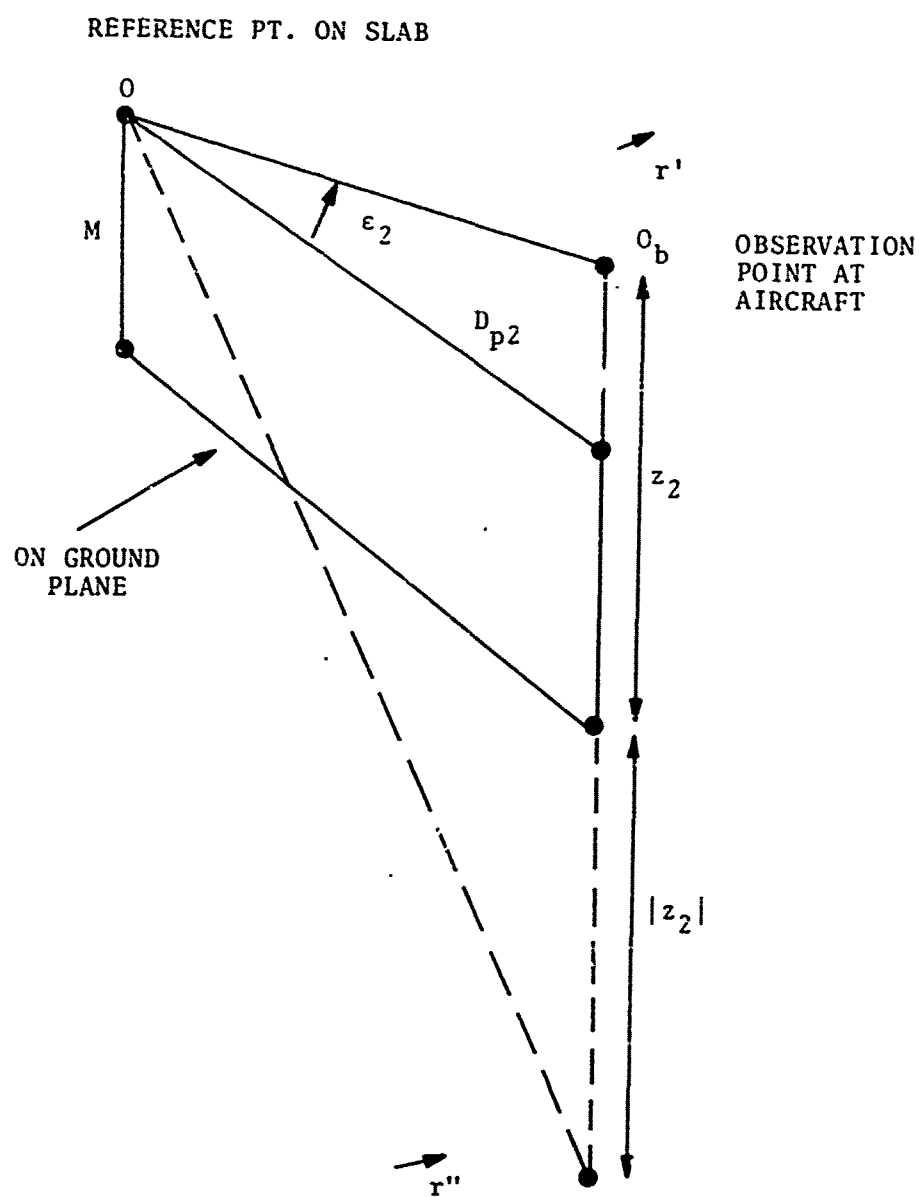
Figure 4.5.   Geometry for Calculating the Scattered Field from
              the Ground Image of the Slab

In order to obtain the scattered electric field from the image of the wall, we first formally compute the scattered field from the wall to a point below the ground plane, which is the same distance as the observation point above the ground plane, and then "reverse" the horizontal component. Since in the voltage equation,

$$v = c_o(\hat{k}x\hat{r}') \cdot \vec{E}_s,$$ (4.101)

$\hat{k} \times \hat{r}'$ is a horizontal vector, after formally calculating the field at the point below the ground plane, one can simply multiply this quantity by -1, since the vertical component is cancelled. Figure 4.5 shows the geometry for this image calculation. The image field at $\vec{r}''$ is obtained by setting

$$\sin\epsilon_2 = - (M+|z_2|)/r''$$ (4.102)

where

$$r'' = \left[D_{p2}^2 + (M+|z_2|)^2 \right]^{1/2}$$ (4.103)

and

$$\cos\epsilon_2 = D_{p2}/r''$$ (4.104)

4.5 SCATTERING FROM A SLANTED RECTANGULAR DIELECTRIC SLAB

The geometry for the scattering is show in Figures 4.4A, B and C. Many of the quantities calculated in the previous section (4.4) for the conductive case apply to the general case treated here.

The scattered electric field is given by Equation (4.17), which can be written as

$$\vec{E}(r') = \frac{ik}{4\pi} \frac{\exp(ikr')}{r'} \overleftrightarrow{\mathcal{J}}(\hat{n}_i,\hat{r}',\hat{n}) \cdot$$

$$\cdot \int_{S_1} ds \, \vec{E}_o(\vec{\rho}) \, \exp\left[i\Delta(\vec{r}'/\vec{\rho})\right]$$ (4.105)

With the same far field approximations as in the previous section, we have for the incident field on the slab,

$$\vec{E}_o(\rho) = F_n \, \hat{U} \qquad (4.106)$$

where

$$\hat{U} = (\vec{e}_1 \cdot \hat{U})\vec{e}' + (\vec{e}_3 \cdot \hat{U})\vec{e}^3 \qquad (4.107)$$

and

$$F_n \cong E_o \, f(\psi) \, \frac{e^{ikR'}}{R'} \, e^{ik\hat{R}' \cdot \vec{\rho}} \left[1 - e^{2ikz'H_A/D_p} \right] \qquad (4.108)$$

Then, defining

$$I'_a = \int ds \, \vec{E}_o(\rho) \, e^{i\Delta(\vec{\rho})} = \hat{U} \, I'_b \qquad (4.109)$$

where

$$I'_b = \int ds \, F_n \, e^{i\Delta(\vec{\rho})} \qquad (4.110)$$

with

$$\Delta(\vec{r}',\vec{\rho}) = - k \, \hat{r}' \cdot \vec{\rho} \qquad (4.111)$$

we have

$$I'_b \cong E_o \, f(\psi) \, \frac{e^{ikR'}}{R'} \, I_c \qquad (4.112)$$

where I_c is given by Equation (4.87) in Section 4.4. Combining the previous equations, we obtain for the scattered field

$$\vec{E}_s = F_2 \, (\overleftrightarrow{\mathcal{J}} \cdot \hat{U}) \qquad (4.113)$$

where

$$F_2 = \frac{i}{2\lambda} \, E_o \, f(\psi) \, \frac{e^{ik(r'+R')}}{r'R'} \, I_c \qquad (4.114)$$

The induced voltage at the aircraft antenna is

$$V = C_o (\hat{k} \times \hat{r}') \cdot \vec{E}_s$$

$$= C_o \, F_2 (\hat{k} \times \hat{r}') \cdot (\overleftrightarrow{\mathcal{J}} \cdot \hat{U}) \qquad (4.115)$$

91

Referring to Equation (4.71) we have:

$$\vec{\mathcal{F}} \cdot \hat{u} = \hat{r}' \times \left\{ \hat{r}' \times \left[\left((\hat{n} \times \vec{e}^3)(-1 + \alpha_D T_H - R_H) \right. \right. \right.$$

$$+ (\hat{n} \cdot \hat{n}_i)(-1 + \alpha_D T_H + R_H)(\hat{r}' \times \vec{e}^3) \right) (\vec{e}_1 \cdot \ddot{u})$$

$$+ \left((\hat{r}' \times \vec{e}^2)(-1 + \alpha_D T_E - R_E) \right.$$

$$\left. \left. \left. + (\hat{n} \cdot \hat{n}_i)\vec{e}^3 (-1 + \alpha_D T_E + R_E) \right) (\vec{e}_3 \cdot \hat{u}) \right] \right\} \tag{4.116}$$

If we denote the quantity enclosed by the square brackets [ ] by $\vec{A}$, the voltage function may be written as

$$V/C_o F_2 = (\hat{k} \times \hat{r}') \cdot \hat{r}' \times (\hat{r}' \times \vec{A}) \tag{4.117}$$

This can be written as a sum of four parts,

$$\frac{V}{C_o F_2} = \left(\frac{V}{C_o F_2} \right)_1 + \left(\frac{V}{C_o F_2} \right)_2 + \left(\frac{V}{C_o F_2} \right)_3 + \left(\frac{V}{C_o F_2} \right)_4 \tag{4.118}$$

We have

$$\vec{e}_3 = \frac{\hat{n} \times \hat{n}_i}{\sin\theta_i} \tag{4.119}$$

$$\vec{e}_1 = \hat{n}/\sin\theta_i \tag{4.120}$$

$$\hat{n} = \hat{\imath} \sin\epsilon \sin\alpha + \hat{\jmath} \sin\epsilon \cos\alpha - \hat{k} \cos\epsilon \tag{4.121}$$

$$\hat{R}_2 = \hat{\imath} \cos\epsilon_2 \sin(\beta_1 - \alpha) - \hat{\jmath} \cos\epsilon_2 \cos(\beta_1 - \alpha) + \hat{k} \sin\epsilon_2 \tag{4.122}$$

After some algebra we obtain

$$\left(\frac{V}{C_o F_2} \right)_1 = \left[- (\hat{n} \cdot \hat{n}_i) \hat{k} \cdot (\hat{r}' \times \hat{n}) + \hat{k} \cdot (\hat{r}' \times \hat{n}_i) \right] \frac{(-1 + \alpha_D T_H - R_H)(\vec{e}_1 \cdot \hat{u})}{\sin\theta_i}$$

$$\tag{4.123}$$

where

$$\hat{k} \cdot (\hat{r}' \times \hat{n}) = \cos\varepsilon_2 \sin\varepsilon \sin\beta_1 \qquad (4.124)$$

$$(\hat{n} \cdot \hat{n}_i) = \sin\varepsilon \cos\theta_1 \cos\gamma_1 - \cos\varepsilon \sin\theta_1 \qquad (4.125)$$

$$\hat{k} \cdot (\hat{r}' \times \hat{n}_i) = \cos\varepsilon_2 \cos\theta_1 \sin(\beta_1 + \gamma_1) \qquad (4.126)$$

$$\sin\theta_i = |\hat{n} \times \hat{n}_1|$$

$$= \Big\{ \sin^2\theta_1 \sin^2\varepsilon + \cos^2\theta_1 \cos^2\varepsilon + \cos^2\theta_1 \sin^2\varepsilon \sin^2\gamma_1$$

$$+ 2\sin\theta_1 \cos\theta_1 \sin\varepsilon \cos\varepsilon \cos\gamma_1 \Big\}^{1/2} \qquad (4.127)$$

Also we obtain

$$\left(\frac{V}{C_o F_2}\right)_2 = - \Big[(\hat{r}' \cdot \hat{n}_i) \ \hat{k} \cdot (\hat{r}' \times \hat{n}) - (\hat{r}' \cdot \hat{n}) \ \hat{k} \cdot (\hat{r}' \times \hat{n}_i) \Big]$$

$$\times \Big[(\hat{n} \cdot \hat{n}_i) (-1 + \alpha_D T_H + R_H) (\vec{e}_1 \cdot \hat{n}) \Big] \Big/ \sin\theta_i \qquad (4.128)$$

where

$$\hat{r}' \cdot \hat{n}_i = -\cos\varepsilon_2 \cos\theta_1 \cos(\beta_1 + \gamma_1) + \sin\varepsilon_2 \sin\theta_1 \qquad (4.129)$$

$$\hat{r}' \cdot \hat{n} = -\cos\varepsilon_2 \sin\varepsilon \cos\beta_1 - \sin\varepsilon_2 \cos\varepsilon \qquad (4.130)$$

and

$$\left(\frac{V}{C_o F_2}\right)_3 = - \Big[(\hat{r}' \cdot \hat{n}_i)(\hat{r}' \cdot \hat{k}) - (\hat{n}_i \cdot \hat{k})$$

$$- (\hat{n} \cdot \hat{n}_i) \Big\{ (\hat{r}' \cdot \hat{n})(\hat{r}' \cdot \hat{k}) - (\hat{n} \cdot \hat{k}) \Big\} \Big]$$

$$\times \Big[(-1 + \alpha_D T_E - R_E)(\vec{e}_3 \cdot \hat{U}) \Big] \Big/ \sin\theta_i \qquad (4.131)$$

93

where

$$\hat{R}_2 \cdot \hat{k} = \sin\varepsilon_2 \qquad (4.132)$$

$$\hat{n}_i \cdot \hat{k} = \sin\theta_1 = (M - H_A)/R' \qquad (4.133)$$

$$\hat{n} \cdot \hat{k} = -\cos\varepsilon \qquad (4.134)$$

and

$$\left(\frac{V}{C_o F_2}\right)_4 = -\left[(\hat{r} \cdot \hat{n}_i)(\hat{n} \cdot \hat{k}) - (\hat{r}' \cdot \hat{n})(\hat{n}_i \cdot \hat{k})\right]$$

$$\times \left[(\hat{n} \cdot \hat{n}_i)(-1 + \alpha_D T_E + R_E)(\vec{e}_3 \cdot \hat{U})\right] \bigg/ \sin\theta_i \qquad (4.135)$$

For the special case where $\hat{u}$ is assumed to be horizontal we obtain

$$\frac{(\vec{e}_1 \cdot \hat{u})}{\sin\theta_i} = -\frac{\sin\varepsilon \, \sin\gamma_1}{(\sin\theta_i)^2} \qquad (4.136)$$

and

$$\frac{\vec{e}_3 \cdot \hat{u}}{\sin\theta_i} = \frac{\cos\theta_1 \cos\varepsilon + \sin\theta_1 \sin\varepsilon \, \cos\gamma_1}{(\sin\theta_i)^2} \qquad (4.137)$$

In general $\hat{u}$ is not horizontal in which case we write out the components of $\vec{e}_1$ and $\vec{e}_3$ from Equations 4.119 and 4.120.

$$\vec{e}_1 = \frac{1}{\sin\theta_i}[\hat{i} \, \sin\varepsilon \, \sin\alpha + \hat{j} \, \sin\varepsilon \, \cos\alpha - \hat{k} \, \cos\varepsilon] \qquad (4.138)$$

$$\vec{e}_3 = \frac{1}{\sin\theta_i} \left[\hat{i}(\sin\theta_1 \sin\varepsilon \cos\alpha + \cos\theta_1 \cos\varepsilon \sin\vartheta) \right.$$

$$- \hat{j}(\sin\theta_1 \sin\varepsilon \sin\alpha + \cos\theta_1 \cos\varepsilon \cos\vartheta)$$

$$\left. - \hat{k}(\cos\theta_1 \sin\varepsilon \sin\gamma_1) \right] \tag{4.139}$$

Accordingly, when the components of $\hat{u}$ are determined the products $\vec{e}_1 \cdot \hat{u}$ and $\vec{e}_3 \cdot \hat{u}$ can be computed for the general case of a non-horizontally polarized electric field incident on the slanted dielectric slab.

APPENDIX A. THE FRESNEL APPROXIMATION

I. INTRODUCTION

Equations (2.47) and (2.48) of this report describe the scattered magnetic and electric fields in the Fraunhofer zone of a perfectly conducting scatterer. These equations represent the leading terms in the asymptotic expansions of Equations (2.39) and (2.42) for large values of the distance between the scatterer and the receiver. Let D denote some characteristic linear dimension of the scatterer, and let r' denote the distance from some point on the surface of the scatterer to the receiver. The assumptions involved in the Fraunhofer approximation can be summarized as follows.

$$r' \gg D \qquad (A.1)$$

$$D^2/2r' \ll \lambda \qquad (A.2)$$

where λ is the wavelength of the incident radiation. In this appendix, condition (A.2) will be relaxed, and Fresnel zone approximations for the scattered fields will be developed and then applied to the problem of localizer signal scattering by a flat, vertical wall. The motivation for this new approximation is the ongoing construction of very tall buildings (motels, 747 hangars, etc.) near airport runways. For such structures, condition (A.2) is often violated, at least over portions of the aircraft approach paths.

II. ANALYSIS

The asymptotic expansions of Equations (2.39) and (2.42) for large values of r' were performed upon the phases and amplitudes of the two-point Green's function $\varphi(\vec{r}',\vec{r})$ and its derivatives which appear in those equations. The function φ is given by

$$\varphi(\vec{r}',\vec{r}) = \frac{e^{ik|\vec{r}'-\vec{r}|}}{|\vec{r}'-\vec{r}|} \qquad (A.3)$$

where $k = 2\pi/\lambda$ is the wave number of the incident radiation, and $\vec{r}'$ and $\vec{r}$ denote respectively, the position vector of the receiver and the position vector of a point on the illuminated surface of the scatterer relative to an origin of coordinates 0 which, for convenience, we locate on the surface of the scatterer. Let D denote the largest value assumed by $r = |\vec{r}|$. D represents some characteristic dimension of the scatterer. If $r' \gg D$ (condition (A.1)), the amplitude $|\vec{r}' - \vec{r}|^{-1}$ of ψ can be approximated very accurately simply by $(\vec{r}')^{-1}$. More care must be exercised in approximating the phase of ψ because of the oscillatory behavior of the complex exponential. Expanding $|\vec{r}' - \vec{r}|$ to terms of second order in r, we find

$$|\vec{r}' - \vec{r}| = r' - \hat{r}' \cdot \vec{r} + \frac{r^2}{2r'} - \frac{(\hat{r}' \cdot \vec{r})^2}{2r'} \qquad (A.4)$$

where $\hat{r}' = \vec{r}'/r'$ is a unit vector in the direction of $\vec{r}'$. If $D^2/2r' \ll \lambda$ (condition (A.2)), we can clearly neglect the quadratic terms in (A.4) and use the first two terms in approximating the phase of ψ for large values of r'. This "linear" representation for the phase of ψ is just the Fraunhofer approximation used in Section 2.0 of this report. If $D^2/2r'$ is not small compared to λ, the quadratic terms in (A.4) cannot be ignored, and we arrive at the following asymptotic representation for ψ:

$$\psi(\vec{r}', \vec{r}) = \frac{e^{ikr'}}{r'} \cdot e^{-ik(\hat{r}' \cdot \vec{r})} \cdot e^{ik\left[\frac{r^2}{2r'} - \frac{(\hat{r}' \cdot \vec{r})^2}{2r'}\right]} \qquad (A.5)$$

Equation (A.5) is the asymptotic representation of the Green's function ψ in the Fresnel zone of the scatterer. It should be emphasized that in deriving Equation (A.5), we have assumed that the phase of the Green's function can be accurately represented by expanding $|\vec{r}' - \vec{r}|$ to terms of only second order in r. That is to say, it has been assumed that all higher order terms are small compared to a wavelength.

When the asymptotic expression for ψ given in Equation (A.5) together with the corresponding asymptotic expressions for the various derivatives of ψ are substituted into Equations (2.37) and (2.39), the following asymptotic expressions for the scattered

fields in the Fresnel zone of a conducting scatterer are obtained:

$$\vec{H}_S(\vec{r}') = - \frac{ik}{2\pi} \frac{e^{ikr'}}{r'} \hat{r}' \times \int_{S_+} (\hat{n}\times\vec{H}_i)e^{-ik\phi(\vec{r}',\vec{r})}ds \ , \qquad (A.6)$$

$$\vec{E}_S(\vec{r}') = \frac{ik}{2\pi} \left(\frac{\mu}{\epsilon}\right)^{1/2} \frac{e^{ikr'}}{r'} \cdot \hat{r}' \times \left[\hat{r}' \times \int_{S_+} (\hat{n}\times\vec{H}_i)e^{-ik\phi(\vec{r}',\vec{r})}ds\right]$$

$$(A.7)$$

where

$$\phi(\vec{r}',\vec{r}) = \hat{r}'\cdot\vec{r} - \left[\frac{r^2}{2r'} - \frac{(\hat{r}'\cdot\vec{r})^2}{2r'}\right] \qquad (A.8)$$

In Equations (A.6) and (A.7), S_+ denotes the side of the surface of the scatterer directly exposed to the incident radiation, $\vec{H}_i$ is the incident magnetic field on S_+ and $\hat{n}$ is the unit inward normal to S_+ at $\vec{r}$.

III. LOCALIZER SIGNAL SCATTERING BY A FLAT, VERTICAL WALL
     IN THE FRESNEL APPROXIMATION

In Section 2.5 the problem of localizer signal scattering by a flat, vertical wall was analyzed using the Fraunhofer approximation. This same problem will now be treated using the Fresnel equations (A.6) and (A.7). The geometry of the problem is illustrated in Figure 2.5.

It was shown in Section 2.5 that the total incident magnetic field $\vec{H}_i$ (direct plus ground reflected) at an observation point (x,y,z) in the far field of a horizontally polarized localizer antenna located at $(0,0,H)$ could be represented as follows:

$$\vec{H}_i = - \hat{e}_z \left(\frac{\epsilon}{\mu}\right)^{1/2} E_0 f(\phi) \frac{e^{ikR}}{R} \left[1 - e^{2ikzH/D_p}\right] \ , \qquad (A.9)$$

where

$$R = \sqrt{x^2 + y^2 + (z-H)^2} \ , \qquad (A.10)$$

$$D_p = \sqrt{x^2 + y^2} \qquad (A.11)$$

A-3

$$\phi = \tan^{-1} (y/x) \tag{A.12}$$

In Equation (A.9), $f(\phi)$ is the horizontal antenna pattern of the localizer, E_o is an amplitude, and $\hat{e}_z$ is a unit vector along the z-axis which is perpendicular to the perfectly conducting, flat ground plane (the x-y plane). Equation (A.9) accurately describes $\vec{R}_i$ at observation points with small elevation angles $(z/D_p \ll 1)$.

As in Section 2.5, we will use the midpoint of the base of the wall as an origin of coordinates for the surface integrals in (A.6) and (A.7). The coordinates of this point will be denoted by $(x_1, y_1, 0)$. The azimuth angle of $(x_1, y_1, 0)$ will be denoted by ϕ $(\phi = \tan^{-1}(y_1/x_1))$. We again assume, as in Section 2.0, that

$$D_{p1} = \sqrt{x_1^2 + y_1^2}$$

is much greater than the length, L, of the wall, so that $f(\phi)$ can be replaced by $f(\phi)$ and D_p by D_{p1} in (A.9) for all points on the wall. The vector $\vec{R}$ from the localizer to any point P on the wall can be represented as follows:

$$\vec{R} = \vec{R}_1 + \vec{r} \quad , \tag{A.13}$$

where $\vec{R}_1 = x_1\hat{e}_x + y_1\hat{e}_y - H\hat{e}_z$ and $\vec{r}$ is a vector in the plane of the wall drawn from the point $(x_1, y_1, 0)$ to the point P. Assuming that

$$R_1 = \sqrt{x_1^2 + y_1^2 + H^2}$$

is much larger than the largest dimension of the wall, the distance R from the localizer to P can be represented to terms of second order in r, as follows:

$$R = R_1 + \hat{R}_1 \cdot \vec{r} + \frac{r^2}{2R_1} - \frac{(\vec{r} \cdot \hat{R}_1)^2}{2R_1} \quad , \tag{A.14}$$

where $\hat{R}_1 = \vec{R}_1/R_1$. In Section 2.5, the quadratic path length difference terms in (A.14) were neglected (cf. Eq.(2.64)). For the present analysis, these terms will be retained for the sake of consistency, since the terms of second order in r in the series expansion of the Green's function Ψ are being retained (cf. Eq. (A.4)).

The vector $\vec{r}$ from $(x_1, y_1, 0)$ to the point P on the wall can be represented as follows:

$$\vec{r} = \eta \hat{\eta} + z \, \hat{e}_z \tag{A.15}$$

where $\hat{\eta}$ is a unit vector in the plane of the wall and parallel to the ground (Fig. 2.5) and η is variable ranging from $-L/2$ to $+L/2$. The variable z is just the elevation of the point P above the ground and varies from 0 to h where h is the height of the wall. In Section 2.5, the following approximate expression for the dot product $(\hat{R}_1 \cdot \vec{r})$ was derived:

$$\hat{R}_1 \cdot \vec{r} = \eta \cos(\theta + \psi) - \frac{zH}{D_{pl}} \quad , \tag{A.16}$$

where θ is the angle between $\hat{\eta}$ and the x-axis (Fig. 2.5). Substituting (A.16) into (A.14) and approximating R_1^{-1} by D_{pl}^{-1} in the last two terms of (A.14), we obtain the following approximate expression for the distance R from the localizer to any point P on the wall:

$$R = R_1 + \eta \cos(\theta + \psi) - \frac{zH}{D_{pl}} + \frac{\eta^2}{2D_{pl}} \sin^2(\theta + \psi) + \frac{z^2}{2D_{pl}} \, , \tag{A.17}$$

where terms of order $(D_{pl})^{-2}$ and higher have been dropped. Substituting Equation (A.17) for R into the complex exponential in Equation (A.9) and replacing the factor R^{-1} by R_1^{-1}, we finally obtain the following approximate expression for $\hat{H}_i$ at a point P on the surface of the wall:

$$\vec{H}_i = 2i \, \hat{e}_z \left(\frac{\varepsilon}{\mu}\right)^{1/2} E_0 \, f(\psi) \, \frac{e^{ikR_1}}{R_1} \, e^{ik\eta \cos(\theta + \psi)} \, \sin \frac{kzH}{D_{pl}}$$

$$\cdot \, e^{ik\left[\eta^2 \sin^2(\theta + \psi) + z^2\right]/2D_{pl}} \quad . \tag{A.18}$$

Let (x_2, y_2, z_2) denote the coordinates of the receiver. The vector $\vec{r}'$ from the base of the wall to the receiver is given by

$$\vec{r}' = (x_2 - x_1)\hat{e}_x + (y_2 - y_1) \, \hat{e}_y + z_2 \hat{e}_z \quad . \tag{A.19}$$

Let R_2 denote $r' = |\vec{r}'|$:

$$R_2 = \sqrt{(x_2 - x_1)^2 + (y_2 - y_1)^2 + z_2^2} \quad . \tag{A.20}$$

The horizontal distance from $(x_1, y_1, 0)$ to the receiver will be denoted by D_{p2}:

$$D_{p2} = \sqrt{(x_2 - x_1)^2 + (y_2 - y_1)^2} \quad . \tag{A.21}$$

Assuming small elevation angles $(D_{p2} \gg z_2)$, it was shown in Section 2.5 that the dot product $\hat{r}' \cdot \vec{r}$ could be represented approximately as follows:

$$\hat{r}' \cdot \vec{r} \approx \eta \cos(\gamma - \theta) + \frac{z\, z_2}{D_{p2}} \quad , \tag{A.22}$$

where γ is the angle between the projection of $\vec{r}'$ onto the ground plane and the x-axis (cf.Fig. 2.5). Substituting (A.22) into Equation (A.8), which defines the phase function $\phi(\vec{r}', \vec{r})$ appearing in (A.6) and (A.7), we obtain the following approximate expression for ϕ:

$$\phi(\vec{r}', \vec{r}) \approx \eta \cos(\gamma - \theta) + \frac{z\, z_2}{D_{p2}} - \frac{\eta^2}{2D_{p2}} \sin^2(\gamma - \theta) - \frac{z^2}{2D_{p2}} \quad , \tag{A.23}$$

where $(r')^{-1} = R_2^{-1}$ has been approximated by D_{p2}^{-1} in the second and third terms of (A.8) and terms of order D_{p2}^{-2} and higher have been neglected.

Equations (A.18) and (A.23) for $\vec{H}_i$ and $\phi(\vec{r}', \vec{r})$ can now be substituted into Equation (A.6) and (A.7) and the integrals evaluated. As in Section 2.5, the range of the z integration is taken to be $-\underline{h} < z \leq +h$ in order to account for the image of the wall in the ground plane. The results of these integrations for the magnitude of the scattered electric field at the receiver is given below:

$$E_s = \frac{2ik}{\pi} E_0\, f(\psi)\, \frac{e^{ik(R_1 + R_2)}}{R_1 R_2} \sin(\gamma - \theta)\, I_1 I_2 \quad , \tag{A.24}$$

A-6

where

$$I_1 = \int_0^h \sin\left[\frac{kHz}{D_{p1}}\right] \sin\left[\frac{kz_2 z}{D_{p2}}\right] e^{ikz^2 \left(\frac{1}{2D_{p1}} + \frac{1}{2D_{p2}}\right)} dz \quad , \qquad (A.25)$$

and

$$I_2 = \int_{-L/2}^{+L/2} e^{ik\eta\left[\cos(\theta+\psi) - \cos(\gamma-\theta)\right]} e^{ik\eta^2\left[\frac{\sin^2(\theta+\psi)}{2D_{p1}} + \frac{\sin^2(\gamma-\theta)}{2D_{p2}}\right]} d\eta$$

$$(A.26)$$

Unfortunately, the integrals I_1 and I_2 cannot be evaluated in closed form. However, they can be evaluated numerically using series representations for the complex Fresnel function $F(x)$.

$$F(x) \equiv \int_0^x e^{i\frac{\pi}{2}t^2} dt \quad . \qquad (A.27)$$

IV. COMPARISONS OF THE FRAUNHOFER AND FRESNEL FORMULATIONS

In the Fraunhofer approximation used in Section 2.5, the integrals I_1 and I_2 defined by Equations (A.25) and (A.26) assume the following simple forms:

$$I_1' = \int_0^h \sin\left[\frac{kHz}{D_{p1}}\right] \sin\left[\frac{kz_2 z}{D_{p2}}\right] dz \quad , \qquad (A.28)$$

$$I_2' = \int_{-L/2}^{+L/2} e^{ik\eta\left[\cos(\theta+\psi) - \cos(\gamma-\theta)\right]} d\eta \qquad (A.29)$$

Of course the integrals appearing in Equations (A.28) and (A.29) can be explicitly evaluated and, in fact, are proportional to the sinc functions appearing in Equation (2.84) which gives the scattered electric Field E_s in the Fraunhofer zone of the wall. However, for purposes of comparison, I_1' and I_2' will be left in integral form.

A-7

It is obvious that the "Fraunhofer" integrals I_1' and I_2' are obtained from the corresponding "Fresnel" integrals I_1 and I_2 by suppressing the complex exponentials in the integrals of I_1 and I_2 which depend upon z^2 and η^2, respectively. The Fraunhofer approximation is thus seen to be based upon the assumption that the following inequalities hold true for all receiver points:

$$A = kh^2 \left(\frac{1}{2D_{p1}} + \frac{1}{2D_{p2}} \right) << 1 \quad , \tag{A.30}$$

$$B = \frac{kL^2}{4} \left[\frac{\sin^2(\theta+\psi)}{2D_{p1}} + \frac{\sin^2(\gamma-\theta)}{2D_{p2}} \right] << 1 \quad . \tag{A.31}$$

The validity of the Fraunhofer approximation as summarized in the inequalities (A.30) and (A.31) will now be examined.

In practice, the inequalitily (A 31) is generally satisfied, since our computer programs automatically segment walls into subsections no more than 50 feet in length. The scattered field at the receiver produced by each subsection is calculated using either Equation (2.84) or (A.24). These partial fields are then summed to give the total field at the receiver due to the entire wall. This segmenting procedure is necessary to ensure the validity of our assumption that $f(\phi)$, the horizontal antenna pattern of the localizer, does not vary significantly as η ranges from $-L/2 \leq \eta \leq +L/2$ and that $f(\phi)$ can be approximated very accurately by $f(\psi)$ for all points on the wall. To get some idea of the magnitude of the parameter B appearing in (A.31), consider the following set of typical parameters:

$$D_{p1} = 4000 \text{ ft}$$

$$D_{p2} = 4000 \text{ ft}$$

$$L = 50 \text{ ft}$$

$$k = 2\pi/\lambda = .706 \ (\text{ft})^{-1}$$

The value of k listed above corresponds to a localizer wavelength of 8.9 ft. Setting $(\theta+\psi)$ and $(\gamma-\theta)$ equal to $90°$ (worst case), we find that $B = .11$. Consequently, the approximation $B << 1$ inherent in the Fraunhofer approximation is reasonably good, and, conse-

quently, differences between the integrals I_2 (A.26) and I_2' (A.29) will generally be negligible in most cases of interest.

On the other hand, the inequality (A.30) involving the parameter A is often violated for tall walls. Consider, for example, the case of a wall 100 feet high (h=100 ft). Using the same values for D_{p1}, D_{p2}, and k that were used in the previous simple calculation of the parameter B, we find that A = 1.77. Consequently, since the Fraunhofer approximation is only valid if A<<1, we can expect to see significant differences between the values of I_1 and I_1' and, hence, between the values of the scattered fields predicted by the Fraunhofer and Fresnel models when very tall scatterers are involved.

Specifically, we can certainly expect to see phase differences between the scattered fields predicted by the two models, since I_1 is complex and I_1' is real. Furthermore, the intensities of the scattered fields predicted by the two models will differ, since the magnitude of $I_1 (|I_1|)$ will generally be less than the magnitude of $I_1' (|I_1'|)$. To demonstrate this fact, we first define the following two functions:

$$f(z) = \sin\left[\frac{kHz}{D_{p1}}\right] \sin\left[\frac{kz_2 z}{D_{p2}}\right] \quad , \qquad (A.32)$$

$$g(z) = \frac{kz^2}{2}\left(\frac{1}{D_{p1}} + \frac{1}{D_{p2}}\right) \quad . \qquad (A.33)$$

In terms of f and g, I_1 and I_1' can be written as follows:

$$I_1 = \int_0^h f(z)\, e^{ig(z)}\, dz \quad , \qquad (A.34)$$

$$I_1' = \int_0^h f(z)\, dz \quad . \qquad (A.35)$$

Clearly, $|I_1|$ must satisfy the following inequality:

$$|I_1| \le \int_0^h |f(z)|\, dz \qquad (A.36)$$

A-9

For the small angles of elevation which we have assumed $(H/D_{p1} \ll 1, z_2/D_{p2} \ll 1)$, the function $f(z)$ will generally be non-negative for all z in the range $o \le z \le h$ even for relatively large values of h. That is to say, in most cases of interest, $|f(z)| = f(z)$ $(o \le z \le h)$. Under this assumption, the inequality (A.36) becomes

$$|I_1| \le \int_o^h f(z)dz = I_1' = |I_1'| \qquad (A.37)$$

As a consequence of the inequality (A.37) we can conclude that, in most cases of interest, the intensity of the scattered field predicted by the Fresnel model is generally less than the intensity predicted by the Fraunhofer model.

Figures A.1, A.2, and A.3 show comparative plots of DDM in microamps, as predicted by the Fraunhofer and Fresnel scattering models. The scatterers involved are flat, vertical walls 50 feet wide and 25, 50, and 100 feet in height respectively. The walls are oriented parallel to the centerline of the runway. The aircraft is assumed to be flying at a constant altitude of 50 feet down the centerline of the runway, so that in the absence of scatterers the DDM would be identically 0. The abscissa in each figure represents distance from the localizer in feet. In each graph, the dashed line represents the predictions of the Fresnel model, while the solid line represents the predictions of the Fraunhofer model.

Referring to Fig. A.1, we note that, for a wall only 25 feet high, there is very little difference between the predictions of the two models. This was to be expected, since for small heights, the parameter A defined in Equation (A.30) is likely to be small compared with unity, and, consequently, the predictions of the Fresnel and Fraunhofer models should be nearly identical.

Referring to Figure A.2, we see that there are slight differences in both phase and amplitude between the predictions of the two models for a wall 50 feet in height.

A-10

Finally, in Figure A.3, we note major differences in both amplitude and phase between the two models for a wall 100 feet in height. The Fraunhofer model predicts DDM magnitudes which are nearly twice the corresponding values predicted by the Fresnel model over portions of the flight path. Differences in the positions of DDM maxima of up to two hundred feet can also be observed.

STATIC RESPONSE
ALPHA(DEG)0.0
X(FT)   3210.0
Y(FT)   470.0
WALL(W*H) 50.0 * 25.0

FRESNEL
FRAUNHOFER

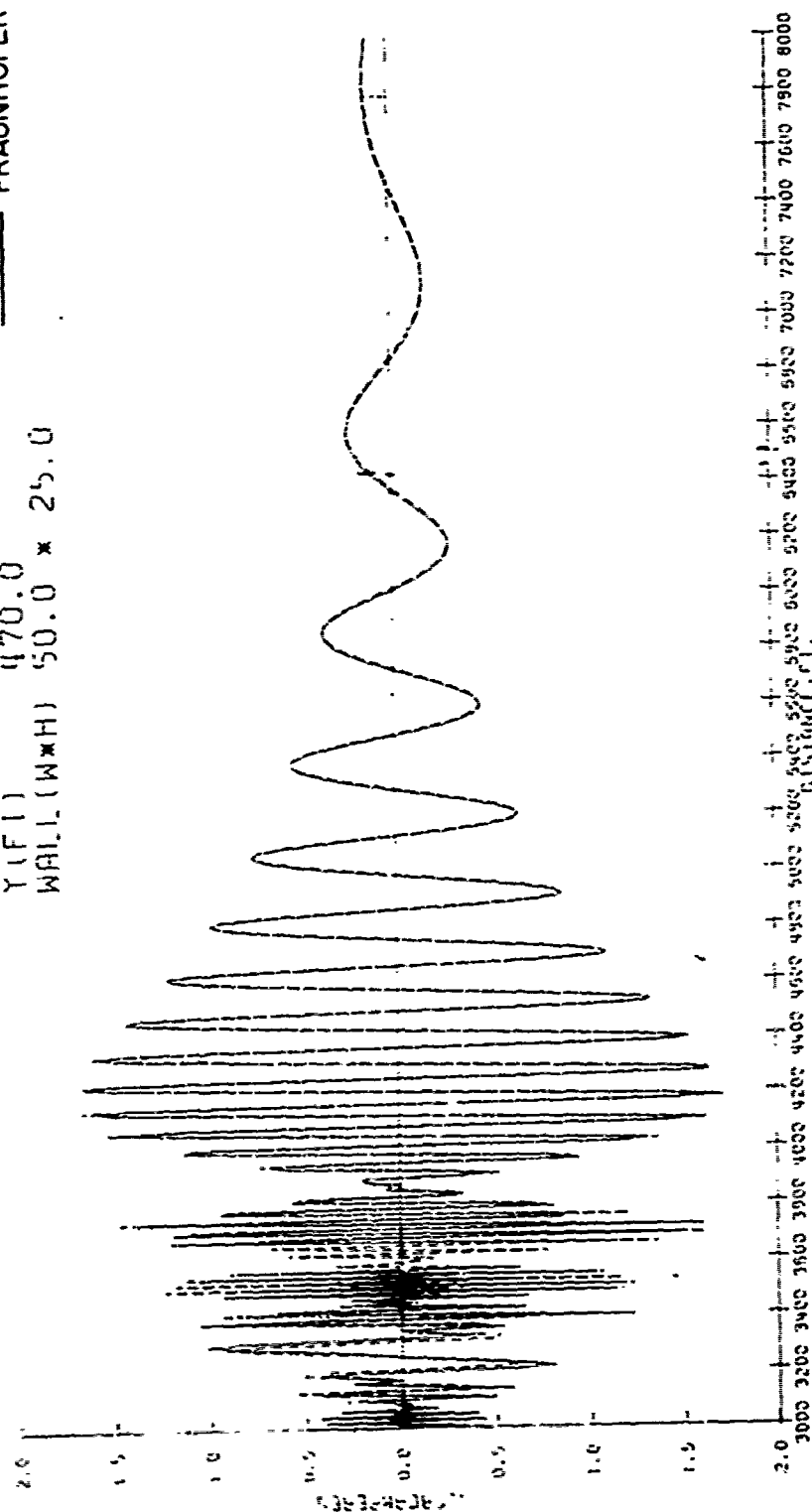Figure A.1 Fresnel and Fraunhofer Approximations Compared, 25-Foot High Wall

A-12
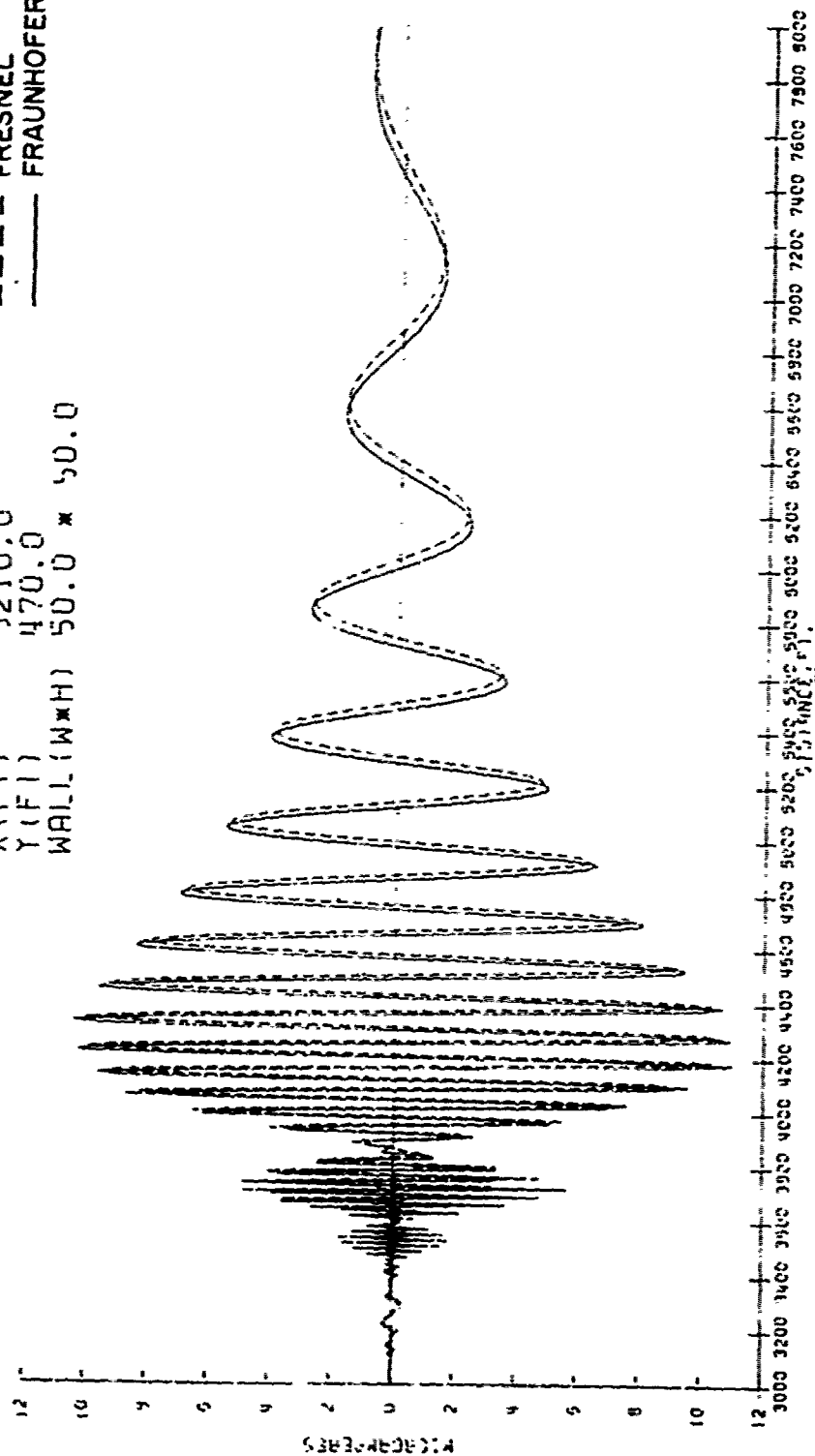
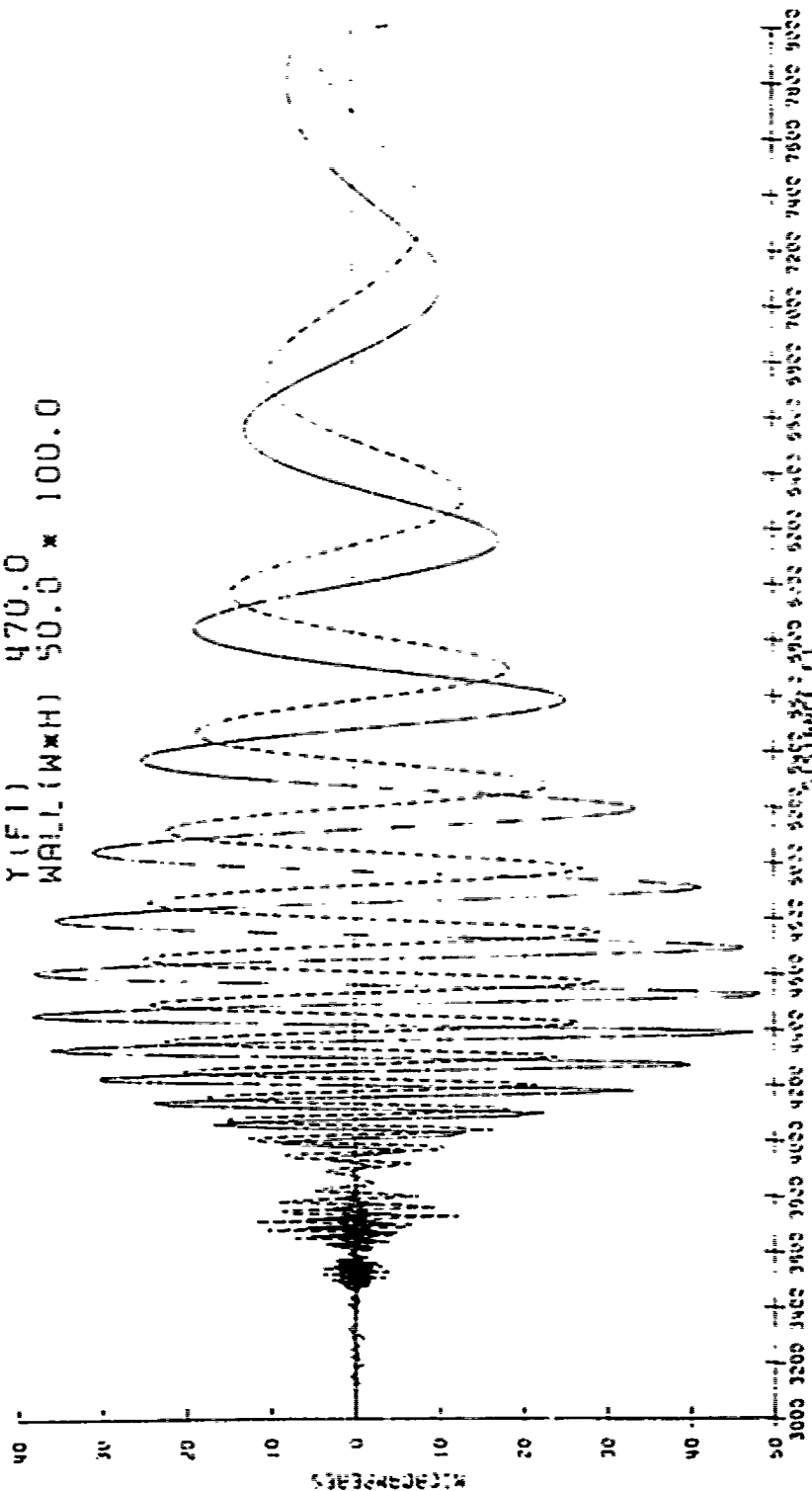Figure A.2. Fresnel and Fraunhofer Approximations Compared, 50-Foot High Wall

A-13

Figure A.3. Fresnel and Fraunhofer Approximations Compared, 100-Foot High Wall

APPENDIX B
SCATTERING FROM A VERTICAL TRIANGLE, NEW FORMULATION

We use the current distribution method to calculate the scattered field for an infinitely conductive triangular surface. The scattered electric far field is (with ground reflections included):

$$\vec{E}_S = \frac{i\omega\mu}{4\pi}\frac{e^{ikR_2}}{R_2}\hat{R}_2 \times \hat{R}_2 \times \vec{I} \tag{B.1}$$

where

$$\vec{I} = 8\left(\frac{\varepsilon}{\mu}\right)^{1/2}\hat{n}E_0 f(\psi)\frac{e^{ikR_1}}{R_1} \int d\xi \int d\eta e^{iA\eta}\sin(m\xi)\sin(n\xi) \tag{B.2}$$

where $A = k(\sin\gamma - \sin\beta)$

$m = kz_2/R_2$

$n = kH_A/D_{pl}$

H_A is the antenna height. For a right triangle with the base on the ground and the vertex to the left the integration, $d\xi$ is from 0 to $h\eta/B + h/2$, and $d\eta$ is from $-B/2$ to $+B/2$. The following result is obtained (Figure B.1):*

$$\vec{E}_S = \frac{k}{2\pi}BE_0 f(\psi)\frac{e^{ik(R_1+R_2)}}{R_2R_1}(\hat{R}_2 \times \hat{k})\cos\beta$$

$$\left\{ \frac{1}{(m-n)}\left[e^{i(m-n)h/2}\text{sinc}\left[\frac{1}{2}(AB+\sigma(m-n)h)\right] \right.\right.$$

$$- e^{-i(m-n)h/2}\text{sinc}\left[\frac{1}{2}(AB-\sigma(m-n)h)\right]\right]$$

$$+ \frac{1}{(m+n)}\left[-e^{i(m+n)h/2}\text{sinc}\left[\frac{1}{2}(AB+\sigma(m+n)h)\right]\right.$$

$$\left.\left. + e^{-i(m+n)h/2}\text{sinc}\left[\frac{1}{2}(AB-\sigma(m+n)h)\right]\right]\right\} \tag{B.3}$$

---

*Note that the angles γ and β defined in Figure B.1 and used here for convenience correspond to the angles $\pi/2-(\theta+\psi)$ and $\pi/2-(\gamma-\theta)$, respectively, used in Section 2.5 and 2.6 of this report.
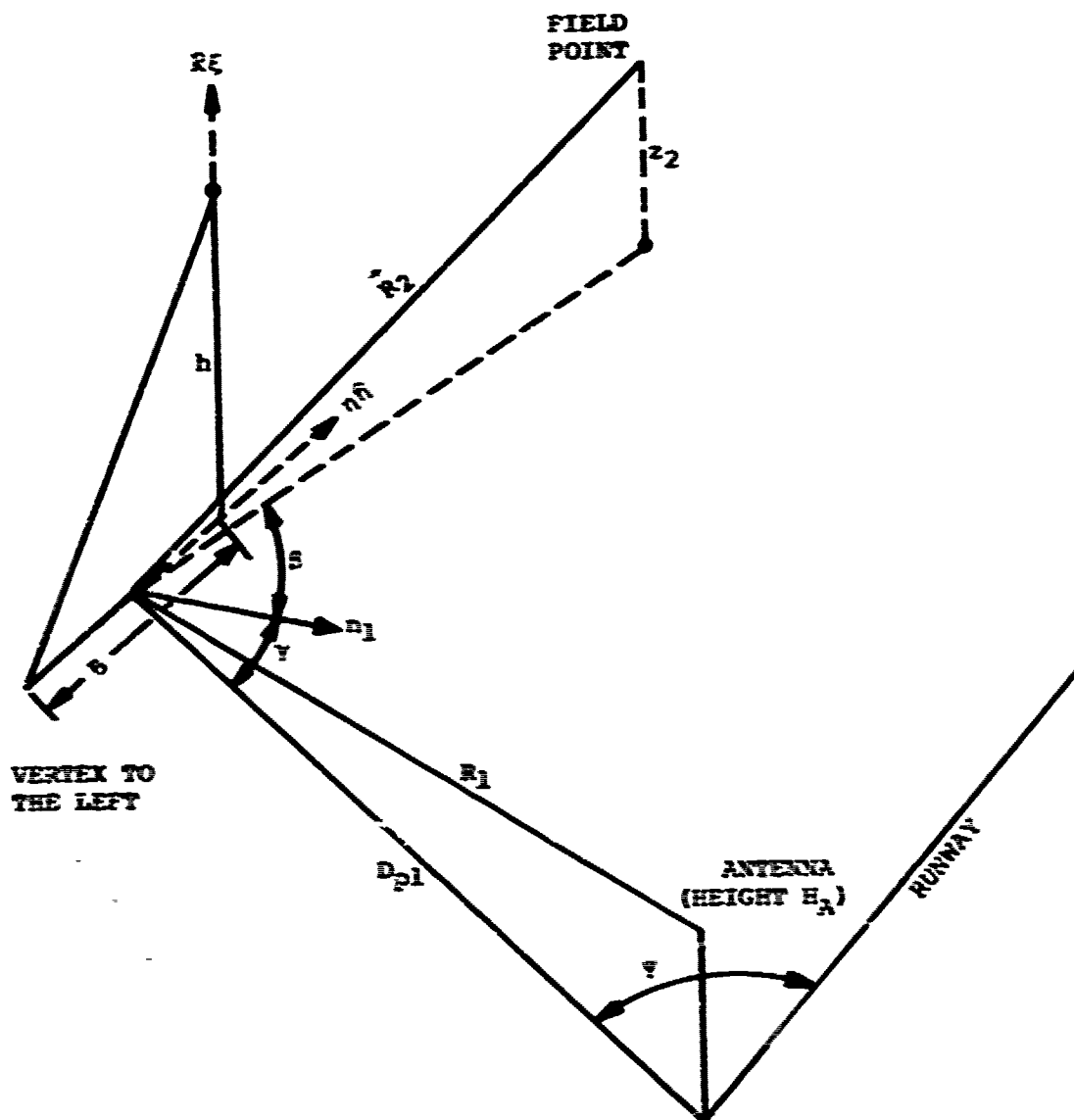
Figure B.1. Geometry for the Scattering from a
Vertical Right Triangle

Figure B.2. Elevated Triangle

For the vertex to the left $c=1$.

For the case of the vertex to the right the integration $d\zeta$ is from 0 to $-h\eta/B + h/2$. The scattered electric field is given by Equation (B.3) with $c=-1$.

For the case of an elevated triangle (Fig. B.2) for the vertex to the left the integration $d\zeta$ is from h_L to $h\eta/B + h/2$ and $d\eta$ from $B(h_L/h - 1/2)$ to $B/2$. The result is then

$$\vec{E}_S = \frac{2k}{\pi}iE_0 f(\psi)\frac{e^{ik(R_1+R_2)}}{R_2 R_1}(\hat{R}_2 \times \hat{k})\cos\hat{s}\times I'$$

(B.4)

where

$$I' = -\frac{1}{4}\left\{\frac{1}{(m-n)}\frac{e^{i(m-n)h/2}}{Y_1}\left[e^{iY_1 B/2} - e^{iY_1 BC}\right]\right.$$
$$-\frac{1}{(m-n)}\frac{e^{-i(m-n)h/2}}{Y_2}\left[e^{iY_2 B/2} - e^{iY_2 BC}\right]$$
$$-\frac{1}{(m+n)}\frac{e^{i(m+n)h/2}}{Y_3}\left[e^{iY_3 B/2} - e^{iY_3 BC}\right]$$
$$\left.+\frac{1}{(m+n)}\frac{e^{-i(m+n)h/2}}{Y_4}\left[e^{iY_4 B/2} - e^{iY_4 BC}\right]\right\}$$

$$+ \left[-\frac{\sin(m-n)h_L}{2(m-n)} + \frac{\sin(m+n)h_L}{2(m+n)} \right] \frac{1}{iA} \left[e^{iAB/2} - e^{iABC} \right] \qquad (B.5)$$

Where

$$Y_1 = A + c(m-n)\frac{h}{B}$$

$$Y_2 = A - c(m-n)\frac{h}{B}$$

$$Y_3 = A + c(m+n)\frac{h}{B} \qquad \qquad (B.6)$$

$$f_4 = A - c(m+n)\frac{h}{B}$$

$$C = h_L/h - 1/2$$
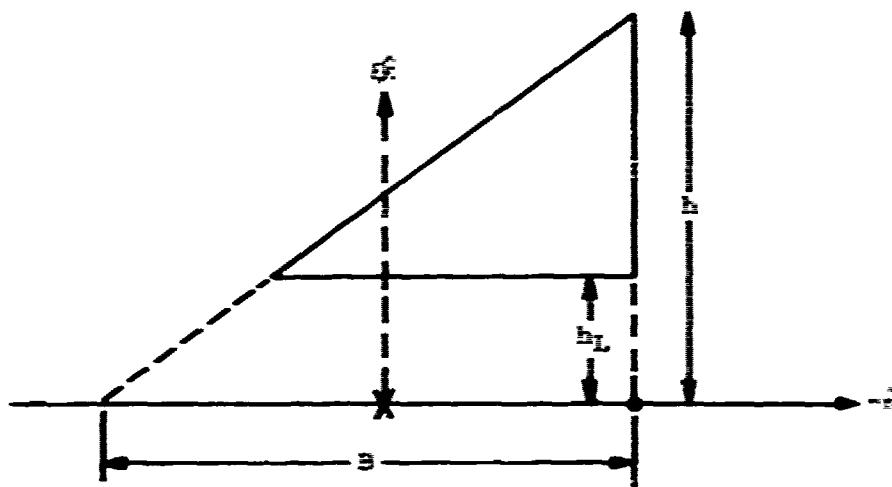
For the vertex to the left $c=1$.

For the case of the vertex to the right the integration $d\xi$ is from h_L to $-h_c/B + h/2$ and $d\eta$ is from $-B/2$ to $B(-h_L/h + 1/2)$. The result is given by Equation (B.4), with

$$I' = -\frac{1}{4} \left\{ \frac{1}{(m-n)} \frac{e^{i(m-n)h/2}}{Y_1} \left[e^{-iY_1BC} - e^{-iY_1B/2} \right] \right.$$

$$- \frac{1}{(m-n)} \frac{e^{-i(m-n)h/2}}{Y_2} \left[e^{-iY_2BC} - e^{-iY_2B/2} \right]$$

$$- \frac{1}{(m+n)} \frac{e^{i(m+n)h/2}}{Y_3} \left[e^{-iY_3BC} - e^{-iY_3B/2} \right]$$

$$\left. + \frac{1}{(m+n)} \frac{e^{-i(m+n)h/2}}{Y_4} \left[e^{-iY_4BC} - e^{-iY_4B/2} \right] \right\}$$

$$+ \left[-\frac{\sin(m-n)h_L}{2(m-n)} + \frac{\sin(m+n)h_L}{2(m+n)} \right] \frac{1}{iA} \left[e^{-iABC} - e^{-iAB/2} \right] \qquad (B.7)$$

where Y_1, Y_2, Y_3 and Y_4 are given by Equation (B.6) but with $c=-1$. Note that Equation (B.7) (with $c=-1$) is just the complex conjugate of Equation (B.5) with $c=1$.

These are the new closed-form solutions for scattering from triangular shapes that are to be incorporated into the computer program.

APPENDIX C
MULTIPLE SCATTERING FROM VERTICAL RECTANGULAR WALLS, NEW FORMULATION

In this appendix we treat the multiple scattering of electromagnetic waves from a set of two vertical rectangular walls where infinite conductivity is assumed. In the double reflection study given by I.B.M.[4] only the reflected field was used in their Equation (2.3). For reflection from a reflecting rectangular wall, the current distribution method yields the same result as given by I.B.M. if the total field is used instead of the reflected field and if the second line integral in the right side of their Equation (2.3) is included. In the following calculation the current distribution method is used to obtain the new equations for double reflection.

The electric field at a point on the second wall is given by (Fig. C.1)*

$$E_p = i \frac{kL_1 h_1 E_o f(\psi)}{\pi R_1 R_2} \exp\left[ik(R_1 + D_{p20} + \eta_2 \sin\gamma_2)\right]$$

$$\cdot \cos\beta_1 \left[\text{sinc}\left[\frac{kL_1}{2}(\sin\gamma_1 - \sin\beta_1)\right]\right]$$

$$\cdot \left\{\text{sinc}\left[kh_1\left[\frac{H}{D_{p1}} - \frac{z_2}{R_2}\right]\right] - \text{sinc}\left[kh_1\left[\frac{H}{D_{p1}} + \frac{z_2}{R_2}\right]\right]\right\} \tag{C.1}$$

where $\text{sinc}(x) = \sin x/x$ and where $k = 2\pi/\lambda$.

At the second wall the incident magnetic field is given by

$$\vec{H}_p \cong \sqrt{\epsilon/\mu} \; E_p(-\hat{k}) \tag{C.2}$$

and the surface current on the wall is given by

---

*Note that the angles γ_1 and β_1 defined in Figure C.1 and used here for convenience correspond to the angles $\pi/2 - (\theta+\psi)$ and $\pi/2 - (\gamma-\theta)$, respectively, used in Sections 2.5 and 2.6.
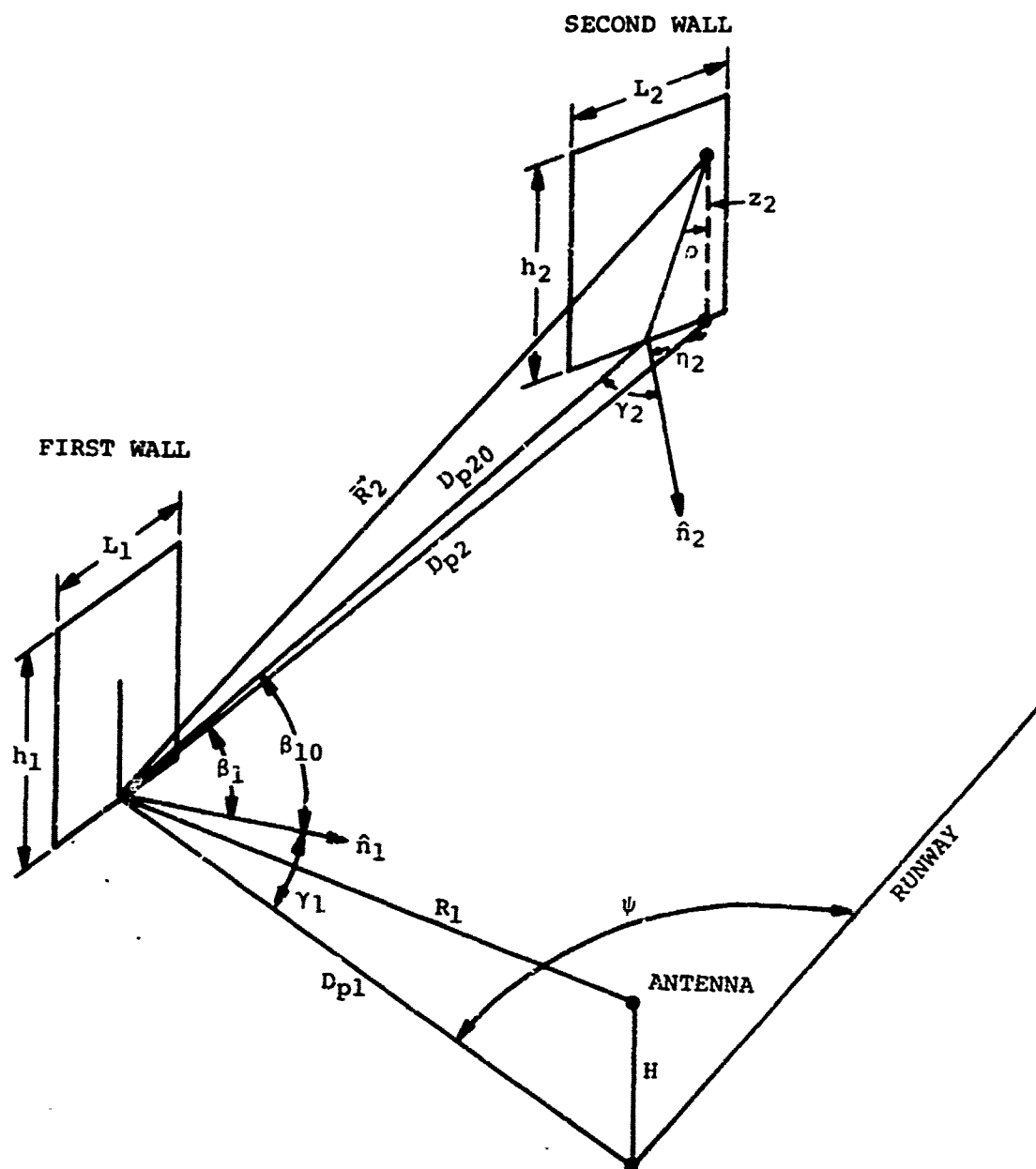
Figure C.1. Double Reflection from Rectangular Walls

$$\vec{J}_2 = - \left(2\vec{H}_p \times \hat{n}_2\right)$$
$$\cong +2 \sqrt{\epsilon/\mu} \, E_p \hat{n}_2 \qquad \text{(C.3)}$$

where n_2 is the outward normal from the scattering surface.

At the receiver the scattered field from the second wall is given by

$$\vec{E}_s = \frac{i\omega\mu}{4\pi} \frac{\exp[ikR_3]}{R_3} \hat{R}_3 \times \left[\hat{R}_3 \times \int -\vec{J}_2 \exp\left[-ik(\vec{\rho} \cdot \hat{R}_3)\right] d\eta_2 dz_2 \right] \qquad \text{(C.4)}$$

Figure C.2. Scattering from the Second Wall

where $\vec{\rho} \cdot \hat{R}_3 \cong \eta_2 \sin\beta_2 + z_2(z_3/R_3)$. $\qquad$ (C.5)

Denoting the integral in Equation C.4 by I,

$$I = -2 \sqrt{\epsilon/\mu} \, \hat{n}_2 i \frac{kL_1 h_1}{\pi} E_0 f(\psi) \frac{\exp[ik(R_1 + D_{p20})]}{R_1 D_{p20}} I_1 I_2 \qquad \text{(C.6)}$$

C-3

where (with ground reflection included)

$$I_1 \cong -2i \int_0^{h_2} \sin\left[kz_2(z_3/R_3)\right] \left\{ \text{sinc}(kh_1\left[\frac{H}{D_{p1}} - \frac{z2}{D_{p2}}\right]) \right. \tag{C.7}$$

$$\left. - \text{sinc}(kh_1\left[\frac{H}{D_{p1}} + \frac{z2}{D_{p2}}\right]) \right\} dz_2$$

and where

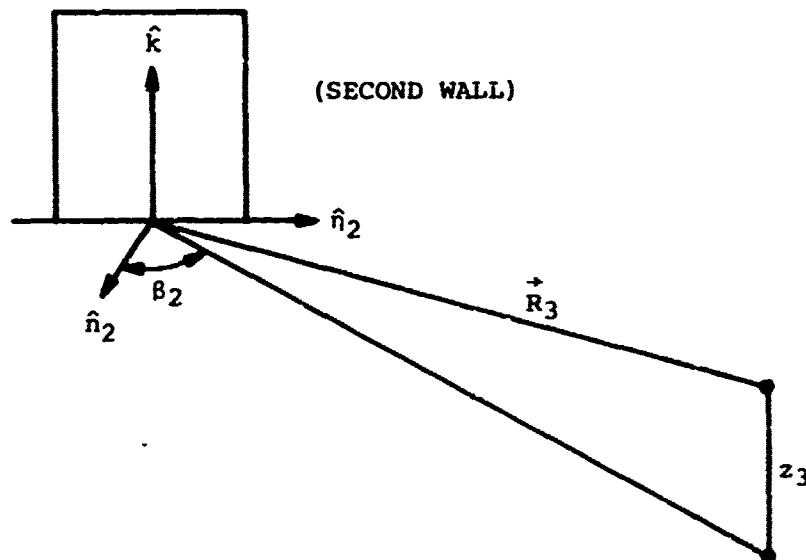$$I_2 = \int_{-L_2/2}^{L_2/2} \exp\left(ik\eta_2\left[\sin\gamma_2 - \sin\beta_2\right]\right) \cos\beta_1 \text{sinc}\left[\frac{kL_1}{2}\left(\sin\gamma_1 - \sin\beta_1\right)\right] d\eta_2$$

$$\cong \cos\beta_{10}\text{sinc}\left[\frac{kL_1}{2}\left(\sin\gamma_1 - \sin\beta_{10}\right)\right] L_2\text{sinc}\left[\frac{L_2}{2}k\left(\sin\gamma_2 - \sin\beta_2\right)\right] \tag{C.8}$$

The scattered electric field at the receiver from the second wall is then given by

$$\vec{E}_s \cong - i\vec{R}_3 \times \hat{k} \frac{k^2}{\pi^2} L_1 L_2 h_1 E_0 f(\psi) \frac{\exp(ik\left[R_1 + D_{p20} + R_3\right])}{R_1 D_{p20} R_3} \cos\beta_2$$

$$\cdot \cos\beta_{10}\text{sinc}\left[\frac{L_2}{2}k(\sin\gamma_2 - \sin\beta_2)\right] \text{sinc}\left[\frac{L_1}{2}k(\sin\gamma_1 - \sin\beta_{10})\right]$$

$$\cdot \left\{ \frac{\sin(AC)}{2B}\left[\int_{C-h_2}^{C+h_2} \frac{\sin(A+B)x}{x}dx - \int_{C-h_2}^{C+h_2} \frac{\sin(A-B)x}{x}dx\right] \right.$$

$$\left. + \frac{\cos(AC)}{2B}\left[\int_{C-h_2}^{C+h_2} \frac{\cos(A+B)x}{x}dx - \int_{C-h_2}^{C+h_2} \frac{\cos(A-B)x}{x}dx\right] \right\} \tag{C.9}$$

where

$$A = kz_3/R_3, \qquad B = \frac{kh_1}{D_{p2}} \cong \frac{kh_1}{D_{p20}}, \qquad C = \frac{D_{p20}H}{D_{p1}} \tag{C.10}$$

and where

$$\int \frac{\sin ax}{x}dx = ax - \frac{(ax)^3}{3\cdot 3!} + \frac{(ax)^5}{5\cdot 5!} - \cdots \tag{C.11}$$

C-4

and

$$\int \frac{\cos\ ax}{x}dx = \log(ax) - \frac{(ax)^2}{2\cdot 2!} + \frac{(ax)^4}{4\cdot 4!} - \dots \qquad (C.12)$$

Combinations of reflections from walls with the lower edge flush against the ground plane can be used to compute the reflection from walls whose lower edges are at a height above the ground plane. The following figures show schematically such a procedure.
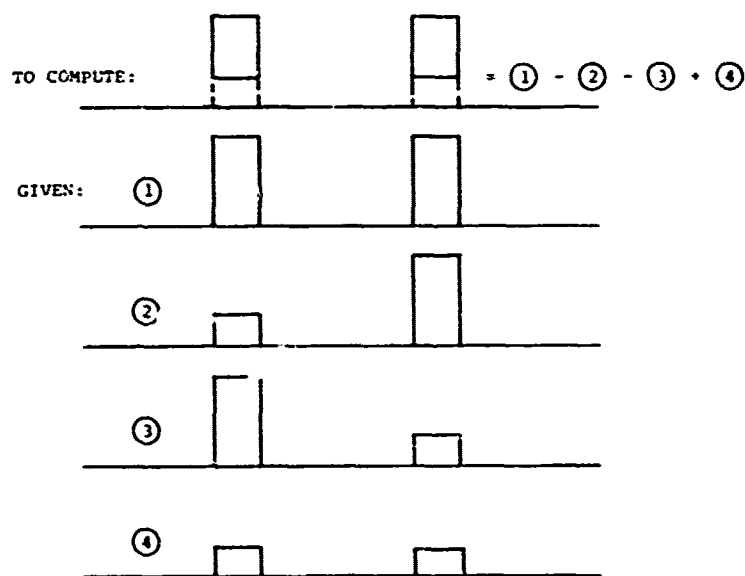
Figure C.3. Elevated Structures

SYMBOLS

R_1 from antenna to reference point on ground plane at 1st wall.

D_{p1} from foot of antenna to reference point at 1st wall.

$f(\psi)$ antenna gain factor.

h_1 height of 1st wall.

L_1 width of 1st wall.

γ_1 angle of incidence at 1st wall.

β_1 look angle from reference point on 1st wall to element of integra. on on 2nd wall.

C-5

β_{1o} look angle from reference point on 1st wall to reference point on 2nd wall.

$\hat{n}_1$ normal vector at 1st wall.

$\vec{R}_2$ vector from reference point on 1st wall to element of integration on 2nd wall.

D_{p20} reference point on 1st wall to reference point on 2nd wall.

D_{p2} reference point on 1st wall to foot of element of integration on 2nd wall.

L_2 width of 2nd wall.

h_2 height of 2nd wall.

$\hat{n}_2$ normal vector at 2nd wall.

$\hat{k}$ unit vector normal to ground plane.

k 2π divided by wavelength.

$\hat{\eta}_2$ unit vector along horizontal direction tangent to wall surface at 2nd wall.

$\vec{\rho}$ vector from reference point on 2nd wall to the element of integration

γ_2 angle of incidence at 2nd wall.

β_2 look angle from 2nd wall to receiver.

$\vec{R}_3$ vector from reference point on 2nd wall to aircraft receiver.

APPENDIX D
DERIVATION OF GAIN VECTOR FOR SMALL CIRCULAR LOOP RECEIVING ANTENNA

We consider a linearly polarized plane wave given by
$\vec{E} = \vec{E}_o e^{i(\vec{k}\cdot\vec{r}-\omega t)}$ incident on a perfectly conducting circular loop
of radius a which is connected to a receiver input impedance Z_L
(Fig. D.1). The current generated in the load impedance Z_L can be
written as

$$I = V/(Z_L + Z_a),\qquad (D.1)$$

where Z_a is the antenna radiation impedance and V is the net
electromotive force (E.M.F. developed in the loop by the incident
field). The E.M.F. is given by the following development of the
basic line integral of E around the loop:

$$\begin{aligned}
V &= \oint \vec{E} \cdot \vec{dl} \\
&= \iint dA\, \hat{n} \cdot \vec{\nabla} \times \vec{E} \\
&= i\vec{E}_o \cdot (\hat{n} \times \vec{k}) \iint r\, dr\, d\phi\, e^{i\vec{k}\cdot\vec{r}} \qquad (D.2)
\end{aligned}$$

Here the vector r lies in the plane of the loop and is perpendicu-
lar to the unit vector $\hat{n}$. We may replace the scalar product in
the exponential by

$$\vec{k} \cdot \vec{r} = k\, r\, \sin\theta\, \cos\phi$$

with the result that the integral reduces to[8]

$$\begin{aligned}
\int_0^a r\, dr \int_{-\pi}^{\pi} d\phi\, e^{2kr \sin\theta \cos\phi} \\
= 2\pi \int r\, dr\, J_o(kr\sin\theta) \\
= 2\pi a^2\, J_1(ka\sin\theta)/(ka \sin\theta) \\
\simeq \pi a^2 \qquad (D.3)
\end{aligned}$$

The latter approximation is valid whenever $a \ll \lambda/2\pi$. Using this
result we find that the current delivered to the receiver can be
expressed as

$$ I = \frac{i\pi a^2 (\hat{n} \times \vec{k}) \cdot \vec{E}_O}{Z_L + Z_a} \tag{D.4} $$

Thus the gain-polarization vector of Equation (D.1) takes the form

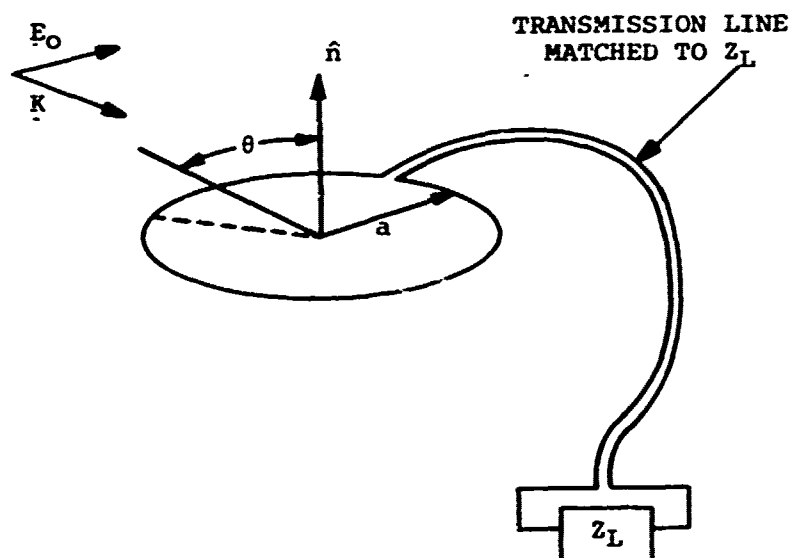$$ \vec{g}(\hat{k}) = C_a \hat{n} \times \hat{k} \tag{D.5} $$

Figure D.1. Illustration of Circular Loop Receiving Antenna Problem

This vector selects the component of $\vec{E}$ normal to the vertical plane of incidence and applies a factor of $\sin\theta$.

APPENDIX E
PROGRAMMING ASPECTS OF THE ILS MODEL

I. INTRODUCTION

The complete simulation of apparent CDI for a large group of ground structures is accomplished by using a sequence of programs. First, the DATGEN set of routines, written for a time-sharing PDP-10 computer, are employed to set up descriptions of antenna patterns, receiver trajectories, scatterer geometry, etc. in the correct formats for input into the ILS-O-E program.

The ILS-O-E program is the basic simulation program, which can be used to calculate static or dynamic CDI along specified receiver trajectories for a variety of antenna and scatterer conditions. The output of this program is usually a formatted listing on tape of CDI versus distance.

If the static CDI has been generated, the dynamic CDI may be obtained with program ILSDYN without further recourse to ILS-O-E. The CDI data are then usually input to the ILSPLOT program for final presentation in graphical form. The ILS-O-E program is a complete operational unit in itself, and its use is detailed below in terms of the input data specifications. However, we do note that since the ILS analysis program and the ILS computer program are presently under development, the ILS-O-E computer program is considered an interim and preliminary, though fully-operational model.

II. DESCRIPTION OF DATA GENERATION PROGRAMS FOR ILS-O-E

A series of programs have been written on the PDP-10 to generate input data for the ILS program. The first of these programs is STRUGN. This is a Structure Generator. It takes section descriptions in free field format and produces a list in the proper format for input to ILS. The sections may be described singly or as polygons or as sections of circles. In the latter case, the arcs will be approximated by a specified number of chords. Any number of sets of sections may be given. Each set is considered a structure and is delimited and numbered in the output list.

E-1

The output of STRUGN (or a combination of the output of several runs) is used as the input to FLDGEN. This is the Field Generation Program. FLDGEN reads in each structure in an input list. It then types out the number of the structure and accepts from the teletype, input, specifying the locations and orientations of the structure. Each structure may appear any number of times on the field or may be omitted completely.

This field description is used as the input to LOCAT. LOCAT takes the field and arbitrary antenna location and orientation and determines where the sections are from the antenna. For each section, LOCAT examines the relative angle of the line of sight and the normal to the section to decide if the section face will receive any incident field from the antenna. It then outputs a list of the sections making up the field. If a section is not illuminated, a flag is set in the output to indicate this. As LOCAT can be run with the same field data and different antenna locations, preparing data for an airport with multiple antenna locations is simplified.

For simple cases, the output of LOCAT can be used as is, but for involved airports, there is a problem of shadowing. A structure section may be facing the antenna location but not have an incident field, because another structure blocks it. To determine if this is the case, a series of programs (SORT 1, SORT 2, SORT 3, PRUN), have been written. These programs take the output from LOCAT and find out which, if any, sections are shadowed and create a new list with flags to indicate the hidden sections. The final program in the series eliminates those that are flagged as shadowed, as well as those flagged by LOCAT. This results not only in an increase in accuracy of the ILS, but, as the hidden sections do not need to have their scattered fields computed, also in a substantial savings in time.

To simplify verification of the input data used in the programs, a plotting program was written. This takes the output from FLDGEN, STRUGN, LOCAT, PRUN or input cards for the 7094 and draws the sections in their proper locations and orientations. The scale

E-2

is variable for convenience in comparing to blueprints, floorplans, etc., and hidden sections may be indicated by dotted lines, if needed.

III. INPUT DATA FOR ILS-O-E

The first input card is the computation mode card. It has the following format:

Col.	Symbol	Contents
1-2	Mode	1 (V-Ring)
		2 (8 Loop)
		3 (Waveguide localizer)
		4 (Not used at present)
		5 (Single measured localizer pattern)
		6 (Measured capture effect localizer pattern)
3-4	IDFC	0 (Fraunhofer approximation)
		1 (Internal switch for Fraunhofer/ Fresnel)
11-20	FRQ	Frequency, MHZ
21-30	THETGS	Glide slope angle, Deg.
31-40	XTH	Distance from loc. antenna to threshold
41-50	Slope	Inclination of runway at threshold, deg.
51-60	ZA (1)	
61-70	ZA (2)	Antenna element heights, ft.
71-80	ZA (3)	

The mode selects the type of antenna pattern used for the simulation. For a single frequency system, a theorectical pattern (V-Ring, 8-Loop, Waveguide) or a measured pattern may be used. Two patterns are used for a dual frequency system, such as the Alford capture effect system. The clearance pattern is chosen first. This is done by using a negative value for the mode number. If a measured pattern is desired for the clearance, a mode of 6 is used. After the clearance pattern is set, the course pattern is chosen. The IDFC switch is used to force the simulation to use the Fraunhofer approximation if desired; otherwise, the Fresnel

approximation will be used for those surfaces with large enough
vertical angles to require it.

If an antenna pattern is to be read in, the following format
is used:

Col.	Contents
1-10	Angle of the measurement in degrees
11-20	Composite sideband pattern as measured
21-30	Composite carrier pattern as measured

The angles must be between plus and minus 180 degrees and in
ascending order. A maximum of fifty measurements is allowed. If
less than fifty are required, the last measurement should be
followed by an angle in excess of 400 degrees.

The next card is the course width card in the following format:

Col.	Symbol	Contents
1-10	XXA (1)	Distance along runway centerline to course array
11-20	XXA (2)	Distance along runway centerline to clearance array
21-30	(Not Used)	
31-40	CW	Course width
41-50	(Not Used)	
51-60	CLS	Relative clearance signal strength

If a course width of greater than three degrees is read in,
this width is used. If a width of less than three degrees is in-
put, the width will be adjusted to FAA specifications according to
the distance to the threshold, as given on the mode card.

The receiver path card follows in the following format:

Col.	Symbol	Contents
1-10	XMIN	Starting distance from origin
11-20	XMAX	Ending distance from origin
21-30	DXR	Spacing between receiver points
31-40	PHIR	Angle of approach
41-50	PSIR	Glide path angle

51-60	(Must be left blank)	
61-70	ZUP	Height above glide path
71-80	(Must be left blank)	

If more than 500 receiver points are requested, the program will increase DXR until not more than 500 will be needed. The number of points is equal to XMAX minus XMIN divided by DXR. If a clearance run is desired, the format of the card is as follows:

Col.	Symbol	Contents
1-10	MIND	Initial angle
11-20	MAXD	Final angle
21-30	DXR	Angular increment
31-50	(Must be left blank)	
51-60	RO	Radius of orbit in feet
61-70	ZUP	Height of orbit
74	ICF	1 (Switch to indicate orbit run)

The next card gives the velocity of the aircraft in feet per second (columns 11-21). As a zero velocity will cause erroneous results, the program sets a minimum velocity of one foot per second.

The next series of cards describe the scattering surfaces. Each surface is a single vertical or tilted flat wall of infinite conductivity.

Col.	Symbol	Contents
1-2	ID	1
3-8	XW (1)	X-Coordinate of center of base
9-14	XW (2)	Y-Coordinate of center base
15-20	XW (3)	Zero
21-24	None	(Blank)
25	C	Zero
26-30	ALPHA	Angle between base line and X-Axis
31-35	DELTA	Zero
36-50	(Must be left blank)	
51-60	WW	Width of wall
61-70	HW	Height of wall from top to bottom
71-30	HL	Height of base above ground

Any number of surfaces may be used, limited only by available computer time. Complex surfaces may be approximated by using sections as chords of arcs, etc. If sections exceeding 50 feet in width are used, they will be broken up into sections of less than 50-foot width by the program. Thus, no time will be saved by using approximating pieces wider than 50 feet, and accuracy will suffer. If an ID of -1 is used, the scattered field is subtracted from the total field. Thus, if a wall is represented by one or more scatterers, a hole in that surface can be represented by a series of scatterers with an ID of -1.

After a series of scatterers is finished, a final ID is inserted. An ID of 10 will cause the direct ray to be added to the field summation and a CDI tape to be generated for the plot program. Then a new series of scatterers may be input. An ID of 11-15 will cause a new receiver path to be read in, allowing multiple runs in one batch. If the ID is less than 14, the plot program will combine the runs into one graph. This allows flight paths containing more than 500 points to be made. However, this will require that all the scatterers be resubmitted for each portion of the flight path. On any one section of the flight, the receiver point spacing must be constant, but between parts of the flight different spacings may be used. This will allow substantial savings in computer time, as those areas with slow changes in CDI (such as near the outer marker and beyond) will not require the density of points that areas with rapid changes in CDI (such as near the threshold) will.

At the end of a series of runs on a flight path, an ID of 20 may be used. This will cause the program to read in a new mode card allowing the program to start over with a new antenna, flight path, and scatterer set.

An ID of 0 will cause the direct ray to be calculated, thus permitting CDI measurements of the undisturbed field. When this ID is used, not only the CDI, but the magnitudes of the carrier and sideband fields are output. This allows verification of antenna patterns and comparison of theorectical and measured results.

To terminate the program, an end-of-file card is inserted. This will cause the program to output the CDI if an unfinished run is in progress and then stop.

REFERENCES

1. Stratton, J. A., "Electromagnetic Theory," McGraw Hill Book Co., New York, 1941.

2. Silver, S., "Microwave Antenna Theory and Design," Dover Publications, New York, 1965.

3. Redlich, R. W., and Gorman, J. T., "Disturbance of ILS Localizer Signals by Reflection from Large Hangars," IEEE Transaction on Aerospace and Electronic System, November 1969, pp. 1001-1002.

4. IBM, Federal Systems Division, "Multipath and Diffraction Effects of Structures on Localizer Systems," FAA-RD-70-20, Final Report, August 1970.

5. McFarland, R. H., Hill, D., and Luttermoser, D., "Earth Cover and Contour Effects," Technical Report RD-65-30 for the Federal Aviation Agency under Contract FA64WA-5060, Department of Electrical Engineering, Ohio University, Athens, Ohio, May, 1965, p. 46.

6. Manney, C., "A Study of Two Frequency Capture Effects on ILS Receivers," Final Report RD-69-12 for the Federal Aviation Administration under contract FA66WA-1556, Wilcox Company, Kansas City, Missouri, March, 1969.

7. Middleton, D., An Introduction to Statistical Communication Theory, McGraw Hill, New York, 1960, p. 98.

8. Abramowitz, M., and Stegun, I. A., Editors, Handbook of Mathematical Functions, National Bureau of Standards, U.S. Dept. of Commerce, Washington, D.C., 1966, p. 360, eq. 9.1.21, and p. 484, eq. 11.3.20.

9. Newsom, D., Memo No. E29200/2EM-88, STC (1972).

10. IBID, Memo No. E29200/2EM-87.